65p.

N64-15793
CODE-1
CR-53058

Space Programs Summary No. 37-25, Volume VI

for the period November 1, 1963 to December 31, 1963

Space Exploration Programs and Space Sciences

OTS PRICE

XEROX $ 6.60 ph.

MICROFILM $ 2.15 mf.

JET PROPULSION LABORATORY
CALIFORNIA INSTITUTE OF TECHNOLOGY
PASADENA, CALIFORNIA

January 31, 1964

Space Programs Summary No. 37-25, Volume VI

for the period November 1, 1963 to December 31, 1963

Space Exploration Programs and Space Sciences

JET PROPULSION LABORATORY
CALIFORNIA INSTITUTE OF TECHNOLOGY
PASADENA, CALIFORNIA

January 31, 1964

(NASA CR - - - ;

Preface

The *Space Programs Summary* is a six volume, bimonthly publication designed to report on JPL space exploration programs, and related supporting research and advanced development projects. The subtitles of all volumes of the *Space Programs Summary* are:

Vol. I. The Lunar Program (Confidential)

Vol. II. The Planetary–Interplanetary Program (Confidential)

Vol. III. The Deep Space Instrumentation Facility (Unclassified)

Vol. IV. Supporting Research and Advanced Development (Unclassified)

Vol. V. Supporting Research and Advanced Development (Confidential)

Vol. VI. Space Exploration Programs and Space Sciences (Unclassified)

The *Space Programs Summary,* Volume VI, is an unclassified digest of appropriate material from Volumes I through III, plus space science instrumentation studies. This instrumentation work is conducted by the JPL Space Sciences Division and also by individuals of various colleges, universities, and other organizations. All such projects are supported by the Laboratory and are concerned with the development of instruments for use in the NASA space flight programs.

W. H. Pickering

W. H. Pickering, *Director*
Jet Propulsion Laboratory

Space Programs Summary No. 37-25, Volume VI

Copyright © 1964, Jet Propulsion Laboratory, California Institute of Technology

Prepared under Contract No. NAS 7-100) National Aeronautics & Space Administration

(NASA

Contents

LUNAR PROGRAM

I. *Ranger* Project 1

A. Introduction 1

B. Systems Testing Operations 2

C. Subsystems Testing Operations 4

D. Lunar Facsimile Capsule 7

II. *Surveyor* Project 9

A. Introduction 9

B. Space Flight Operations 9

THE PLANETARY–INTERPLANETARY PROGRAM

III. *Mariner* Project 11

A. Introduction 11

B. Systems Testing 12

C. Atlantic Missile Range Launch Complex Facility Design 13

D. Spacecraft Design and Development 14

THE DEEP SPACE INSTRUMENTATION FACILITY

IV. Introduction 19

V. Communications Research, Development, and Facilities 20

A. Tracking Station Operations 20

B. Engineering Developments 20

C. Research and Development 21

D. Advanced Antenna System 23

OPERATIONAL AND TEST FACILITIES

VI. Test and Support Equipment 25

A. Environmental Test Laboratory 25

B. Operational Support Equipment 27

References 39

SPACE SCIENCES

VII. Space Instruments Development 41

A. *Mariner* Television Subsystem Optical Subassembly 41

B. *Mariner C* TV Development Support Equipment 43

C. Efficiency of Video Data Utilization in a Space TV Camera System 46

D. Investigation of Micropolish Oxides for Recording *Ranger* Block III Data 50

References 52

Contents (Cont'd)

VIII. Space Instruments Systems 53

A. Mechanization of the Nonreal-Time Data Automation System 53

B. Planetary Simulation for *Mariner C* Planetary Scan Subsystem 56

C. Analysis of Anomalies in *Mariner 2* Data 58

References 60

LUNAR PROGRAM

I. *Ranger* Project

A. Introduction

The *Ranger* Project was established to develop a space flight technology for transporting engineering and scientific instruments to the Moon and planets. This technology is then to be utilized for deriving information regarding the nature and history of the Moon. Nine *Ranger* launchings, using *Atlas D–Agena B* rockets, are now planned; five of these flights have been made.

Rangers 1 and *2* (Block I) were not lunar-oriented, but were engineering evaluation flights to test the basic systems to be employed in later lunar and planetary missions. Several scientific experiments were carried on a noninterference basis. The *Ranger 3, 4,* and *5* (Block II) spacecraft carried a gamma-ray instrument, a TV camera, and a rough-landing seismometer capsule. All three of these flights experienced failures. The objective of the *Ranger* Block III (*Rangers 6* through *9*) flights is to obtain TV pictures of the lunar surface which will be of benefit to both the scientific program and the U.S. manned lunar flight program.

All aspects of the project had been proceeding toward the December launch for *Ranger 6,* which was established early in 1963 as a result of the modified objectives and outcome of the design review. However, in September it was discovered that certain diodes used in the spacecraft and launch vehicle could possibly cause a mission failure. On October 21, when the spacecraft was ready for shipment to the Atlantic Missile Range (AMR), it was decided to postpone the launch in order to replace the diodes.

The suspect diodes (*Rangers 6* and *7*) in the central computer and sequencer (CC&S) and Sun sensor subsystems were replaced as these were critical circuits. The *Ranger 6* spacecraft was reassembled after receipt of the reworked hardware. System, environmental, and mission verification tests were conducted and successfully completed. The spacecraft was packaged for shipment and

left Pasadena on December 19, 1963, arriving at the AMR on December 23.

The PTM completed testing at the Deep Space Instrumentation Facility (DSIF). The tests included command and data threshold, compatibility with DSIF and space flight operations, and compatibility between the TV subsystem and the DSIF video recording equipment. Also, outside photographs and calibration pictures were made.

The operational support equipment (OSE) was checked out in the Spacecraft Checkout Facility at AMR by December 31. The only problem encountered was a somewhat higher ground noise. Preparation of the spacecraft for initial systems tests was completed December 31.

The *Atlas* and *Agena* launch vehicles for *Ranger 6* have been delivered to AMR, checked out, and erected on the launching pad. Additional guidance system units were furnished which included silver paste diodes.

The Deep Space Instrumentation Facility (DSIF)/space flight operations (SFO) compatibility test, SFO training test, command procedure test and SFO/DSIF integration test have been successfully completed. All DSIF stations have been prepared for the *Ranger 6* launch, and operational readiness tests are scheduled for January 1964.

The reworked (CC&S) and Sun sensor subsystems of *Ranger 7* were received and the spacecraft was reassembled. Subsystems tests, separation tests, and vibration tests have been completed successfully. A problem noted in the TV subsystem during high-frequency vibration tests was traced to the mixer in the Transmitter-A chassis; this unit was subsequently replaced. The spacecraft is being prepared for mission tests beginning January 3, 1964.

Ranger 7 launch vehicles are scheduled for delivery to AMR in January 1964.

Ranger 8 spacecraft is presently in assembly and is scheduled to be completed on January 4, 1964. Subsystem deliveries for *Ranger 9* are being made, and assembly of the spacecraft is scheduled to begin January 27, 1964.

The *Ranger* Block V Project comprised a series of six flights to be accomplished in 1965 and 1966. On December 13, 1963 the Block V series was cancelled by NASA Headquarters for budgetary reasons.

B. Systems Testing Operations

1. Ranger 6 Spacecraft Assembly and Test Operations

All available Spare 1 electronic assemblies were assembled to the *Ranger 6* bus and an abbreviated power turn-on and a subsystem test were accomplished. A systems test with these spares was then performed. No problems with the spare equipment were encountered, and the system performed as designed. The spare units which were not qualified in this test were: central computer and sequencer (CC&S), attitude-control gas system, TV subsystem, Sun sensors, and ring harness.

Following the systems test, the spares were removed and the hexagonal frame was moved to the JPL Spacecraft Assembly Facility pit for an attitude-control leak test. Results indicated a leak rate of less than 30 cm^3/hr.

The spacecraft was reassembled with all available flight hardware. A directional antenna deflection test, attitude-control subsystem test, a subsystem test of the CC&S, and a systems test, with all flight equipment, were performed.

A Space Flight Operations Facility spacecraft compatibility test was performed. No spacecraft problems were observed.

A mission test was conducted in the JPL 25-ft Space Simulator. No difficulties were experienced until the terminal (yaw) maneuver, when a hard-over gyro indication after approximately 80 sec resulted in an improper maneuver. Investigation revealed that in the power subsystem digital scan OSE an isolated chassis was grounded to frame by a mounting screw. Close evaluation verified that no damage to flight hardware had occurred. Since the objectives had been met, the test was not repeated.

The spacecraft and support equipment were shipped from JPL to the Atlantic Missile Range (AMR). The launch complex equipment arrived at the AMR and was installed in the blockhouse. Checkout of this equipment was started.

2. Ranger 7 Spacecraft Assembly and Test Operations

A transmitter power supply engineering change requirement was made on the TV subsystem. The new

hybrid ring, new RF cables, F-shutters, and all shutter grommets were replaced.

The following tests were made on the spacecraft: (1) the attitude-control gas system was inspected for faulty regulators and pressure transducers, (2) a directional-antenna deflection test was performed, and (3) a power survey was conducted. Results of the tests were satisfactory.

After checkout on the spacecraft, a systems test was performed. The only problem was with the antenna preset angles. This problem was isolated to the antenna control electronics module in the attitude-control subsystem. The module was replaced with a flight spare unit and checked out.

After the systems test, the following operations were performed on the spacecraft with satisfactory results: vibration tests, weight and center-of-gravity determination, and another systems test.

3. *Proof Test Model (PTM)*

The Block III PTM was tested in conjunction with the Deep Space Instrumentation Facility (DSIF) to establish compatibility between the spacecraft and the DSIF equipment. The tests included command, DSIF, and data threshold, with considerable evaluation of the TV equipment at received RF signal strengths below those which would be experienced when the spacecraft is at lunar distances. Preliminary test results indicated that:

(1) No incompatibilities existed between the DSIF equipment and the spacecraft.

(2) The spacecraft and TV data recovery system operated at threshold signal levels.

(3) No noted RF interferences between TV and spacecraft transmitters affected the data or command capability at threshold levels.

(4) Outside picture quality at lunar-distance RF levels was good; it is still being evaluated. New sync circuits in TV data recovery equipment seemed to function properly, even at levels 10 db below lunar-distance levels.

The spacecraft bus and TV subsystem were given another torsional vibration test in the JPL Spacecraft Assembly Facility. A systems test, including the terminal maneuver and TV operation, was also performed. Test results indicated no spacecraft problems.

After these tests, the TV subsystem was tested in the horizontal vacuum chamber with the new-design (stripline) hybrid ring. No RF power dropouts or other abnormal operation were noted during four tests. Based on these tests and other tests at RCA, the decision was made to change hybrid rings in all Block III spacecraft to the new design.

The spacecraft bus was then tested in the JPL celestial simulator. The purpose of this test was to determine the effects of light reflections from the Sun shade and other spacecraft surfaces on the Earth sensor. Special tests were also made in the JPL 7-ft Space Simulator, on the data encoder and communications system. No problems were encountered in these tests.

A series of special design evaluation tests was conducted on the spacecraft bus. A special solar panel test was conducted to verify zener and panel operation at high and low booster regulator input voltages. Solar panels performed as designed. Following these tests, another systems test indicated all spacecraft operations were normal.

A special attitude-control systems test was conducted, using the *Ranger 6* power scanner with circuit corrections. No failure was noted while the spacecraft was in an extended pitch and yaw maneuver. The attitude-control failure observed on *Ranger 6* was duplicated on the PTM. This was an operational-support-equipment problem and was corrected.

4. *Electromagnetic-Interference and TV Compatibility*

Electromagnetic-interference Cape simulation tests and extension systems verification tests were run to ensure pyrotechnic safety and absence of susceptibility of the *Ranger* Block III spacecraft systems to electromagnetic interference generated by ground and launch vehicle sources. Also, TV compatibility tests were run at 890 Mc to determine if the TV subsystem had any spurious interference output at this frequency.

Simulating sources for the flight spacecraft are designed to establish average power densities 3 db higher than those created by the Cape and launch vehicle sources. On the proof test model (PTM), 6-db margins are used. With the exception of the *Ranger 7* dummy run, pulsed

power sources have been simulated on an average power basis. During the *Ranger 7* dummy run, the *Agena* radar beacon was simulated by a nonflight-type pulsed beacon whose peak power density at the spacecraft was 14 db above levels calculated to exist in flight configuration. No malfunction was noted during this test. An effort will be made in future tests to use pulsed power simulation sources where applicable. The only interference noted during the electromagnetic-interference simulation tests was in the Block III dummy run on August 9, 1963, and the *Ranger 6* systems test on August 28, 1963. Interference to the data encoder caused by the *Agena* telemetry simulator was discovered. Subsequent tests, made with a flight spare *Agena* telemetry antenna installed, indicated no interference problem existed. This implies that, for local (launch vehicle) transmitter sources with antennas in general facing away from the spacecraft, the simulated incident power density level has exceeded the 3- and 6-db margins previously mentioned.

Power density measurements have been performed on Pad 12 at the Atlantic Missile Range (AMR) to substantiate levels calculated to exist at the spacecraft.

During the extension systems verification tests RF power absorption by squibs was monitored. Power absorbed by squibs was so minute that no further squib measurements will be made on *Rangers 7* through 9 unless there is a change in AMR, launch vehicle, or spacecraft RF transmission conditions.

The TV compatibility tests were run on the *Ranger 6* and 7 PTM during the space simulation mission verification test and the final systems test. These tests consisted of a search for 890-Mc noise generated by the TV subsystem, radiating into the omni-antenna, induced into the omni-antenna cable, or leaking through the high-gain antenna coupler. No indication of signal levels above the 890-Mc transponder receiver threshold was observed. Further 890-Mc tests were performed on the PTM to determine if voltage standing wave ratio and load phase angle variation at the high-gain antenna cable (antenna end) would create any spurious outputs of the TV subsystem. No problem of interference was noted for this test. Attenuation tests were made on the spacecraft shroud in the frequency range of 200 Mc to 4.2 Gc. While the area in which the measurements were made was not ideally suited for such measurements, it appears that the shroud gives a minimum 15- to 50-db attenuation, depending upon the frequency.

Measurements of the JPL transponder transmitting frequency 960.046 Mc have been performed to ensure freedom of interference from the RCA TV transmitter in this frequency band. A frequency band of approximately 100 kc has been scanned. Some interference signals have been noted which are above the specification level of −15 dbm. Performance of the transponder has, however, been satisfactory.

5. Spacecraft Simulator

A spacecraft simulator has been designed for *Ranger* Block III. The specific characteristics to be tested were duplicated so as to allow a minimum of procedural modifications when effecting the transition from simulator to actual spacecraft tests.

The Block III simulator is comprised of two basic units: (1) data encoder and (2) the remaining functions of power, CC&S, pyrotechnics, and attitude control. Both units are equipped with a waterproof carrying case. Power activation cables and support documents are contained in the lid of the case; large cables enabling the simulator to be connected to several electrical interfaces are supplied separately. This equipment was used for the *Ranger 6* dummy run and for space simulation checks prior to spacecraft hookup.

C. Subsystems Testing Operations

1. Midcourse Propulsion System

All functional type-approval (TA) testing of explosively actuated valve squib assemblies was completed. Serious problems were encountered in two areas: (1) an unusually large number of squibs exhibited venting around the connector assembly, and (2) three nitrogen valves failed to close completely. There was also a fuel valve problem; one partial opening was observed.

During the TA testing, the squib failure rate increased from approximately 1 in 40 to about 1 in 5. The failures appear to be related to a particular lot that is being used

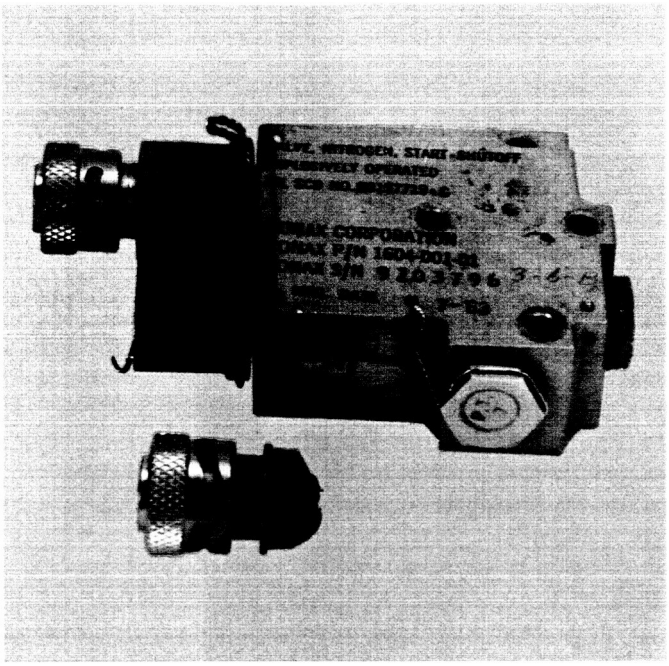

Fig. 1. Post-firing view of nitrogen valve showing both squib venting and connector failure

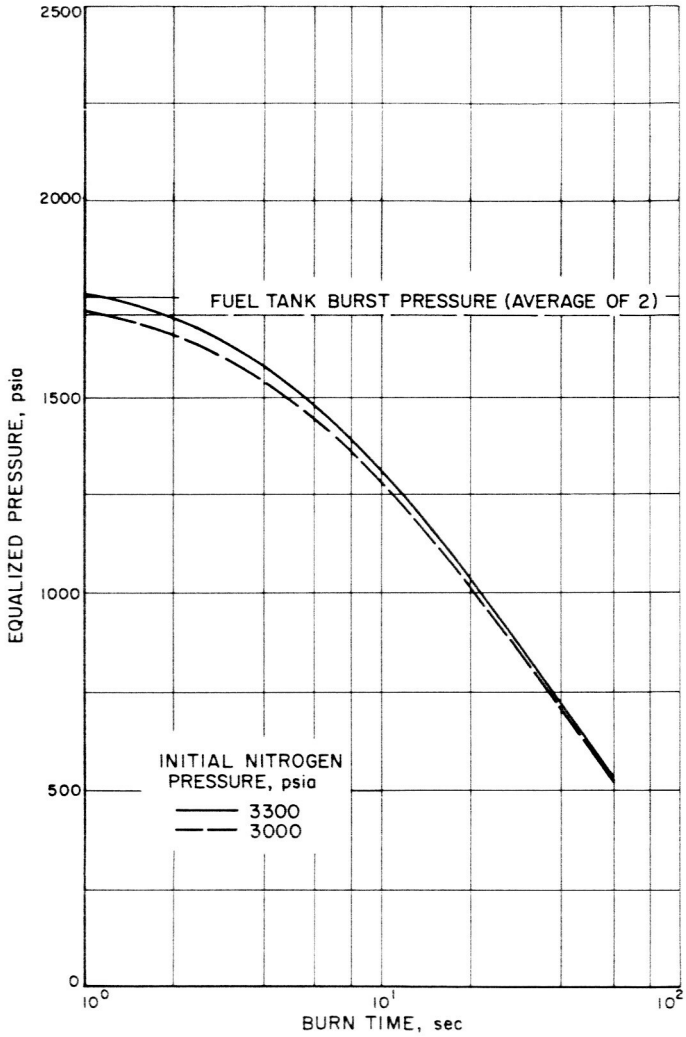

Fig. 2. Final fuel and nitrogen tank pressure vs burn time, assuming equalization of pressures

for test only. A portion of this lot is presently being tested for lot acceptance prior to flight. A typical squib failure is illustrated by Fig. 1. In this particular case shroud burn-through is evident, as well as connector failure.

The valve failures are the first adverse experience with these explosive valves after approximately 500 firings. The valve failures fall into two categories: (1) leakage through the normally open port after actuation, and (2) failure of the normally closed actuator ram to effect complete opening.

The nitrogen valve failures resulted in leakages through the valves of from 180 cm^3/hr (STP) to in excess of 2760 cm^3/hr (STP). The nitrogen valve closing cycle is the least critical valve function since the downstream pressure regulator allows a maximum leakage of only 10 cm^3/hr. The maximum permissible leakage for a 66-hr mission is 1400 cm^3/hr; thus, dual failures (nitrogen valve and regulator) would be required in order to cause fuel tank over-pressurization and rupture. If an engine burn time of approximately 6 sec is accomplished, the equalized pressure would be well below the fuel tank burst pressure (Fig. 2).

The fuel valve problem falls into two areas: (1) reduced flow to the rocket motor because of a partial opening, and (2) no fuel flow in the event of no opening. The effect of the former would be to reduce the thrust produced by the engine; this should result in no other propulsion problems if the resultant thrust is at least approximately 20 lb. Complete loss of fuel flow would result in failure of the system to deliver any thrust.

Despite these problem areas, which are being extensively investigated, there is still considerable confidence in the ability of the fuel valves to function properly. The one partial opening that was observed still allowed full fuel flow through the test system. Only one no-opening case has ever been observed in any valve during some 500 operations.

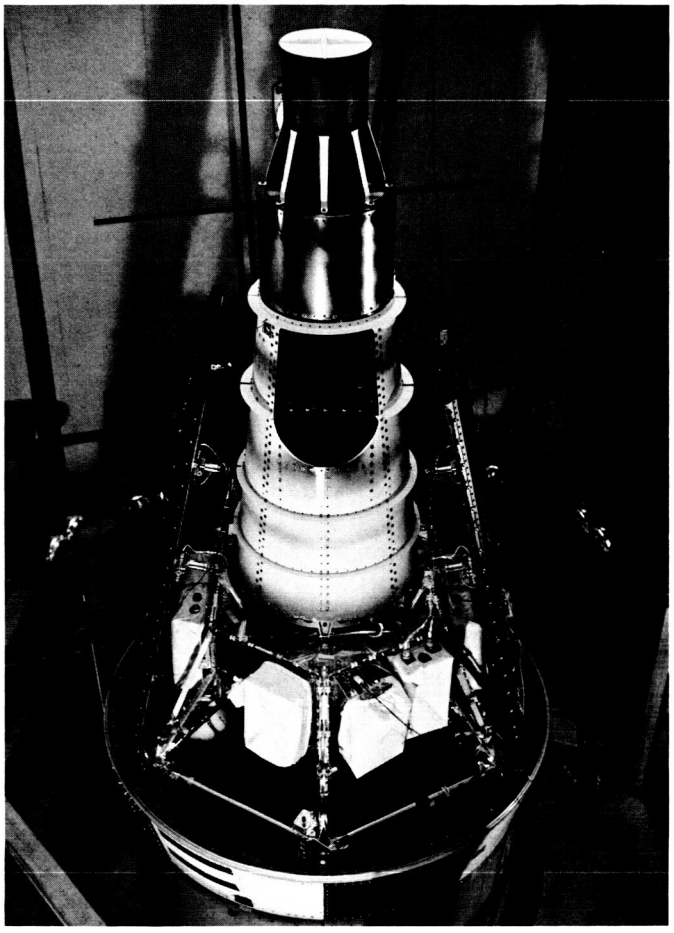

Fig. 3. Solar panel pin-puller test configuration

2. *Solar Panels*

Solar panel TA 2 and a dummy panel were mounted on the PTM spacecraft for: (1) environmental testing in the launch configuration; and (2) vibration tests in each of the three axes, x, y, and z. A post-PTM electrical performance test was conducted. The TA 2 and dummy solar panel underwent a pyrotechnic pin-puller test with the *Ranger 6* spacecraft (Fig. 3).

During solar panel TA 1 testing, an initial transportation vibration test and additional electrical performance testing were completed. Opening of solar cell circuits occurred during the transportation vibration test due to an incorrectly designed test fixture and incorrect location of the control accelerometer.

Final TA verification of the Mark IV solar panel design began on September 21. The tests performed were: (1) humidity, (2) electrical performance, (3) vibration, (4) electrical performance, (5) vacuum-temperature and thermal shock, (6) electrical performance, (7) transportation vibration, and (8) electrical performance.

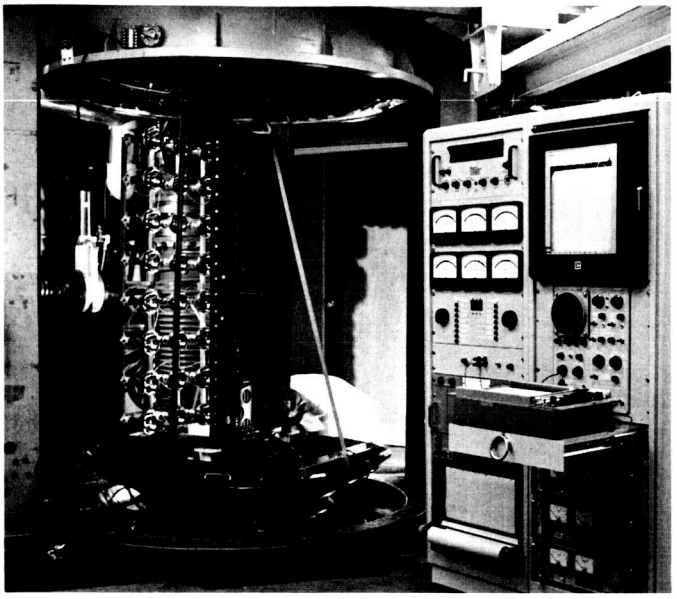

Fig. 4. Solar panel thermal shock test configuration and test rack

The TA humidity test was performed in a Bemco humidity chamber. The subsequent vibration test was performed on the JPL vibration exciter and consisted of: (1) a low-frequency run between 20 and 100 cps, (2) a high-frequency run between 100 and 2000 cps, and (3) a high-frequency run of Gaussian noise, band-limited between 100 and 2000 cps, in each of the three mutually orthogonal x, y, z axes. Vibration of the panel took place without any problems after a wire solder connection, (which had failed during the low-frequency x-axis run) was repaired.

The vacuum-temperature and thermal shock test was performed on solar panel TA 1 during a 7-day period in the JPL 6 × 7-ft simulator, with the solar panel mounted as shown in Fig. 4. A bank of 32 infrared lamps was used to heat the panel to an average temperature of 80°C for 116 hr after the thermal shock test had been conducted.

Modifications were made to the solar panel mounting fixture for the repeat TA 1 transportation vibration test. Fig. 5 shows the modified fixture used. The panel was held at the four transportation attachment points much more securely than for the first test. The two control

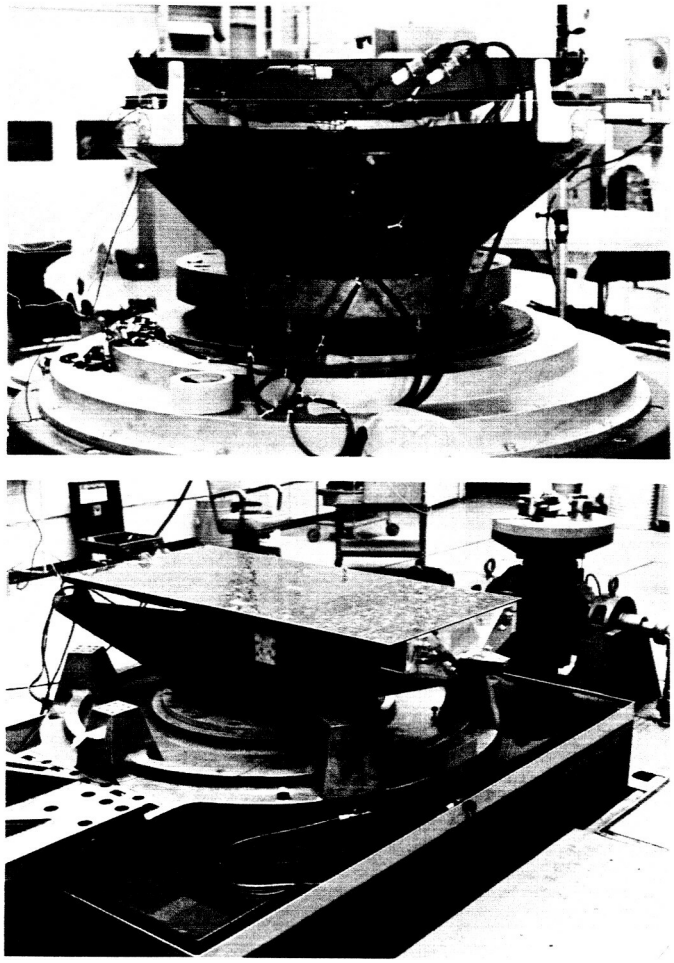

Fig. 5. Modified attachment configuration for transportation vibration testing

accelerometers were placed so as to give better control of the input acceleration levels during the test.

Environmental and electrical performance tests are considered as sufficient criteria for the qualification of the design of the *Ranger* Block III flight solar panels. For the TA electrical performance tests run on solar panel TA 1, the total panel electrical performance requirement of 100 w at 26.0 v and also the specified zener diode requirements were met in every instance.

The *Ranger* Block III solar panels comprise the first solar cell space power supplies to be electrically evaluated using primary standard solar cells which have been calibrated at Earth-space conditions. These primary standard cells had been calibrated earlier atop a balloon at 77,000-ft altitude above sea level on June 13, 1963.

3. Batteries

The three batteries subjected to the type approval (TA) test program all passed successfully. To date, fourteen batteries have been used in spacecraft and power subsystem testing; all have met the requirements of an actual flight battery.

The TA testing was divided into two sections: (1) tests conducted in the environments which simulate the on-the-ground stand and operating conditions, and (2) tests conducted in the environments which simulate the flight aboard the spacecraft from the launch/boost phase to lunar impact. The battery was tested between each of the environmental exposures to assure that it had survived and was able to be subjected to the next environment.

D. Lunar Facsimile Capsule

1. Introduction

Aeronutronic Division of Philco Corporation, a subsidiary of the Ford Motor Company, has been developing major subassemblies for a lunar facsimile capsule (LFC).

Further development of the switch drum on the scanning drive shaft and the solid-state flip-flop circuit in the signal electronics (both in the top tube subassembly) was indicated by results of Prototype 2 assembly checkout and functional testing. A simple change of switch drum materials and a simplified switch geometry are being investigated.

Under development efforts of the breadboard porting mechanism, dynamic porting characteristics were investigated. The purpose of porting action is to create an opening for the extension of the top tube subassembly from the LFC payload while maintaining the tube's vertical alignment. From this task it was discovered that, without the aid of external stabilization, excessive bounce would be induced by cutting through the balsa wood impact limiter at high velocity. Consequently, effort was initiated to conduct a study of impact limiter separation, stabilization, and shaped-charge porting mechanisms.

The following material relating to the lunar facsimile capsule was extracted from the Aeronutronic document: *Bimonthly Technical Progress Report No. 6, Lunar Fac-*

simile Capsule Program, November 15, 1963, covering the period August 31, to October 25, 1963.

2. Top Tube Subassembly

The LFC sync switch failure experienced during prototype testing was due to surface oxidation of the aluminum contact material, which was caused by arcing. The switch drum was designed with gold-plated contact points to prevent this, but the gold-plating process was found to etch away the insulating material.

The new switch drum will be fabricated from Neyoro G, a high-gold-content alloy containing platinum, silver, and copper. This material has resistance to tarnish and corrosion, high strength, hardness, and relatively low resistivity. The switch block contacts will be fabricated from Paliney 7, a pallodium platinum, gold, and copper alloy.

The redesign of the preamplifier circuit requires the switch drum design to be 180 deg on and 180 deg off for each switch cycle. The switch block will have a bifurcated contact to reduce switch noise and provide circuit redundancy.

A method of switching, utilizing a single blanking switch, is shown in Fig. 6. When the switch is open, both sensors are on and operating. The gate-source diodes of the field-effect transistors act as a preferential *or* gate and pass only the signal of Sensor 1. Closing the switch removes the bias from Sensor 1 and leaves Sensor 2 on.

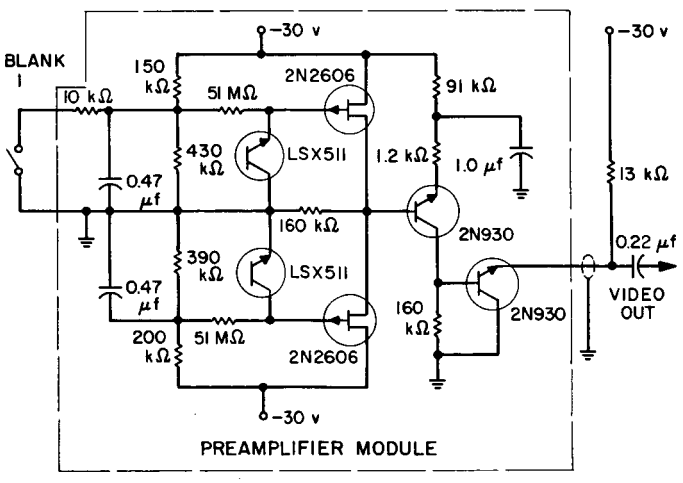

Fig. 6. Modified preamplifier circuit with single blanking switch

With this method one good picture results, regardless of any switch failure mode.

The simplicity and reduced number of components result in high reliability. The addition of a redundant output stage would assure the transmission of a video signal in the event of a transistor failure. The output is not appreciably degraded with the additional amplifier stage. Although the failure of one of the two transistors in the original circuit (Fig. 6) would be a "catastrophic" failure, the possibility is so remote that the additional circuitry to guard against it does not appear to be justified.

3. Porting and Stabilization Subsystem

It was previously determined that a 20-grain RDX flexible linear shaped charge (FLSC) is capable of providing an adequate 5.5-in.-D cut through 0.187-in.-thick flat fiberglass coupons. Then tests were run with both 20- and 40-grain RDX FLSC to evaluate the effect of adding an additional 0.030-in.-thick aluminum sheet between the FLSC and the fiberglass coupon. From the results of these tests, it was decided that all future porting tests will be run using a 40-grain FLSC with a 2.75-in. D. It is estimated that this will reduce the impulse by a factor of 2, and will result in an energy equivalent to that of dropping the ball 3.75 in. onto the lunar surface.

Configurations for limiter and stabilization legs were considered. The approach selected is the use of radial legs mounted on three orthogonal axes, which are folded up and passively deployed when the limiter is removed. These legs will be stiff (i.e., metal) and may allow energy absorber pads on the end to reduce the rebound on the lunar surface. The orthogonal legs will allow the reduction of the FLSC diameter from 5.5 to 2.75 in., with a subsequent reduction in impulse from 5.2 to 2.6 lb-sec.

A dynamic analysis was made to determine the behavior of the payload sphere when subjected to a 5.62-lb-sec impulse on the lunar surface. A lunar model was devised which is considered conservative for all cases. The analysis considered portions of this model and selected a soil modulus of elasticity equal to 16.67 times the bearing strength (the worst case for sand found in the literature). For low compressive strengths, the stored elastic energy is low due to plastic deformation of the lunar surface. At relatively high compressive strengths, very little plastic deformation occurs and the ball approaches the perfectly elastic case of a 12-in. rebound for 5.62 lb-sec impulse.

II. *Surveyor* Project

A. Introduction

The *Surveyor* Project will take the next step in advancing lunar technology by making soft landings on the Moon, beginning in 1965 with a group of four test missions whose objective is to demonstrate successful soft landing by post-landing spacecraft operation. An engineering payload including elements of redundancy, increased diagnostic telemetry, touchdown instrumentation, and survey TV will be used. A possible backup mission is under consideration.

The general objective after 1965 is to perform operations on the Moon contributing new scientific knowledge and basic data in support of manned lunar landings. A group of four flights planned for 1966 will carry a scientific payload selected from the following experiments: two-camera TV, micrometeorite ejecta, single-axis seismometer, alpha-particle scattering, soil properties (surface sampler), and touchdown dynamics.

In 1965 and 1966, the 2150-lb (separated weight) spacecraft will be injected into the lunar trajectory by direct ascent, using single-burn *Atlas–Centaur* vehicles.

Hughes Aircraft Company is under contract to develop and manufacture the first seven spacecraft. Studies are under way at the Bendix Corporation, Systems Division, and the General Motors Defense Research Laboratories on the feasibility and design of lightweight lunar roving vehicles as possible later payloads for *Surveyor*.

B. Space Flight Operations

The *Surveyor* operations planning effort during this reporting period has been concerned with further defining and establishing procedural concepts for flight operations in both the standard and nonstandard cases. Included in this activity is the formulation of specific procedural methods by which spacecraft commands will be generated, verified, and transmitted.

The terrestrial communications capability which can be made available for *Surveyor* operations has been

specified, as have Deep Space Instrumentation Facility (DSIF) tracking coverage commitments. The *Surveyor* missions will be supported by DSIF 11 (Goldstone Pioneer Station), DSIF 42 (Canberra, Australia), and DSIF 51 (Johannesburg, South Africa). Each overseas station will be provided with three teletype circuits, one simplex high-speed data circuit, and two voice circuits for operational use. The Goldstone station will be provided with six teletype circuits, two simplex high-speed data circuits and one duplex high-speed circuit, six voice circuits, one microwave system video channel, and one microwave system wideband message channel. The DSIF-11 teletype and high-speed data circuitry will utilize the microwave system as the transmission medium between the Space Flight Operations Facility (SFOF) and Goldstone.

The SFOF has been committed to support the *Surveyor* Project and will provide the means by which control of the missions can be exercised by the Project Office. SFOF data processing, communications, display, and support capabilities have been allocated to the *Surveyor* Project, as well as SFOF technical areas where analysis of the spacecraft performance and flight path may be performed.

THE PLANETARY—INTERPLANETARY PROGRAM

III. *Mariner* Project

A. Introduction

The early objective of the Planetary-Interplanetary Program is the initial probing of the planets Mars and Venus by unmanned spacecraft. The initial probing of Venus was successfully accomplished by *Mariner 2*. The next step toward this objective is the initial probing of Mars by a *Mariner C* spacecraft planned for the 1964–1965 opportunity.

The primary objective of the *Mariner C* mission (*Mariner* Mars 1964 Project) is to conduct close-up (flyby) scientific observations of the planet Mars during the 1964–1965 opportunity and to transmit the results of these observations back to Earth. The planetary observations should, to the greatest practical extent, provide maximum information about Mars. A TV system and a reasonable complement of field and particle experiments will be carried. An effort will be made to identify organics in the atmosphere and on the surface of the planet.

A secondary objective is to provide experience and knowledge about the performance of the basic engineering equipment of an attitude-stabilized flyby spacecraft during a long duration flight in space farther away from the Sun than the Earth. An additional secondary objective is to perform certain field and/or particle measurements in interplanetary space during the trip and in the vicinity of Mars.

It is planned to conduct two launchings of *Mariner C* missions from two separate launch pads. In order to exploit the limited launch period to the maximum extent, spacecraft and launch vehicles will be processed in parallel, so that following the launch of the first space vehicle the second vehicle may be launched without delay, no earlier than two days after the first launch.

The proof test model (PTM) spacecraft is assembled and checkouts have begun in the JPL Spacecraft Assembly Facility. Some of the equipment presently on the spacecraft is prototype; however, this will be replaced by the PTM serial number equipment as soon as it is available. It is expected that all PTM equipment will be on board the spacecraft for the system testing.

The decision has been made to proceed with the development of an over-the-nose shroud for *Mariner C*. This decision requires certain spacecraft changes which are currently being incorporated into the design.

B. Systems Testing

1. Proof Test Model Assembly and Test Operations

On November 1, 1963, assembly was begun on the *Mariner C* proof test model (PTM) at the Spacecraft Assembly Facility (SAF). Installation and checkout of related facility support equipment (FSE) and operational support equipment (OSE) progressed concurrently.

The PTM will be used for design verification of the *Mariner C* flight spacecraft to be assembled at SAF in early 1964. This prototype of the final flight spacecraft is scheduled to be subjected to a variety of tests (many at more severe environmental levels than would normally be encountered in flight). Detailed test procedures are released just prior to the performance of each test on the PTM or system test complex (STC). PTM testing provides the means of validating the test procedures for use on the flight spacecraft and STCs.

During the assembly period, a controlled disassembly and inspection of all delivered PTM equipment were performed. This inspection uncovered some discrepancies which, in most instances, were corrected. As a result, the *Mariner C* PTM was assembled to the electrical test configuration without solar panels, solar pressure vanes, thermal shields, and temperature control louvers, with very few major mechanical or electrical interface problems occurring. The assembly was completed on schedule; however, because of variances in hardware delivery to SAF, the actual sequence of installation of the individual subassemblies differed somewhat from the optimum installation sequence, and prototype equipment was used in many instances where PTM hardware was not available.

The *Mariner C* STC and its related FSE were installed and tested during the spacecraft assembly period. The following tests of the STC and FSE were satisfactorily completed:

(1) Cabling continuity test.

(2) STC ground integrity test.

(3) Initial application of power to the STC.

(4) Self-test of the OSE of each spacecraft subsystem.

(5) Testing of the interfaces among OSE.

(6) Measurement of the electromagnetic interference produced by each item of OSE and FSE on the STC.

The initial application of spacecraft power (as opposed to OSE power) to each of the spacecraft subsystems was satisfactorily completed. Photographs were taken of the various voltage and current waveforms for comparison with photographs previously taken during laboratory-type testing.

Testing of the complex inter-relationships among spacecraft subsystems was started. During this series of tests, each subsystem is operated through all possible modes of operation and its effect on the other spacecraft subsystems is determined.

2. Electromagnetic Interference (EMI) and Magnetics

A Franklin Electronics high-speed printer was tested according to JPL specifications. Test results indicated conducted interference in excess of specification limits. The addition of a line filter reduced the interference level to an acceptable value.

Similar tests were performed on a prototype central computer and sequencer (CC&S) and the narrow angle Mars gate subsystem as part of the preliminary subsystem testings. Data from these levels indicate no interference above specification.

The RFI limit for the *Mariner C* communications system has been determined. A preliminary EMI spacecraft test plan has been written. Design work is near completion for parts for a low-noise parametric S-band receiver for interference measurements on *Mariner C*.

An evaluation has been made of materials used on spacecraft which may be detrimental to magnetic measurements. A specification has been written to provide proper magnetic restraints. A large percentage of the *Mariner C* hardware meets the requirements of the specification. Where specifications are not met and schedule has prohibited substitutions, magnetic shielding has been considered. Shields have been successfully fabricated, annealed, and evaluated with flight hardware, providing shielding factors of approximately 1200 using mumetal or molypermalloy.

3. *System Control of Spacecraft Low Frequency Wiring*

A large fraction of the spacecraft proof test model (PTM) tests is devoted to verifying electrical interfaces between the various functional subsystems. Included are static continuity checks, useful in uncovering the first three of the four main types of fault possibly present in any of the hundreds of interface circuits: (1) incorrect wiring of the active line, (2) incorrect wiring of the return line, (3) incorrect wiring between lines, and (4) incorrect end-circuit. All circuit faults must of course be found and corrected, but it is considered advantageous to perform *detailed* postassembly continuity checks for faults of just the second of the four types. Normal diagnostic procedures are time consuming in determining the Type 2 faults which are prone to generate crosstalk and other symptoms of improper performance not obviously related to the fault.

Evolution of tools employed in the return-line circuit checks, and the method of application are shown in Fig. 1. The Connector Summary Sheet is made entirely from data in the Return-Side Tree Diagram and predicts what will be found with an ohmmeter "looking into" a connector junction in the spacecraft. A sheet is prepared for each connector to be checked. The format of the Tree Diagram greatly facilitates the preparation of these sheets.

The Ohm Sheet is prepared from the measurements made on the spacecraft. Measurements are accomplished with the aid of a break-out box which maintains connection of all lines through the connector junction, except the line under test.

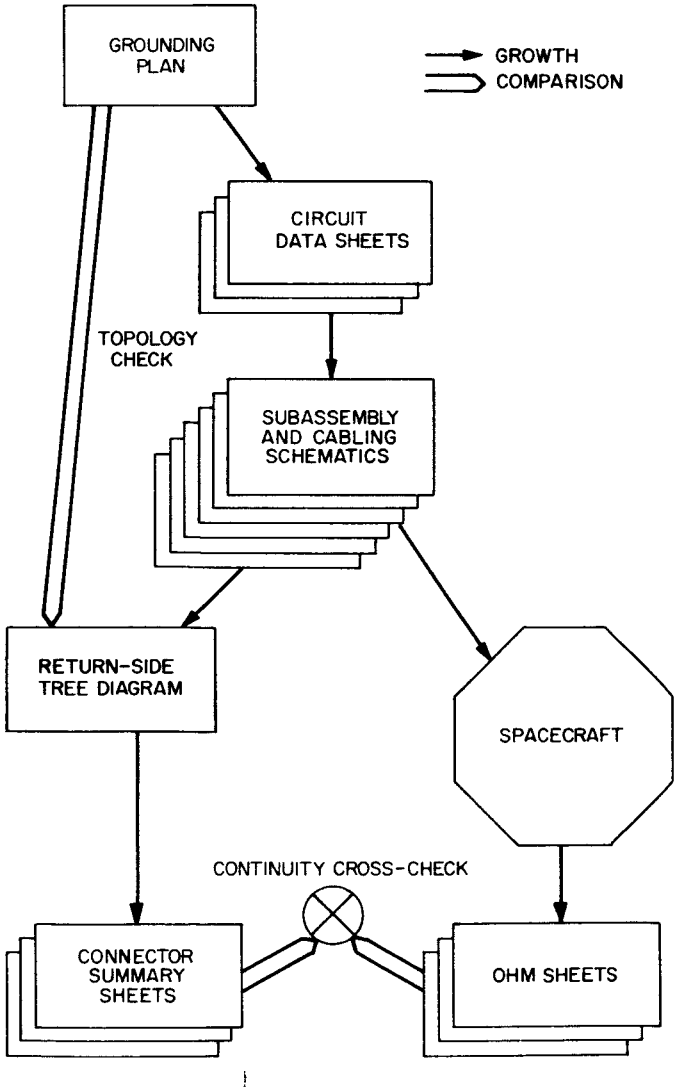

Fig. 1. Return-line continuity checks

C. Atlantic Missile Range Launch Complex Facility Design

To meet the requirements of *Mariner C*, several design changes are scheduled for the spacecraft or "payload" portion of Atlantic Missile Range Complex 12 cable installation; a functionally identical installation is planned for Complex 13 to provide the dual countdown capability. Because of the tight schedules between projects, maximum consideration was also given to design compatibility between the *Ranger* and *Mariner* projects. Basic differences between Complex 12 and 13 have been resolved in the JPL system hardware design while maintaining the direct interchangeability feature of "like" JPL-supplied equipment on each complex.

Since the basic concepts governing spacecraft launch complex system design apply to all current programs and much of the hardware is identical, a general design specification has been released detailing the basic concepts and establishing the minimum requirements for electrical systems on current programs.

Design of the cable link between the spacecraft and the first JPL equipment interface (umbilical tower junction box) has been improved.

The original Pad 12 installation used a special cable retractor which pulled the 50-ft catenary (boom) cables clear of the retracting boom during launch. The advantages gained were: (1) a minimum cable length (50 ft), and (2) an installation using the fewest interfaces. The new installation will use 75-ft cables permanently routed down the boom (although still replaceable). The added length and extra boom plate interface will be compensated for by designing the cables with adequately low resistance lines for external power and charging functions (no splices) and by including special low-capacity wiring for critical functions. The remaining link to the spacecraft consists of a catenary cable (or cables) approximately 12 ft long incorporating all special project requirements between the spacecraft and the boom plate.

The requirement for low-capacity lines is coupled with a requirement for temperature stability. This follows since most critical ac-type signals are not only affected by the total capacity of the line but also by changes in capacity (generally resulting from changes in temperature). An acceptable type of low-capacity wire was incorporated into the design of two of the boom cables. Only a portion of the conductors in each cable are special, however, since use of this type of line reduces the physical ruggedness of the cable.

The requirement for extensive signal conditioning and amplification of spacecraft signals and the present relatively severe environmental penalties imposed by the umbilical tower location of the JPL umbilical tower junction box have resulted in a requirement for extensive expansion of the video-pair installation at each complex. The present plan is to permanently install six video-pair lines between the umbilical tower (JPL J-box area) and the launch complex OSE area (launch control shelter/launch pad building on Pad 12 and first-stage-vehicle room/launch pad building on Pad 13). Also, six lines will be installed between the launch complex OSE area and the transfer room on each pad where connection can be made to existing pothead terminations of the permanently installed and existing video-pair lines routed throughout the complexes.

In addition to the remote control of JPL-supplied 400-cps generators (as formerly provided for *Mariners 1* and *2* on Pad 12), additional remote control of 60-cps power used to support the JPL equipment located on the umbilical tower and in the launch complex OSE are being provided. The control panels for these circuits will be located in each blockhouse.

D. Spacecraft Design and Development

1. Structural Test Model Testing

Developmental vibration testing was conducted on the *Mariner C* structural test model (Fig. 2). Several solar panel corrugations buckled and tore at frequencies of about 90 cps and about 16 cps during the x-axis test at a level of 1.0 g rms. Other test damage included the propagation of a crack at a stress concentration on the low-gain antenna support channel and loosening of the rod end bearings at the solar panel hinge.

Analytical and test results indicate that the failure of the solar panel corrugations is attributable to below tolerance corrugation skin thicknesses. The present corrugation design is believed to be adequate with a minimum allowable thickness of 3.5 mil. Corrugations with a thickness of 3 mil can be made structurally adequate by the addition of cap stiffeners. Handling of this thin material remains a problem.

2. Launch Vehicle Interface

After a series of design reviews and investigations by Lockheed Missiles and Space Company (LMSC), Lewis Research Center (LeRC), and JPL personnel, it was concluded that a mechanical over-the-nose shroud would

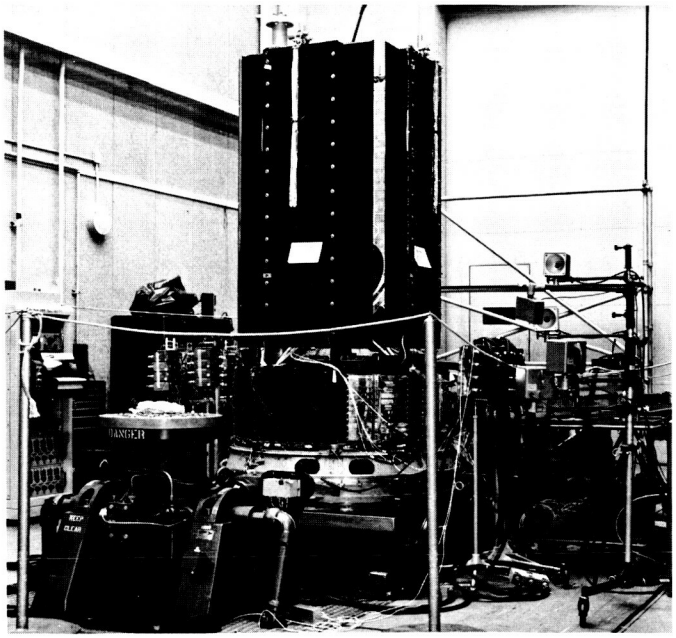

Fig. 2. STM lateral vibration test setup

be used for *Mariner C* instead of the pyrotechnically-separated clamshell shroud. Several changes have to be made to the spacecraft to accommodate the over-the-nose shroud. These include: (1) addition of two skid rails to the back of each solar panel, (2) tilting the top of each solar panel inward 0.62 in., and (3) relocating the solar pressure vane, actuator deployment mechanism, and latch.

3. Temperature Control

The thermal shield design has been modified as a result of the temperature control model simulator tests, which indicated that the spacecraft bus temperature would be too cold at Mars. The objective is to both reduce the emissivity of the lower and side shields as much as practical and to minimize the heat losses from seams and attach points. Only minor improvements will be made in the upper shield to simplify its construction. It will continue to consist of 30 layers of ¼-mil aluminized Mylar film with an outer layer of black Dacron fabric. The shields around the perimeter of the spacecraft will be changed from multilayered Mylar shields to thin-gage polished aluminum shields. These shields will be attached to the spacecraft structure with non-metallic standoffs. The lower shield will continue to consist of 20 layers of ¼-mil aluminized Mylar, but the exterior surface will be 1-mil aluminized Teflon (Teflon side out) instead of black Dacron.

Results of the temperature control model simulator tests also indicated that the planet science storage and operating temperatures were within limits, with the exception of the ultraviolet photometer, which was about 30°F below the minimum desired operating temperature at Mars. To raise the temperature of the planet science, particularly the ultraviolet photometer, the lower shield will have a rotary joint. This will allow the planet science to be radiatively coupled to the octagon and to be enclosed within the shielded volume. Both of these features will raise the temperature of these instruments and will reduce the uncertainty of the temperature predictions.

4. Pyrotechnics

A series of tests was conducted in the pyrotechnics area to verify the adequacy of the design. The prototype pyrotechnic control assembly successfully fired a quantity of 1-w squibs which are similar to the *Mariner C* pinpuller and postinjection propulsion system squibs. The results showed that the circuit functions satisfactorily at −10°C and at greatly reduced energy. At 19 v, the capacitor bank has 48% of its nominal energy.

Another series of tests was conducted to determine the effectiveness of the capacitor to prevent noise from triggering the silicon-controlled rectifiers. The results of these tests indicate that the 4.7-μf Sprague-type 350D capacitor is acceptable in this application.

5. Gyro Control Assembly

Fabrication and assembly have progressed to the stage where a gyro control assembly prototype has been built and tested, a proof test model completed, tested, and delivered to the JPL Spacecraft Assembly Facility, and a type approval (TA) unit is in the final stages of assembly. No significant areas of design deficiency have been encountered.

The normal schedule of events for the TA system calls for an extended life test period after all TA testing is complete. A similar procedure was used on the *Mariner 2* system. The life test of a *Mariner-2*-type gyro package is still in progress after over 1 yr of constant operation. To this date, the three Kearfott 2519 gyros used in the tested *Mariner* subassembly have accumulated over 11,000 hr of spin motor operation at 24,000 rpm.

The spin motor and its associated ball bearings are the subject of largest concern in any gyro design as they are the only parts that can wear out due to use. In order to test for ball bearing wear-out, two important parameters must be measured. These are the components of mass unbalance which lie along the gyro spin axis and along the input axis. From results of data analysis, a *Mariner-2*-type gyro design can be expected to survive and operate through a typical 6000-hr *Mariner C* mission.

The bearing and motor design used in the *Mariner 2* gyro is very similar to the present *Mariner C* Kearfott 2565 gyro. As an advance check of the *Mariner C* gyro, all units used in the prototype, proof test model, and TA gyro control assemblies have been operated in such a manner as to obtain as much spin motor running time as possible. A total of about 13,000 hr of spin motor time has been accumulated on a group of nine gyros without any spin motor problems to date. Over-all performance data for three *Mariner C* TA gyros indicated that all but one of these gyros showed satisfactory stability of torquer scale factor and reaction torque.

6. Narrow Angle Mars Gate

The narrow angle Mars gate (NAMG) is located on the planetary scan platform of the *Mariner C* spacecraft.

It provides an acquisition signal to the data acquisition system when Mars enters its field of view. This signal causes initiation of the science planetary encounter sequence.

During a normal encounter, the planetary platform scanning will have stopped and the wide-angle planet sensor will be causing the platform to track Mars at the time of NAMG acquisition signal occurs. If there is a malfunction in the planet sensor or if the miss distance is too great for proper tracking, the NAMG can still provide an acquisition signal as it scans across the planet. This will stop the scanning motion and hopefully permit the obtaining of a limited amount of planetary data.

Fig. 3 shows the exploded view of the assembled NAMG. The NAMG is cylindrical shaped, 4 in. long × 1 in. D with a mounting flange 1 in. from the back end. It weighs 0.16 lb and nominally consumes 20 mw.

The front 3 in. consist of a lens and a system of baffles which define the field of view and eliminate the effects of stray light. The baffling is effective enough to prevent interferences from the Sun if it is more than 22 deg off axis.

The rear 1 in. contains the welded electronic module, which consists of a trigger circuit activated by a cadmium sulfide photoconductive cell (Fig. 4). The photocell, trigger circuit, and external connection terminals are all integrated into the one welded module which is interchangeable between units. The components within the module have been selected to produce a uniform response from all modules.

The trigger level has been defined as equivalent to viewing Mars from a distance of 800,000 km. This provides an overdrive of about 50 times when viewing Mars

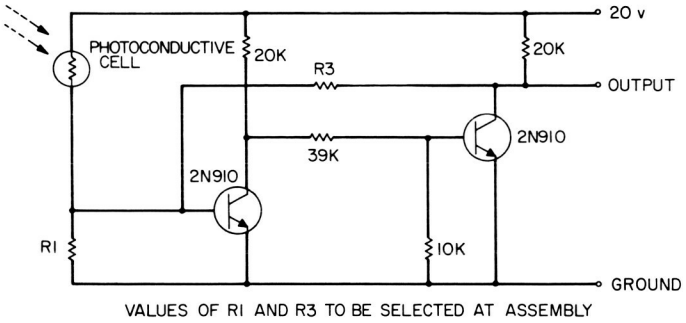

Fig. 4. Narrow angle Mars gate circuit diagram

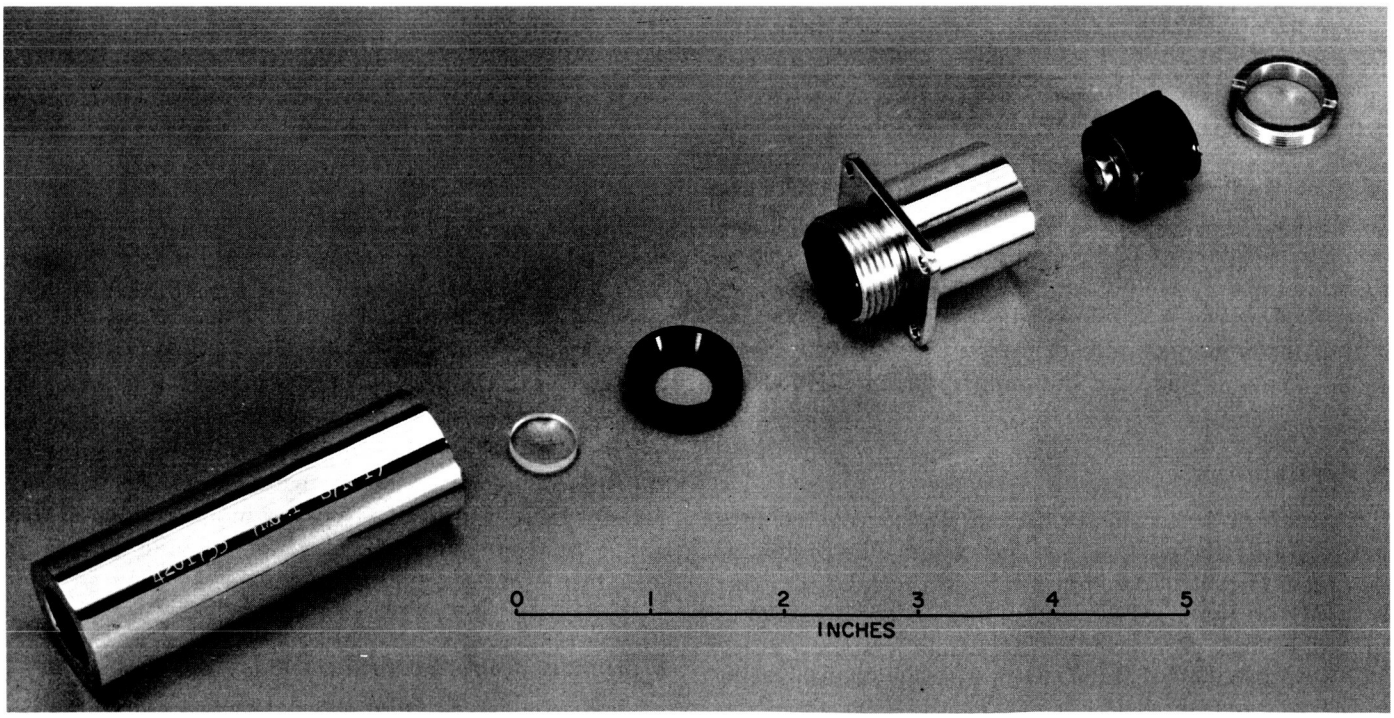

Fig. 3. Narrow angle Mars gate (exploded view)

from the nominal miss distance of 20,000 km. This level is also greater than 100 times the output of the cell when dark or when viewing the star background. The nominal encroachment on the Mars limb necessary to trigger the NAMG is 0.3 deg.

Figs. 5 and 6 show the encounter geometry for a typical trajectory. The NAMG field of view is 2.5 deg along the line of flight and 1.5 deg in the planetary platform scan direction. The center of this field of view is within 0.25 deg of being perpendicular to the NAMG mounting surface.

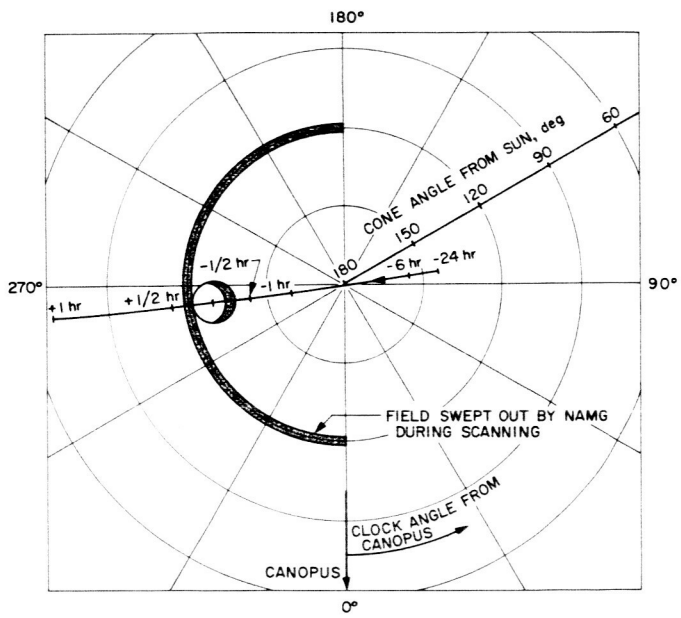

Fig. 5. Typical trajectory encounter geometry

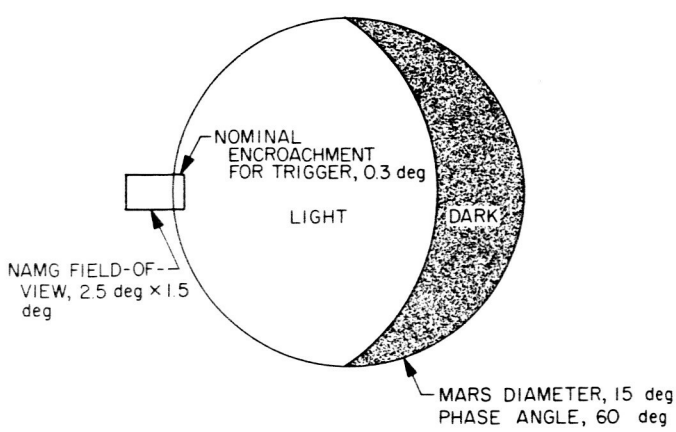

Fig. 6. Nominal encounter geometry

On board the spacecraft, the Sun shield which protects the science instruments also provides a light stimulus to permit verification of proper operation of the NAMG.

7. Postinjection Propulsion System

After assembly of the TA-1 propulsion system it was subjected to a series of modal tests. A typical test setup is shown in Fig. 7. This series of tests was concerned with determination of the structural resonant frequencies and the corresponding modes of vibration. Very good correlation was noted between the actual test data and the analysis upon which the structural design was based.

The TA-1 system was then subjected to a series of preliminary vibration tests to determine amplification factors at selected points on the structure. It was found that the first resonant frequency of the structure was at approximately 140 cps. At this resonant frequency, an amplification factor of five was measured at the center of gravity of the structure.

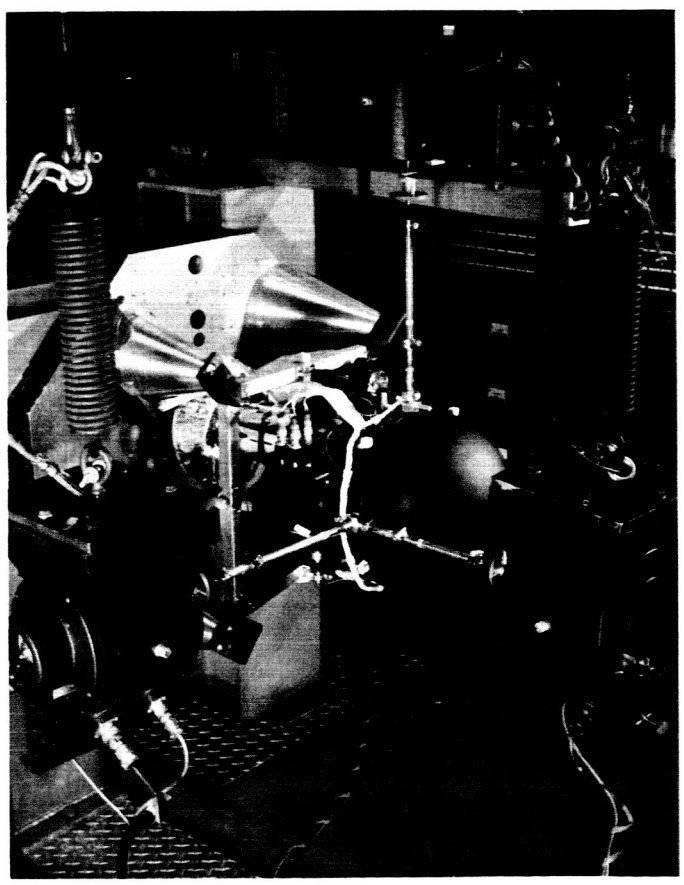

Fig. 7. Test setup for modal test of TA-1 propulsion system

The TA-1 system was installed in a shipping container, and subjected to the transportation and handling drop and vibration tests. The system was then subjected to the spaceflight shock and static acceleration tests. After each of these tests, a thorough leak check was performed with no leakage or other system failures being noted.

Testing of the TA-2 propulsion system consisted of conducting firings at various tank pressures so as to define system start transients and steady-state operation under a variety of starting conditions. Good results were obtained in these tests after a filter problem which caused a pressure regulator malfunction was solved.

THE DEEP SPACE INSTRUMENTATION FACILITY

IV. Introduction

The DSIF is a precision tracking and data acquisition network which is designed to track, command, and receive data from deep space probes. It utilizes large antennas, low-noise, phase-lock receiving systems, and high-power transmitters at stations positioned approximately 120 deg around the Earth. Its policy is to continuously conduct research and development of new components and systems and to engineer them into the DSIF so as to continually maintain a state-of-the-art capability.

The DSIF is comprised of three permanent deep space stations, one mobile station, and one launch station. The three permanent stations are located to provide continuous coverage of a deep space vehicle. Their locations are Goldstone (Pioneer and Echo), California; Woomera, Australia; and Johannesburg, South Africa. The Mobile Tracking Station (MTS) is presently located near the permanent station in South Africa and is used mainly for early acquisition, and tracking and communications with spacecraft from injection into orbit to an altitude of about 10,000 mi. The Launch Station is used to provide real-time telemetry during the spacecraft prelaunch tests and to record spacecraft transmitted telemetry data from launch to the end of the visibility period.

The testing and development engineering of new equipment for the DSIF are performed at the Goldstone Space Communications Stations. In most cases new equipment is installed and tested at Goldstone before it is integrated into the system. An 85- and a 30-ft Az–El antenna are installed at the Goldstone Venus site for primary use in research and development.

Section V of this Report, regarding the DSIF Program, is abstracted from *SPS 37-25*, Vol. III.

V. Communications Research, Development, and Facilities

A. Tracking Station Operations

1. Goldstone

In order to meet the *Ranger 6* video bandwidth requirements, unity gain 30-Mc isolation amplifiers were installed at the Echo and Pioneer Stations to feed data to the ground TV equipment and to the noise monitoring equipment. Similar modified equipment was sent to the overseas stations to feed the video recorders. A new quadripod (Fig. 1) and an equipment cage have been installed on the Goldstone Pioneer antenna.

2. Woomera

The Woomera Station successfully acquired, tracked, and received data from the *Atlas–Centaur* (AC-2) which was launched on November 27, 1963. Tracking operations lasted from 20:07 to 20:26 GMT. The AGC voltage exhibited a very predominant ripple at 0.67 cps. The Woomera Station accomplished this mission in addition to making preparations for tracking the Interplanetary Magnetic Probe (S-74) which was also launched on November 27, 1963.

B. Engineering Developments

1. S-Band Systems Engineering

Systems engineering has completed: drawings of antenna cage and equipment, control building floor layouts, S-band receiver and CDC compatibility tests, tests of commands generated in the CDC, plans for making a compatibility test with a *Surveyor* spacecraft, system performance tests with a *Ranger 6* PTM and a preliminary function description of the Ames/DSIF *Pioneer* Program.

Fig. 1. New quadripod on Pioneer site antenna

2. Computer Programs

a. Trajectory program for on-site computers. A spacecraft trajectory program has been developed for small size digital computers which is accurate enough to generate prediction data and antenna drive tapes. Position and velocity components at injection are used, and a variable step size numerical integration is used to improve accuracy and to reduce the computation time required.

b. Method of rejecting possible blunder points. Tracking data which is used in the orbit determination computer program has a tendency to be contaminated with what are known as "blunder points." To reduce the effect of these "points" a method of using auto regression smoothing is proposed, which is accomplished by differencing the sampled time series of tracking data with a predicted time series based on the trajectory's initial conditions. Preliminary tests indicate that there is merit to the proposal.

3. Mariner C 100-kw Transmitter

The 100-kw transmitter at the Venus site will be used in *Mariner C* operations when the spacecraft is on its way to Mars in 1965. In order to accomplish this at the operations frequency range of 2110 to 2120 Mc, a complete Cassegrain cone with two klystron amplifiers (one for redundancy) and switching capabilities will be constructed. This will be done on a fixed price basis because of the availability of complete documentation.

C. Research and Development

1. Ground Antennas

a. Boresight calibrations for DSIF antennas. Several techniques for boresighting DSIF ground antennas using radio star sources have been developed. One of these methods uses an ephemeris angle drive tape to drive the antenna to the source location and angular offsets to steer the antenna exactly on course. The offsets required determine the boresight error. Using this method on the 85-ft Venus antenna, a 0.035-deg peak-to-peak cyclic error was discovered which was corrected by replacing the elevation angle encoder.

b. Antenna instrumentation. An automatic typewriter (Flexowriter) has been added to the transportable antenna instrumentation system to permit simultaneous line printing of scanned data, the punching of a paper tape, and the later verification of punched data. The system will be used to make additional measurements on the 85-ft Venus antenna and also to check the 210-ft antenna when it is erected.

c. Radio frequency interference tests. Although fluorescent lighting fixtures have several advantages, they have not been used in DSIF Stations because of the danger of potential RF interference. A new unit with RF shielding has been tested and was found not to increase the noise temperature by more than 0.02°K when illuminating an isotropic side lobe at a distance of 50 ft.

Similarly, a dc tachometer was tested and no noticeable interference was noted. It is estimated that it would cause a maximum of 0.1°K increase in noise temperature in an operational situation.

d. 30-ft antenna reflector calculations. Recent structural deflection measurements which were made on the Venus 30-ft antenna have made it posible to check the STAIR Computer Program which is being used in the design of the 210-ft antenna. When the computed

deflection values were compared to the actual measurements, the results were considered to be within reasonable tolerance except for one joint. This is being investigated.

e. 85-ft antenna, reflector resurfacing. A new reflector surface has been installed on the 85-ft antenna at the Goldstone Venus site and has been measured to have 0.4-db more gain than the old surface.

An improvement installed with the new surface was the use of new panel mounting assemblies which were specially designed to minimize temperature effects, to allow adjustments from the front of the panel, and normal to the reflector surface.

2. Planetary Radar Project

a. Water rotary joint for Az–El antenna. Continued surveillance of the water rotary joint installed in the 85-ft antenna at the Goldstone Venus site indicates that the carbon seals are satisfactorily wearing in.

b. High-power transmitter. The series limiter for the 100-kw klystron at the Goldstone Venus site is a water cooled triode, operated as a diode, which uses an emission limited cathode. Limiting is controlled by varying the filament voltage. A new klystron filament supply has been designed and built. This includes a new solid-state rectifier assembly, protective diodes, and a filter choke. A lightweight, sensitive, shielded unit for measuring incidental phase modulation has been built and tested.

c. Mod IV planetary radar receiver—a note on reliability. The Mod IV planetary radar receiver has operated for more than 7400 hr without a tube failure. This is attributed to a 100-hr tube aging test made prior to use in the receiver and the reduction of plate voltage from 150 to 120 v. The receiver is also more stable and drift free.

d. Nine-channel autocorrelator. A nine-channel autocorrelator is being built which will resolve the received planetary radar signal into nine separate and adjacent geographical zones, detect the power in each zone's signal using bandwidths from 25 to 400 cps, accumulate 50 autocorrelation points for each signal and feed the data to a stored program computer for control, integration, recording, and display. The nine channels are obtained by modulating the transmitted signal with a pseudonoise (PN) code and demodulating the received signal with nine separate demodulators, which are fed with the same PN code, each displaced in phase by 1 code bit.

e. Central frequency synthesizer. A central frequency synthesizer is planned for use at the Venus site to supply all the coherent reference frequencies for the receiver–transmitter systems at both the 85- and 30-ft antennas. By consolidating all the equipment, considerable reduction is possible. Improvements will be made in some cases in that all reference frequencies will be coherent.

3. Lunar Radar Project

a. A range-gated lunar radar experiment. In a previous *SPS* (*37-23*, Vol. III), a proposed method of making radar experiments on the Moon was discussed. This system has been implemented and used with satisfactory results. A PN code modulation of the carrier (length 16,383) was used, running at a 1-Mc digit rate. Correlation of the return signal, using a fixed delay between the transmit and receive coders, provided a measurement of a range-gate increment of 150 m. System temperatures are considerably degraded at low elevation angles. Range calibrations using the collimation tower agree within the system uncertainty. Actual measurements on the Moon revealed lunar ephemeris inaccuracies which are being corrected. Data on lunar surface characteristics is now being reduced.

b. Lunar radar range measurements. Preliminary results from the lunar radar measurements indicate that the observed response curves may be a powerful means of studying the lunar topography over regions of 45-km sizes, and will require a major research effort to improve the lunar ephemeris for the purposes of calculating significant astronomical constants from radar observations.

4. Ranging and Tracking System Development

a. Monostatic radar operating parameters. Preliminary test results of the anti-sideband system coupled with the effects of target dynamics (discussed in *SPS 37-24*, Vol. III) have pointed up several areas of compromise in the selection of receiver loop bandwidth, keying rate, and predetection bandwidth. Inherent in the problem are the uncertainties of prediction of range and range rate at the time of satellite acquisition.

b. Monostatic satellite and lunar radar transmitter. The 10-kw transmitter, which will be used on the 30-ft antenna at the Venus site, will have improved directional couplers to reduce the uncertainty of back power measurements, a photo diode arc detector near the klystron

window with a 5-μsec response time instead of several milliseconds, new power meters that are linear and not temperature sensitive, a waveguide switch to eliminate the necessity of manually connecting the transmitter to the antenna feed on the water load, and water flow gages. All are expected to improve reliability.

5. S-Band Implementation for DSIF

a. TWM for DSIF. The closed cycle refrigerators (CCR) for two traveling wave masers (TWM) have been received and tested. The compressor unit has been repackaged and is more compact than the old version. Two TWM units are nearly complete.

b. Acquisition aid for DSIF. The S-band acquisition aid antenna will use the basic 85-ft S-band feed horn as an antenna and will have its own angle tracking channels in the receiver. An erectile, close-in collimation tower is being designed to provide a rapid multipath free means for phasing and collimating the acquisition antenna.

c. DSIF microwave switch control assembly. In order to rapidly and safely control the various microwave switches in the S-band system, an automatic control system has been developed. Logic circuits are used to interlock the controls so specific modes of operation may be switched without endangering equipment or personnel.

D. Advanced Antenna System

1. Synopsis

At the Mars site, excavations for the antenna pedestal and the instrument tower have been completed, and placement of forms and reinforcing steel for pouring of concrete is in process. The outside diameter of the pedestal is 88 ft, 8 in. and that of the tower is 26 ft. The foundation depths are 11 and 35 ft, respectively. A 5-mi road 24½ ft wide has been completed, and erection of the 315-ft-high guyed derrick is in progress. Preliminary design and engineering analysis of the antenna is nearly completed. Progress as of November 8, 1963 is shown in Fig. 2.

Fig. 2. Mars site progress as of November 8, 1963

OPERATIONAL AND TEST FACILITIES

VI. Test and Support Equipment

A. Environmental Test Laboratory

1. Thermal-Vacuum Testing

a. Heat exchangers. Fluid-type heat exchanger units were used for testing *Ranger* Block III assemblies which mount in cases on the spacecraft bus. The heat exchangers are used to insure a uniform temperature on the surfaces of the test components. Cold or hot nitrogen gas may be circulated through the heat exchanger copper tubing to attain temperature control at desired levels. These heat exchangers satisfy the requirements detailed in JPL *Ranger* Block III type-approval, (30277) and flight-acceptance (30278) environmental specifications.

During this reporting period the heat exchangers were used by JPL and its subcontractors on the *Ranger* Block III test program with satisfactory results. Fig. 1 is a typical heat exchanger controller test temperature curve with the corresponding temperatures, as measured by thermocouples mounted on the test specimen and various heat exchanger surfaces.

An upgrading program was initiated in December, at which time two heat exchangers were supplied with stainless-steel micro-adjusting fasteners in place of the existing steel clamps (Fig. 2). The micro-adjusting fasteners (which will be incorporated into all units) simplify assembly of components in the heat exchanger and provide a careful means of ensuring adequate contact between the test specimen and the heat exchanger.

b. Miniature ionization gages. To meet an increasing need for accurate vacuum measurements in restricted volumes inside spacecraft and other systems being tested in vacuum chambers, miniature ionization gages (GE gage 22-GT-102) have been recently developed. The new portable miniature gage is 2½ in. long with a 1 in. D, as compared to a standard Veeco ionization gage, which is 6 in. long with a 2¼-in. D. Because of its small size, the gage may be installed anywhere inside the vacuum chamber in any desired position. Another of its features is a low filament power dissipation. The maximum dissipation is 4.3 w, as contrasted to a maximum possible dissipation of more than 20 w in a Veeco gage. This reduces chances of upsetting a critical thermal equilibrium or overheating components near the gage.

The controls are similar to those used for standard gages. A switch on the controls allows the introduction of either a tungsten or a thoriated iridium filament into

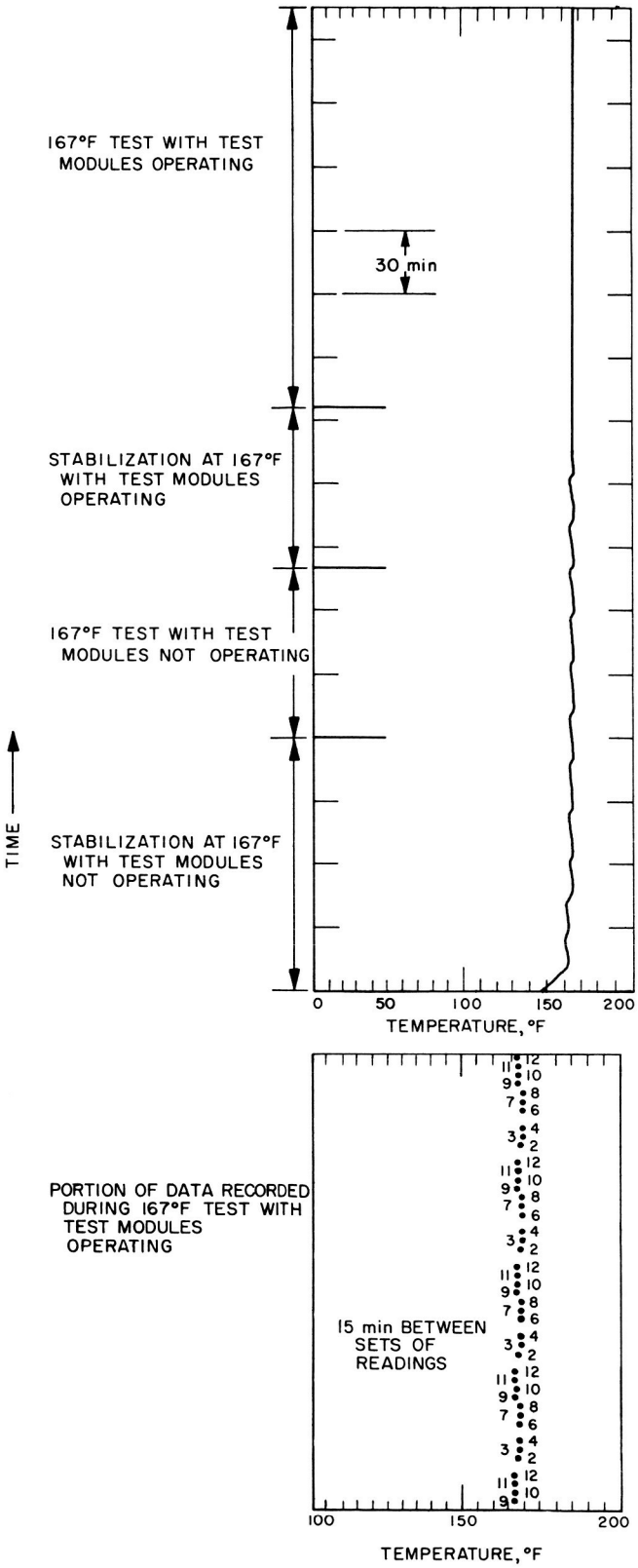

Fig. 1. Typical curve obtained during thermal-vacuum testing with new fluid-type heat exchangers

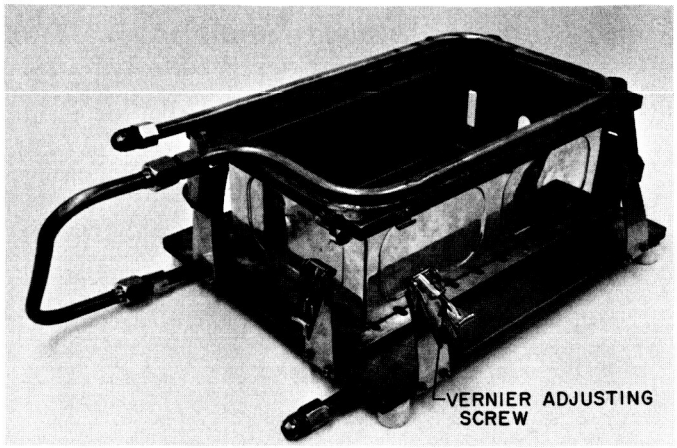

Fig. 2. New heat exchanger with micro-adjusting fasteners

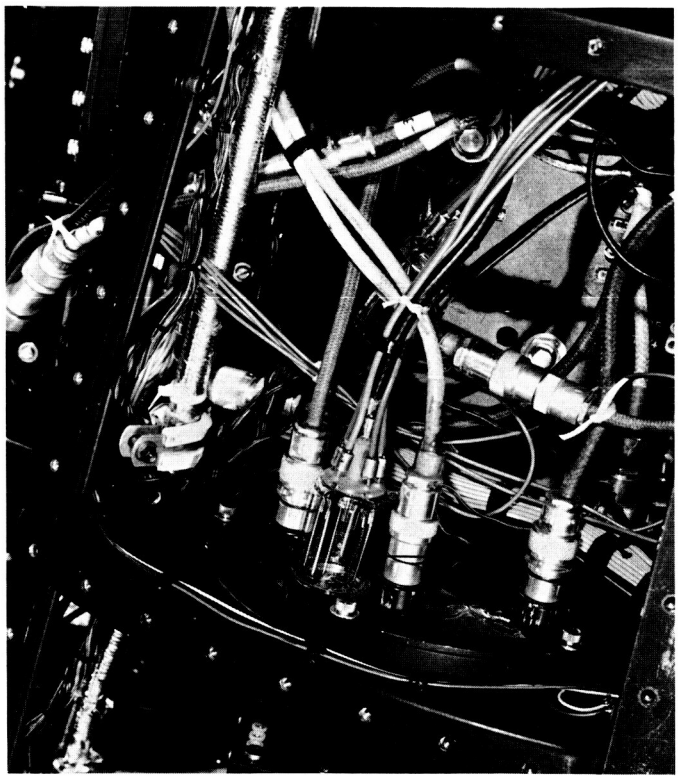

Fig. 3. Miniature ionization gages inside TV tower of *Ranger* proof test model

the circuit, even while under vacuum. The thoriated iridium filament must be used when measuring pressures from 250μ to 10^{-3} torr, while either filament may be used from 10^{-3} to 10^{-10} torr. The tungsten filament is preferred at high vacuum conditions when high emission currents are desired, such as those required for outgassing. If one filament burns out during a test, the other

filament may be substituted without aborting the test. Special cables consisting only of materials which have low outgassing and low contaminative properties have been made for internal use in the vacuum chamber. Outgassing of the gage is normally accomplished by electron bombardment while under vacuum.

Gage applications are being developed in the Environmental Test Laboratory (ETL). Fig. 3 shows two gages installed on and near the four-port hybrid located in the *Ranger* Block III proof test model TV tower. These internal spacecraft pressures are compared to the chamber pressure (as measured at the chamber wall) in Fig. 4. This chart is from a test performed in the 7- × 14-ft chamber in JPL Building 144. Another use of the gages would be to determine the pressure profile in a vacuum chamber under different test conditions so that the spacecraft or test environment can be more accurately known.

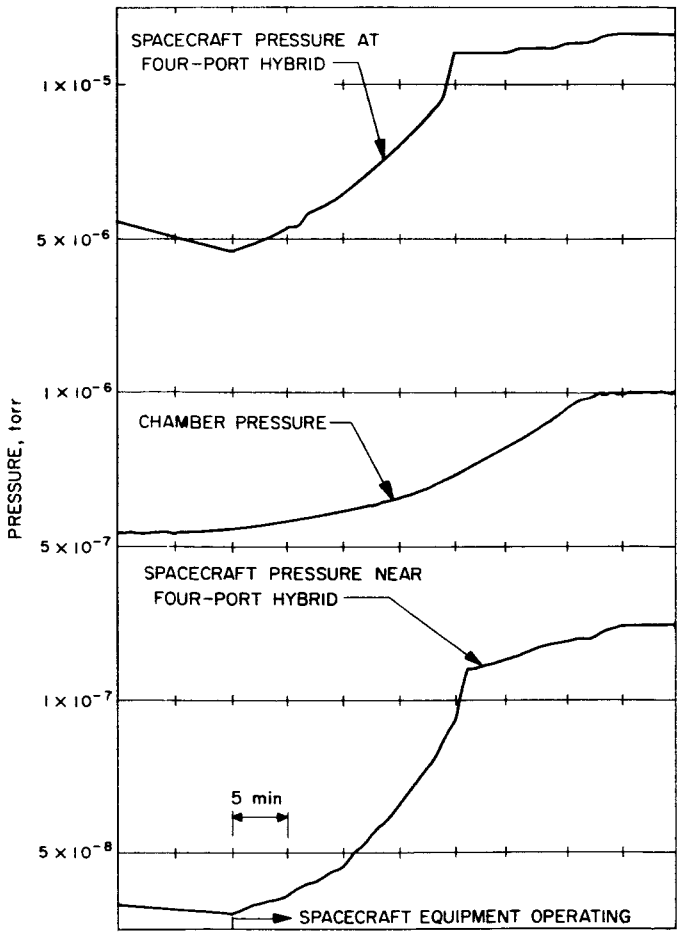

Fig. 4. Comparison of internal spacecraft pressures and vacuum chamber pressure

Currently available in the ETL are 3 gage controls and 4 gages, and 16 more gages have been ordered. Not enough experience has been gained on these new devices to determine meaningful failure-rate information.

2. *25-ft Space Simulator*

A test was made to determine the electrical performance of the *Ranger* Mark IV solar panel and to examine its temperature distribution. The present solar simulation system uses mercury-xenon arc lamps and is, therefore, deficient in energy at the wavelengths to which the solar panel responds electrically. Consequently, it was necessary to determine the electrical performance of the panel at a total energy input somewhat above an Earth constant. To eliminate this experimental problem in the future, some of the mercury-xenon lamps will be replaced with xenon lamps so that it will be possible to closely approximate the spectrum of the Sun. The temperature distribution was determined for several total energy inputs centered around one Earth constant. Test conditions were: vacuum, 2×10^{-6} torr; wall temperature, $-270°F$. The test duration was 7 days.

B. Operational Support Equipment

1. *Mariner C Central Computer and Sequencer Simulator*

The central computer and sequencer (CC&S) simulator is a portable test instrument capable of functionally qualifying the *Mariner C* CC&S system test set (STS). This simulator was designed to satisfy the need for a portable test instrument to be used at three primary program test areas. First, in the operational support equipment (OSE) fabrication, the simulator is used to assist in qualifying every OSE interface at either the connector inputs to the OSE or at the spacecraft end points of all OSE cabling. In addition, the simulator is used to automatically cycle the STS on a continuous basis, thus allowing an adequate number of operational hours to be accumulated by the STS prior to its use with an actual CC&S. Second, in spacecraft test operations, the simulator is used to assist in verifying the operational readiness of a CC&S system test set prior to its participation in any test operation. Third, at the Kennedy Space

Center prior to all launch complex spacecraft test operations, the simulator is used to assist in qualifying all CC&S umbilical signal lines.

The CC&S simulator is packaged in an all-weather aluminum industrial carrying case and weighs approximately 37 lb. All connectors, controls, and meters are located internally for maximum protection within one-half of the unit. The other half of the case is an enclosed accessory compartment. Both halves of the test unit, once opened, can be separated (Fig. 5). This results in easier handling of the test instrument. The simulator may be operated in any position without degradation of meter indications. The simulator is normally powered from the CC&S system test set, but when necessary the simulator may be used remotely from the STS by utilizing internal plug-in power supplies furnished as accessory hardware with each simulator. The weight of the simulator is increased by approximately 10 lb when using the plug-in power supplies. There must be a source of 115 v ac, 60 cps power at the remote location.

Accompanying each simulator is a cable carrier (Fig. 6) that insures protection against damage to test cables during transportation. This carrier is a case of the same size and material characteristics as that for the simulator. The total weight of the carrier and cables is 45 lb. Both halves of the case are enclosed cable compartments that cannot be separated when opened.

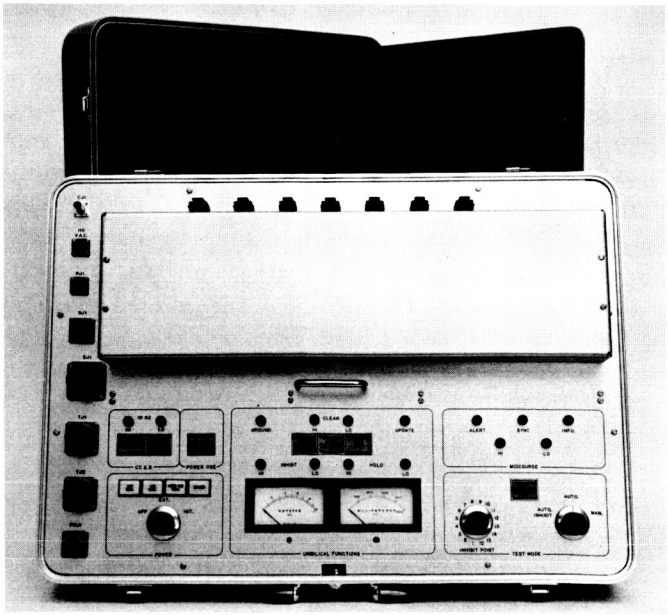

Fig. 5. CC&S simulator control panel

Fig. 6. CC&S simulator cable carrier compartments

2. Ranger *Attitude-Control Operational Support Equipment*

The *Ranger* attitude-control operational support equipment (OSE) consists of the systems test set (STS), the launch complex set (LCS), and the laboratory test set (LTS). During systems testing, various stimulus generators and readout devices are used to provide the interface between the OSE and the spacecraft. The LTS simulates all the interfaces between the attitude-control system case and the rest of the spacecraft.

Both the system and subsystem tests may be broken down into the following five phases:

(1) *Prelaunch.* The counter for the preset antenna angle is tested and the gyro loops are monitored to assure that the loops are closed and that the gain is correct.

(2) *Sun acquisition.* The Sun sensor phasing is tested and the pitch and yaw switching amplifier characteristics are measured.

(3) *Earth acquisition.* This is divided into two subphases:

(a) *Hinge.* The phasing of the hinge circuitry is monitored, the hysteresis and deadband of the hinge switching amplifier are determined, and the hinge preset angles are checked.

(b) *Roll.* The roll phasing is tested and the roll switching amplifier deadband is determined.

(4) *Midcourse maneuver.* The gyro loop response is tested and the frequency of the accelerometer pulses is counted and is correlated to the acceleration of Earth's gravity.

(5) *Terminal maneuver.* Tested in the same manner as the midcourse maneuver.

The STS is required to completely test and evaluate the attitude-control system. This set (Figs. 7 and 8) is used in integrated spacecraft systems tests in conjunction with the attitude-control spacecraft system interfaces.

The LCS uses a portion of the system test set to monitor the gyro loops. The inputs to the LCS are the pitch, yaw, and roll gyro rebalance amplifier outputs. These voltages are used to determine the gyro loop gain and to monitor the gyro loop closure.

In addition to the test points used by the STS, the LTS provides the following functions:

(1) *Power.* Provides the 31-v dc primary power and the 800-pps trigger for the inverters.

(2) *Central computer and sequencer (CC&S).* Simulates the CC&S inputs to the attitude-control system by means of switches.

(3) *Command subsystem.* Simulates the command subsystem inputs to the attitude-control system by switches.

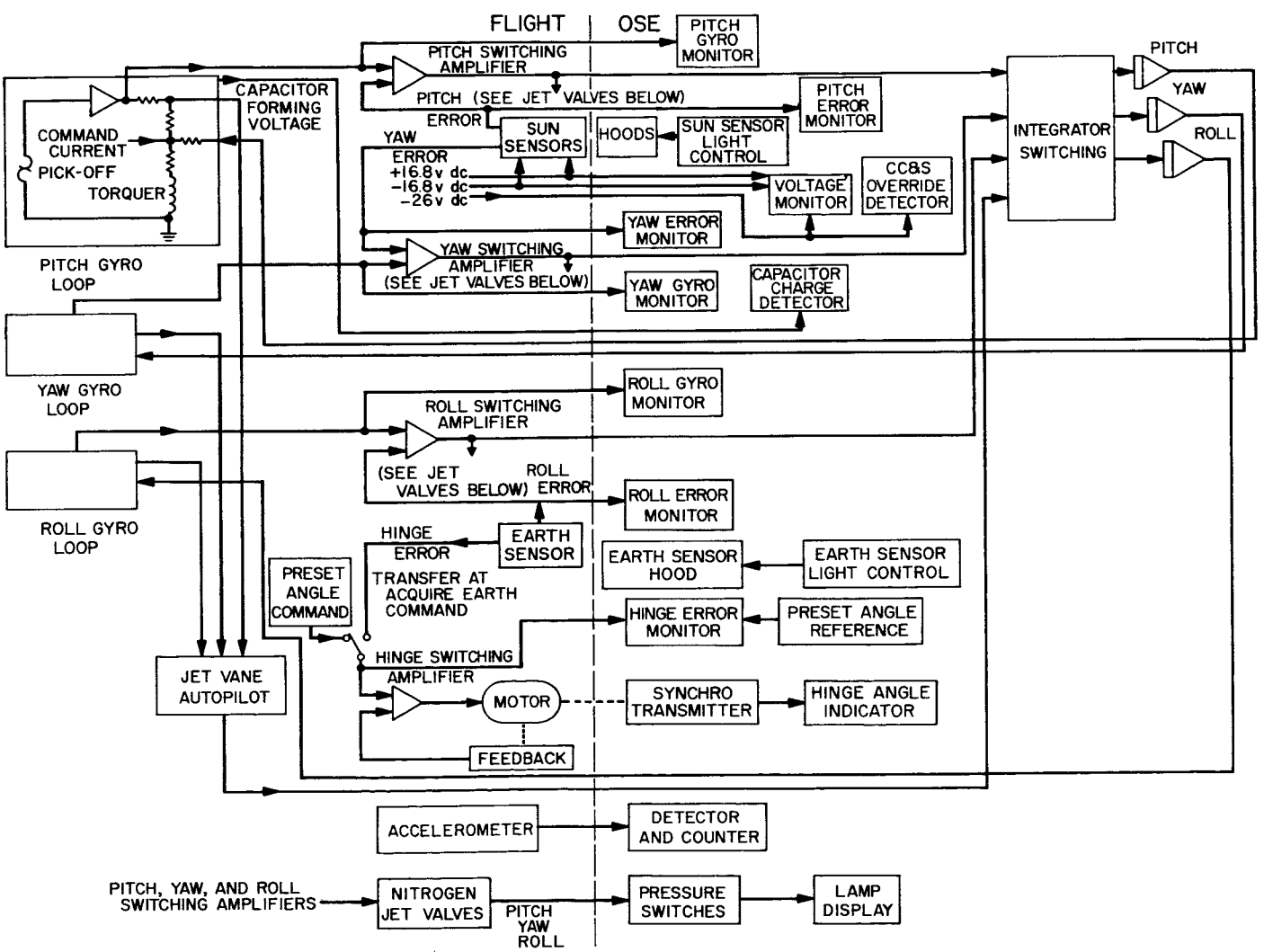

Fig. 7. Block diagram of the attitude-control system test set

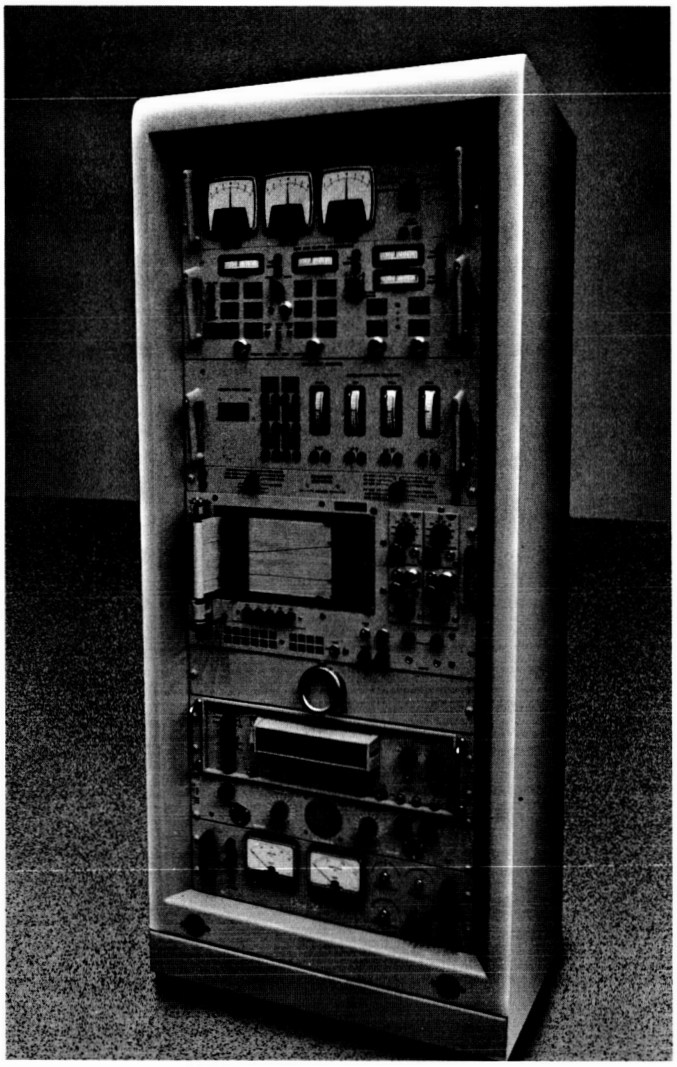

Fig. 8. Attitude-control system test set

(4) *Attitude-control system components.* Duplicates by nonflight hardware the system components which are not mounted within the attitude-control system case. These include the Earth sensor, Sun sensors, gas system, and antenna drive.

3. Mariner C *Attitude-Control Operational Support Equipment*

Among the new capabilities that have been incorporated in the *Mariner C* attitude-control operational support equipment (OSE) to monitor new subsystems are the solar vane monitors and the gyro rebalance loop.

a. Solar vane OSE. A block diagram of the monitoring circuitry for the solar vane system is shown in Fig. 9.

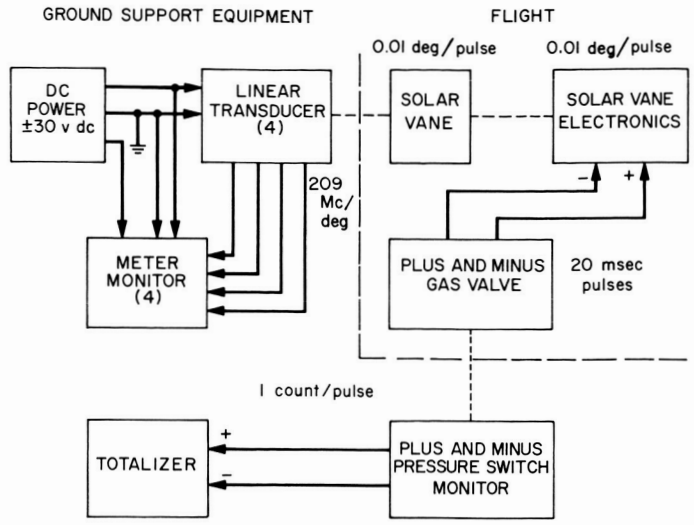

Fig. 9. Solar vane monitor system

A brief description of its operation and monitoring technique follows: The attitude control switching amplifier is forced to switch, at a rate no greater than 1 pulse per second (pps), by injecting an error signal slightly larger than the dead-band switch point through control of the illumination of the cruise Sun sensors and using the derived rate feedback as the shutoff signal. The solar vane electronics will force the solar vane to step +0.01 deg for every pulse from a counterclockwise (CCW) gas jet. A pulse from a clockwise (CW) gas jet will result in a −0.01-deg step. Monitoring of this action is accomplished by totalizing the number of CW and CCW gas jet actuations algebraically until a count of 100 is registered. At this time, the switching amplifier forcing function is removed, and the solar vane net movement is read on the solar vane meter monitors. Since 100 pulses were monitored, a difference of 1 deg should be noted on the solar vane meters.

b. Gyro rebalance OSE. Comprehensive analysis of the rate and position gyro system is accomplished by employing a dynamic rebalance loop in the system test set (STS). This rebalance loop simulates the dynamics of the spacecraft. With this capability, the gyros are less susceptible to damage, and long duration turns become attainable. A block diagram of this system and a typical curve of the gyro rebalance amplifier output voltage versus time for error rates and commanded turns are shown in Figs. 10, 11, and 12, respectively.

The operation of the gyro rebalance loop during spacecraft error rates follows: As the gyro senses an error rate,

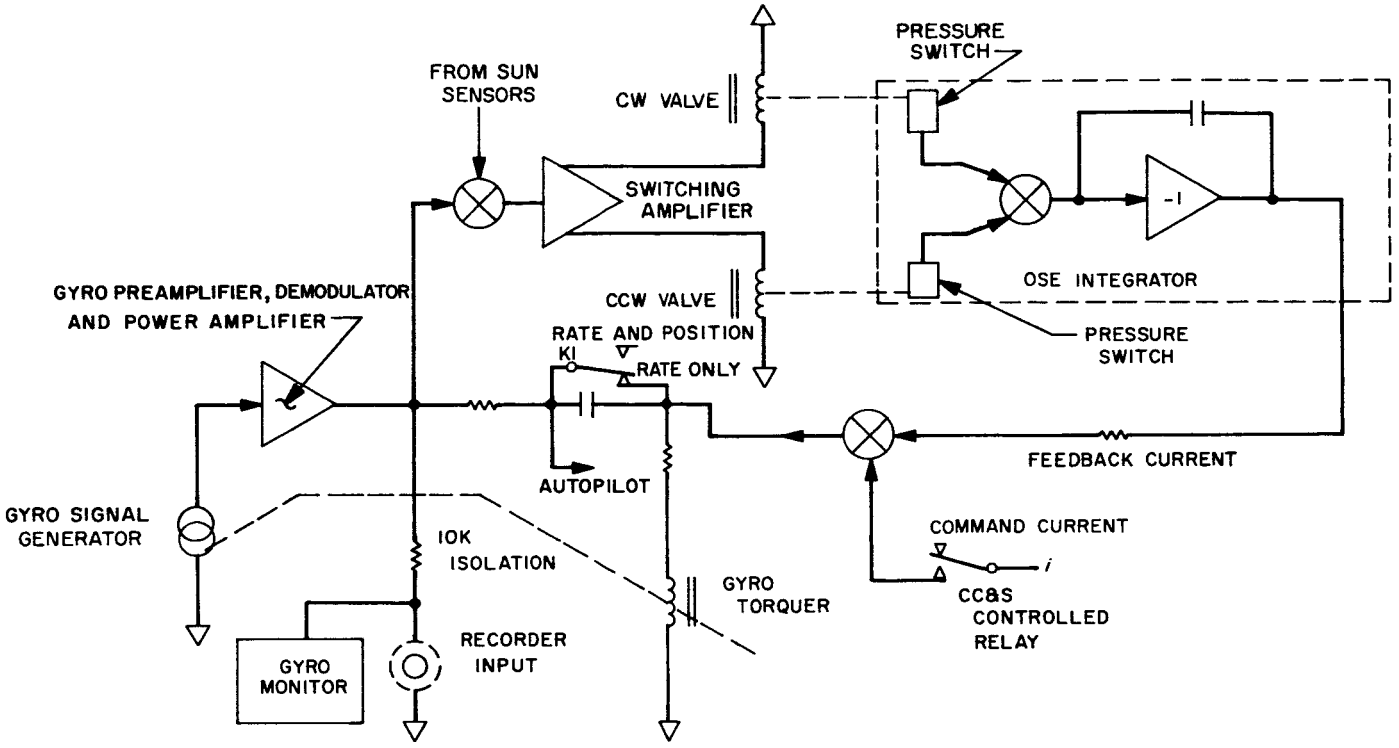

Fig. 10. Typical command turn monitor

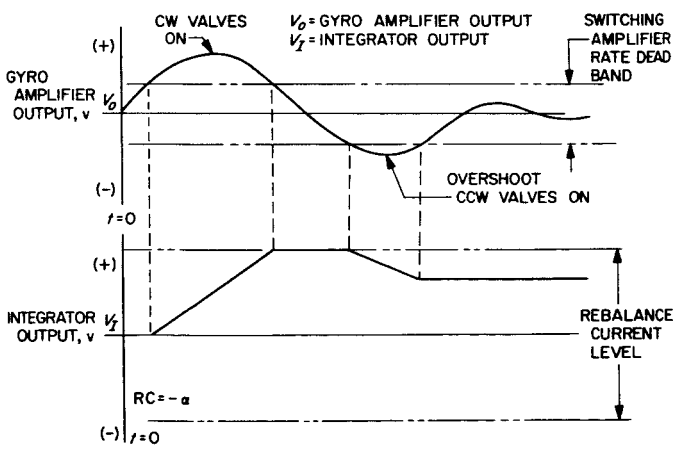

Fig. 11. Plot of gyro amplifier and OSE integrator output versus time for a constant CCW spacecraft error rate

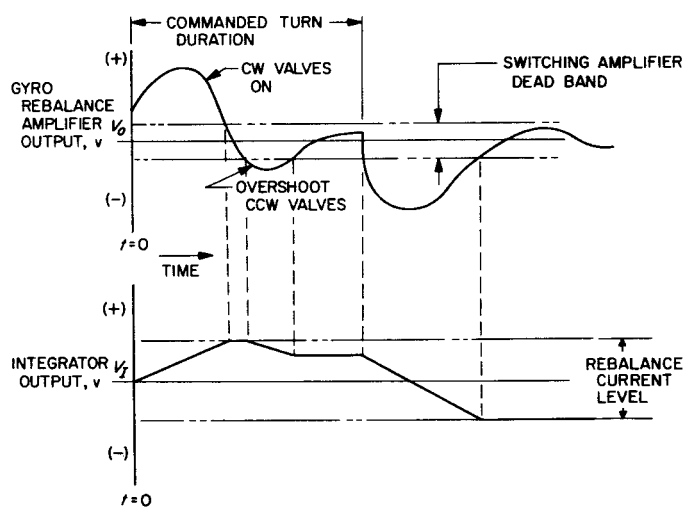

Fig. 12. Anticipated gyro output for commanded turns

an out-of-phase voltage will appear at the gyro power amplifier output, e.g., a plus voltage for a CCW error rate. The voltage amplitude is directly proportional to the error rate, and will exceed the switching amplifier (SA) rate threshold at approximately 0.02 deg/sec in the roll channel and 0.07 deg/sec in the pitch and yaw channels.

If a CCW error rate occurs, operation of this system would be as follows: Exceeding the switching amplifier rate threshold will activate a CW valve; the OSE pressure switch senses nitrogen flow and applies an integrator input which is in phase with the gyro amplifier output. This input is integrated according to a spacecraft acceleration (deceleration in this case) constant and supplies

a torquer current (rebalance current) which is out of phase with the gyro amplifier torquer current. As torquer current is reduced to the value corresponding to the switching amplifier lower rate threshold limit, the CW valve turns off and grounds the integrator input. The gyro amplifier output will remain at the switching amplifier lower rate threshold limit for a constant error rate and/or until integrator decay of sufficient magnitude occurs that will reduce the torquer rebalance current.

This cycle will continue until spacecraft motion is stopped. Any change in the direction of rate will reverse this sequence. Fig. 11 shows the relationship between gyro amplifier output and integrator output versus time, and Fig. 10 shows the rate gyro loop when the command current equals zero.

During commanded turns the operation sequence is basically the same, with the exceptions that the current to be balanced out is the turn command current initiated by the Central Computer and Sequencer (CC&S), and a position storage capacitor is inserted in the gyro loop. Fig. 10 would show the command gyro loop if Relay K1 is open and command current i equals the commanded turn current from CC&S. Fig. 12 shows the relationship between gyro amplifier output and integrator output versus time.

A brief description of the commanded turn rebalance operation follows: Command current i is injected into the gyro torquer, causing the gyro gimbal to take an initial offset. The offset is balanced by a gyro amplifier output within several milliseconds, shown by the step function at $t = 0$ in Fig. 12. This "step" function surpasses the switching amplifier rate dead band upper threshold and actuates a gas valve. The integrator rebalance action is identical to that of the rate mode when the valve is actuated and is shown in Fig. 12 as gyro amplifier output versus time. When the command current i is removed, the cycle reverses as shown in Fig. 12.

The integrators will balance the three gyro loops and hold the gyro gimbal system at a relatively constant position thus reducing the chances of possible damage to the gyro from such things as sudden disturbances to the spacecraft while the gyro loop is saturated.

4. Space Sciences Operational Support Equipment

The following is a description of some of the equipment being used in the checkout of the *Mariner C* science subsystem. These instruments have already been used in the subsystem checkout (Ref. 1) conducted in the Space Science Building and will be used in subsequent checkouts and tests conducted by the *Mariner C* Project.

a. Count rate accumulator and ion chamber interval counter. The count rate accumulator (CRA) and ion chamber interval counter (ICIC) (Fig. 13g), although built on two separate chassis, function as a single unit. The CRA contains buffer counters for the trapped radiation detector and the ICIC contains dual interval counters for measuring the period between ion chamber pulses and a counter display which is capable of selecting any of the inputs to either chassis.

The CRA accepts six data inputs; four of the inputs are commutated between two counters and the remaining two inputs are connected to separate counters continuously. The two separate counters have the capability of either being reset after readout (destruct) or accumulating input pulses (nondestruct).

The timing, commutation and print command portion of the CRA is shown in Fig. 14, Section 1. The timing section requires 10 pps and 1 ppm as the basic time references. The 1 ppm is used as the period over which all counters are allowed to count. The 10 pps is used to generate 200-msec pulses that are used for print commands.

The four counters are five-decade binary-coded-decimal (1-2-4-8) and are shown in Section 2 of Fig. 14. Counters 3 and 4 have commutated inputs and are reset at the end of each readout cycle. Counters 1 and 2 are not commutated and have switches (SW_1 and SW_2) in their reset lines so that either counter may be in a destruct or nondestruct mode.

The transfer and readout portion of the CRA is shown in Section 3 of Fig. 14. Only one transfer and readout gate is shown for each counter for the purpose of illustration. Transfer gates are connected to the outputs of each decade and only one set of transfer gates may be activated at one time. The data is transferred through the transfer gates, through an *or* gate and then through an output gate to the data printer.

The operation of the CRA is as follows: Assume that all counters have been operating for some period of time and it is time for the 1-min pulse (readout). When the

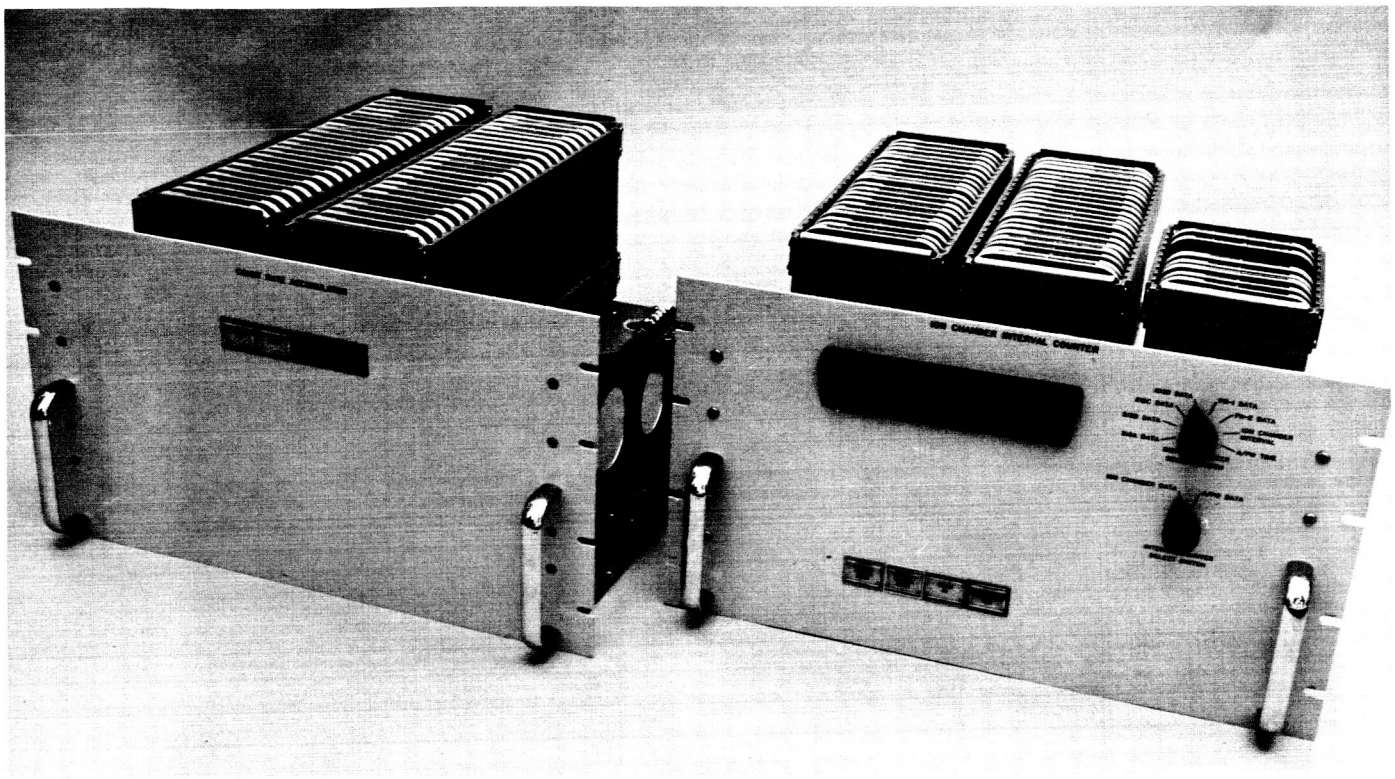

Fig. 13. Count rate accumulator and ion chamber interval counter

pulse occurs flip-flop (F/F) 1 is set, which enables one-half of the *and* gate input to the 8-bit counter, and disables the data inputs to all counters. The other half of the *and* gate has pulses occurring at 200-msec intervals which can now be entered into the counter.

As the first pulse enters the counter, it is detected by the transfer *and* gates and a transfer level is produced for Counter 1. When the second pulse enters the counter, Transfer 2 is generated. Transfers 3 and 4 are generated by the third and fourth pulses entering the counter. When Transfer 4 is generated a delay one-shot is activated; at the end of this delay a pulse is generated that resets all counters.

The pulses that enter the 8-bit counter are used as the print command signals after being conditioned by a one-shot. F/F 2 is the commutation F/F and alternates every one minute to enable or disable the four data input lines to Counters 3 and 4, thus allowing Inputs 3 and 5 or Inputs 4 and 6 to be counted at the same time.

The ion chamber interval counter (Fig. 15) contains two buffer counters, commutation, print command and reset circuitry, and a six-decade display counter which can display the CRA data pulses, the time between ion chamber pulses or analog-to-pulse width conversion time (Ref. 2).

The interval counter operates as follows: when each ion chamber pulse is received, F/F 1 alternates. The state of this flip-flop determines which counter (A or B) is activated. Assuming that a pulse had just occurred and Counter A was activated by this pulse, the reference frequency of 100 pps is allowed to enter Counter A. When the next data pulse is received, F/F 1 toggles and enables Counter B to count the 100 pps. At the same time that F/F 1 toggles, a print command is generated and the number of counts contained in Counter A is transferred to a data printer and Counter A is reset. Since 100 pps is used as the frequency reference, the counters contain the period between ion chamber pulses to a resolution of 10 msec. The state of F/F 1 is used to select the data to be printed.

The ion chamber data pulses may be replaced by the analog-to-pulse width, (A/PW), start and stop pulses as the input to the interval counter. When the A/PW data are used as the input the reference frequency is changed

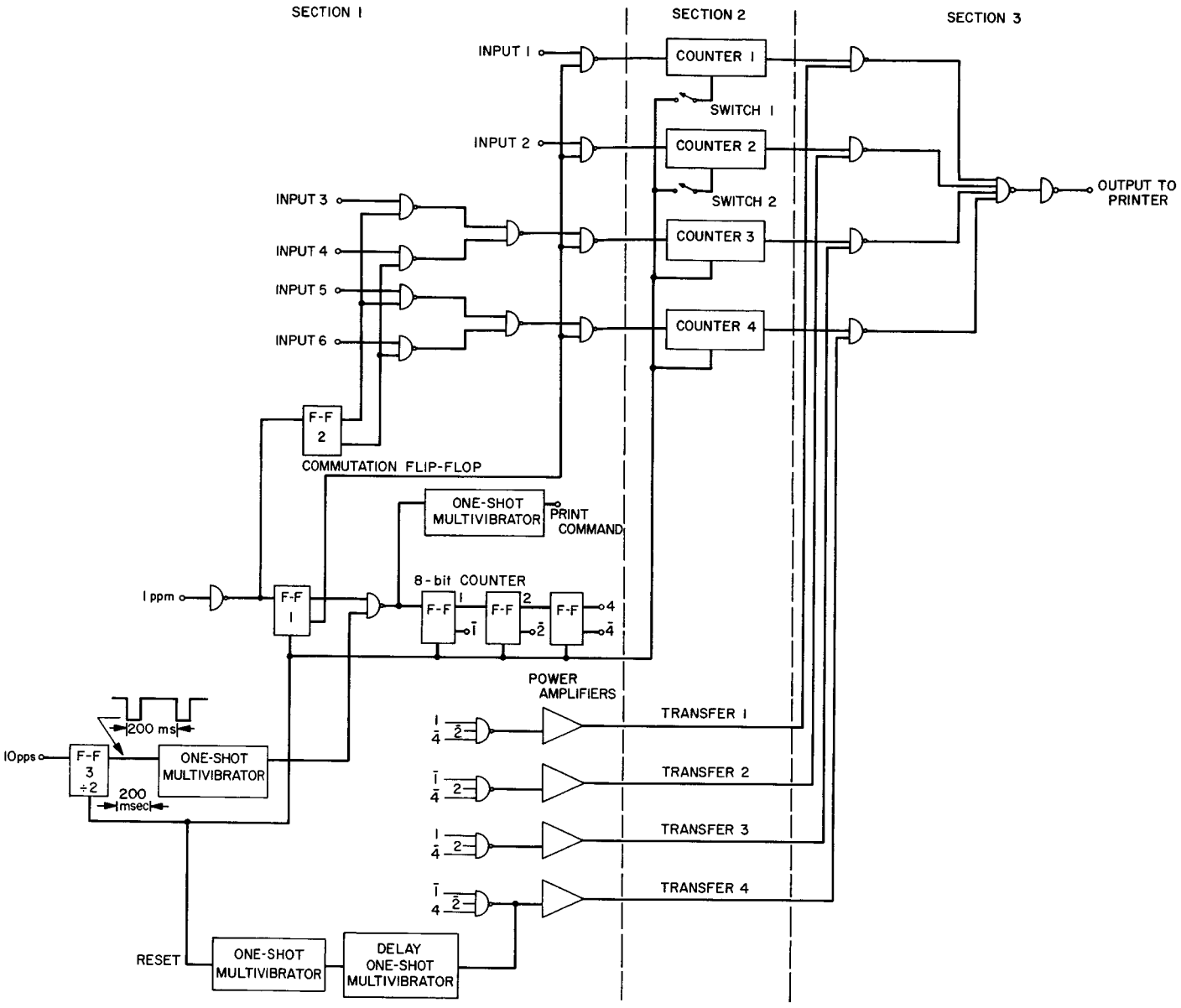

Fig. 14. Count rate accumulator block diagram

from 100 pps to 100 kc, thus allowing a resolution of 1/100 kc or 10 msec.

The display portion of the interval counter consists of a six-decade binary coded decimal (BCD) counter, BCD to decimal converters, and a decimal display. The input to the display counter can be switched to any of the six data lines from the CRA, and these data pulses will be displayed as they are received.

When the display counter is used to display the time between ion chamber pulses or the A/PW conversion time, the display counter input is switched to the reference frequency, and the decimal display is the time interval between pulses, in seconds.

The display counter reset is switched as the data input lines are selected. If the data from a counter that is in destruct mode are selected, the display counter is reset at the end of the print cycle whereas if a nondestruct counter is selected, the display counter is not reset. If the A/PW input is selected, there is no automatic reset, and the counter must be manually reset.

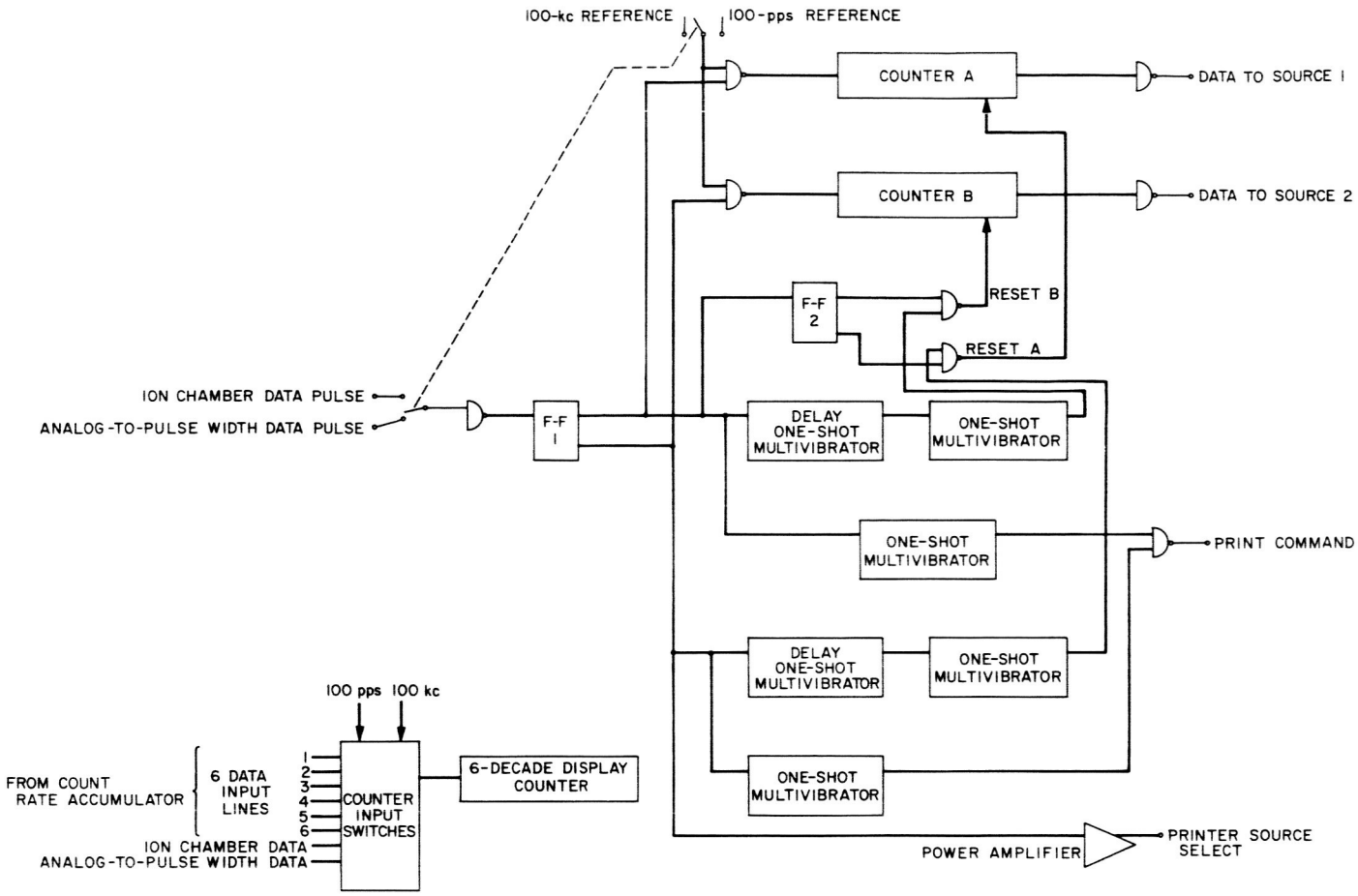

Fig. 15. Ion chamber interval counter block diagram

b. Real-time data translator. The real-time data translator (RTDT) (Fig. 16) is a unit composed of logic elements that will accept coded data from a data automation system (DAS) on board a spacecraft (via hard line or the telemetry and demodulation system), convert this information into more appropriate engineering units and apply it to an output mechanism for quick-look operation evaluation.

The RTDT can be used in the AMR blockhouse for prelaunch evaluation of the science system on board the spacecraft, or it can be used at DSIF tracking stations to obtain science data.

The RTDT consists of three physically separate elements: (1) a logic drawer; (2) four output mechanisms—electric typewriter, cathode ray tube printer, binary-coded decimal (BCD) recorder, and a magnetic digital

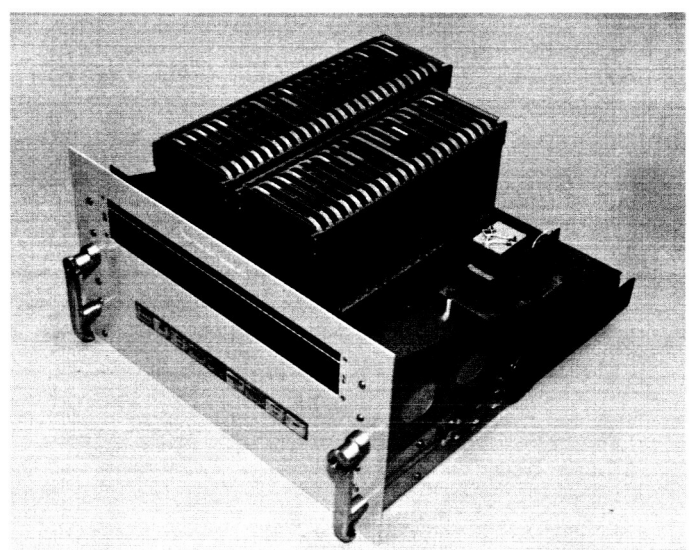

Fig. 16. Science OSE real-time data translator

recorder; and (3) power supply. Following is a discussion of the three elements:

(1) *Logic drawer.* The logic drawer consists of a standard chassis (Ref. 3) which holds three logic card files and a front panel. The drawer is equipped with drawer slides having tilt mounts, permitting access to the equipment for maintenance and is designed for installation in a standard relay rack type of equipment cabinet.

The front panel has status display indication lights and all the controls necessary for operation and/or maintenance. To facilitate fabrication the front panel is removable and all connections are made through connectors.

All input and output connections to the RTDT are made on the rear panel through Pygmy connectors.

(2) *Output mechanisms.* The RTDT has the capability to drive several types of output mechanisms.

(a) At all times data is presented to a digital magnetic tape recorder in parallel teletype (TTY) format for permanent recording.

(b) At low-bit sync rates (less than 10 bps) an electric typewriter can be connected to the RTDT. The information is presented to the typewriter in a parallel TTY format (Ref. 4).

(c) For bit rates between 10 and 50 bps a BCD printer is required. The data is presented to the printer in a 1-2-4-8 BCD code.

(d) For bit rates up to 300 bps a cathode ray tube (CRT) printer can be used. The input to the CRT printer is the same as the tape recorder data.

(3) *Power supply.* Power for the logic drawer is supplied by a Computer Control Co. RP-31 power supply mounted beneath the logic drawer and an indicator lamp power supply mounted on a standard subchassis (Ref. 3) contained within the logic drawer.

Functional description. The RTDT serves as a data processing unit between the spacecraft data system and an observer. Inputs to the RTDT may be obtained directly from the DAS for bench checkout, or from the telemetry decoder for system test or flight data reduction.

The RTDT consists of three basic parts: (1) an input/output data register; (2) a timing system; and (3) data readout and output circuits.

Fig. 17 is a block diagram showing the functional operation of the RTDT. Data flow is shown by the heavy lines and timing or control functions by dotted lines.

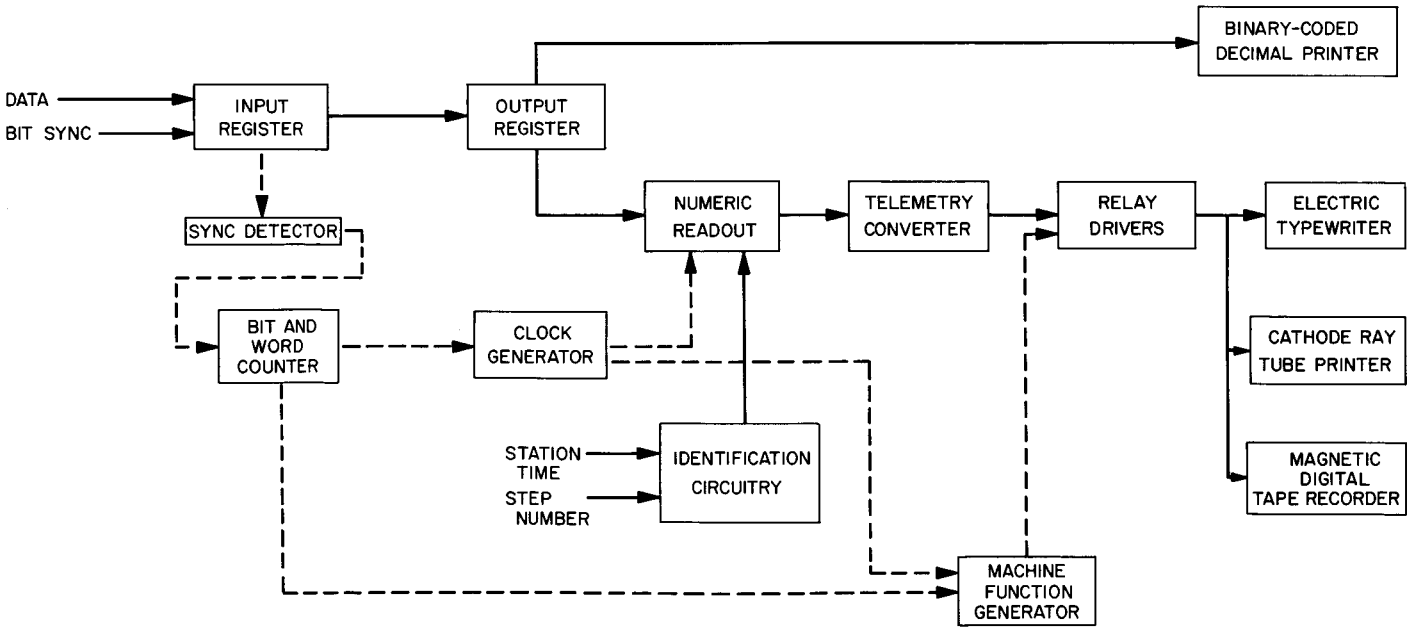

Fig. 17. Real-time data translator block diagram

The data is applied to the input register through an *and* gate and is examined for the presence of the pseudonoise (PN) sync word. The data also flows directly from the input register to a 10-bit output register. The data is stripped from the output register at a predetermined time governed by an internal clock, and passed in parallel to the numeric readout. The output of the numeric readout is connected to the TTY format converter which is connected to the output circuitry.

For BCD printer operation the input data lines to the printer are connected to the output register. A transfer/print command is generated when the 10-bit data word is in the output register. Thus for printer operation the numeric readout, TTY converter and TTY output circuits are not required.

Data shifting pulses known as bit sync are obtained from either an external source (data display or the DAS directly) or from the internal bit sync generator. The internal generator is a multivibrator which operates at either 8⅓ or 33⅓ bps and is used for self-test purposes.

The input register is a 15-stage shift register which has a sync detector connected to it. As data is being shifted through the register, it is continually being checked for the presence of the PN sync word.

After the data has shifted through the input register it enters the 10-bit output register. When a complete data word is present in this buffer register, the process of stripping the data begins.

Bit and word counters. Both the bit and word counters are necessary to detect certain bits and words which are used in the logical development of readout and machine functions.

When the sync word has been detected in the input register, the bit counter is activated which counts the shift pulses applied to the input-output register.

The bit counter is a 10-bit counter, which is equal to the DAS word length, followed by a flip/flop designated F/FA. The purpose of F/FA is to separate the odd-numbered words from the even-numbered words. This is necessary so that machine functions may be performed during even words and readout performed during odd-numbered words.

Clock generator. The clock generator is the heart of the timing system of the RTDT. It generates the pulses to strip the data from the output register and the pulses to allow station time to be entered into the output data.

The generator consists of a series of *and* gates with selected bit and word combinations used as the inputs. It is inherent in the clock generator that no two outputs of the generator may occur at the same time. For this reason, the clock generator is the basic time reference in the RTDT, where time refers to bit and word time instead of chronological time.

Numeric readout/TTY converter. This portion of the RTDT converts the binary data in the output register to 1-2-4-8 BCD. The numeric readout section consists of four separate sets of gates, one for each of the BCD numbers 1, 2, 4, and 8. One input to each gate is the output of the clock generator and the other input is either connected to the output register or to other data input lines.

The output of the numeric readout section is connected to a "BCD to teletype format converter" and is simply a set of gates connected to convert the BCD input combinations to a five-level teletype code.

Station time/step number generator. As was mentioned before, the input to one side of all the readout gates is either connected to the output register or to other input data lines. These other input data lines are station time and step number.

The RTDT must record the station time in order to be able to correlate its output data to other spacecraft events, and it should also have the procedure step number to correlate output data to the input conditions as dictated by the system test procedure. This is accomplished by sensing all input step number lines; if any of them changed, the station time which is always printed is replaced for one subframe by the new step number.

Machine function generator. This section generates the commands to the output mechanisms that require a teletype format. The inputs to the machine function generator are obtained from the clock generator; therefore, no two commands can be given at the same time. These commands are: (1) carriage return; (2) line feed (paper advance); (3) figures shift; and (4) space.

The data output from the teletype converter and the output of the machine function generator are gated together to obtain the desired output machine function sequence and the printout of the TTY data.

c. Standard isolation box. An important element of operational support equipment (OSE), although not housed in the OSE racks, is an isolation box (IB). On all spacecraft programs an IB has existed in some form and its purpose is to provide signal conditioning between the instrument being tested and the OSE. Since the instruments may be 60 to 125 ft from the OSE, signals from and commands to the instruments must be conditioned such that:

(1) The OSE will detect them,

(2) The instrument will accept them,

(3) They will not be degraded by the cable capacitance.

On *Mariner C* a standard IB was designed, developed and built that meets these objectives and can be reused on future projects. Considerations given to the mechanical design of the IB were:

(1) Flexibility such that wiring changes can be made or wiring errors corrected readily.

(2) Of sufficiently small size to be mounted on the spacecraft structure within 10 ft of instruments.

(3) Enough cable capacity to support future projects.

(4) A card cage concept for printed circuit boards to house the necessary signal conditioning circuits.

Fig. 18 shows the IB with the card cage in the open position. All the necessary circuitry for signal conditioning are mounted on individual printed circuit cards which are readily accessible. The card cage contains six card files, with a 14-card capacity, providing a total of 84 individual signal conditioning circuits. The card cage is hinged to allow access to the terminal blocks and the connectors located at the bottom of the IB. The terminal blocks provide the flexibility to make wiring changes to some of the functions coming from the instruments and additional terminal blocks may be added if necessary.

When in use, the IB is mounted on the spacecraft holding fixture just below the spacecraft (Fig. 19). The IB also serves as a support for all the cables between the instruments and the OSE.

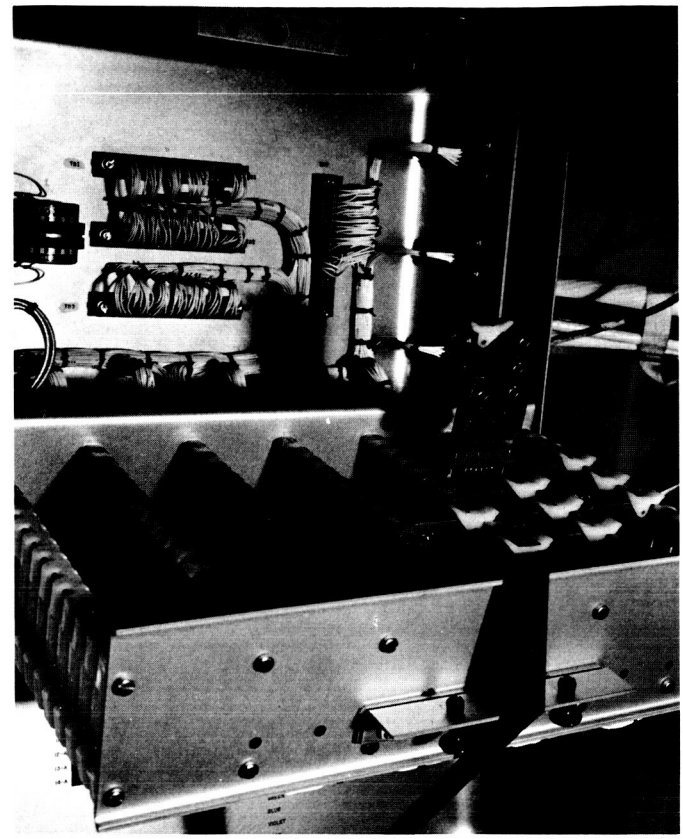

Fig. 18. Isolation box

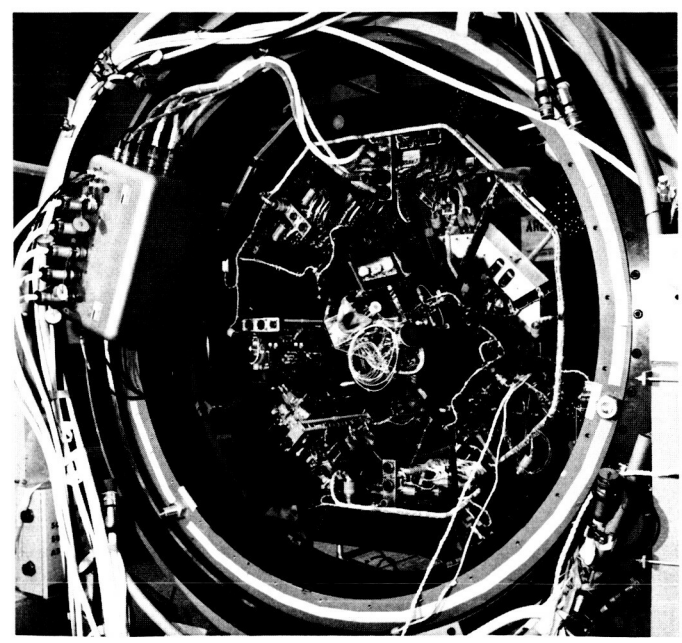

Fig. 19. Isolation box mounted on spacecraft holding fixture

References

1. "Scientific Instruments Subsystem Test Complex," *Space Programs Summary No. 37-24*, Vol. VI, pp. 33–35, December 31, 1963.

2. "Analog Data Conditioning of the Scientific Instruments," *Space Programs Summary No. 37-24*, Vol. 51, pp. 84–87, December 31, 1963.

3. "A Standard Chassis for Space Science OSE," *Space Programs Summary No. 37-23*, Vol. VI, p. 44, September 30, 1963.

4. *Reference Data for Radio Engineers*, Fourth Ed., International Telephone and Telegraph Corp., 1956, New York, N.Y., pp. 842–849.

SPACE SCIENCES

VII. Space Instruments Development

A. *Mariner* Television Subsystem Optical Subassembly

The optical design has been described previously in Ref. 1. Essentially the design is an $f/8$ Cassegrain system with a 12-in. equivalent focal length. The primary mirror, made of beryllium, has a diameter of 1.62 in. and an f-ratio of 2.47. The beryllium secondary provides an amplification of 3.0. The linear occultation[1] by the secondary cell and stray-light shield is 0.51, which seems to represent a practical minimum value under the design constraint that the focal plane must be located 1.35 in. behind the primary vertex.

If it were not for the requirement for the stray-light shield, the occultation would only be 0.38, which would, of course, give somewhat better resolution. Herein lies one basic difference between Cassegrain systems designed for astronomical use and those designed to photograph landscapes (*Mariner*). The astronomical Cassegrain telescope, when used at night to view celestial objects subtending a smaller diameter than its field of view, requires no stray-light shielding. This is true only if the sky background is dark. Theoretically, at least, the limiting magnitude of astronomical telescopes used under moonlit sky conditions could be increased by stray-light shielding. However, stray-light shielding is generally not found on astronomical telescopes.

It may be of interest to inquire into the following questions regarding the *Mariner* television optical design:

(1) What quality of optical performance might be expected of a system such as the one described above?

(2) What performance is required of the system?

(3) How well must the system be built to meet these requirements?

The theoretical limit of resolution performance of an optical system is a function of the diameter of the aperture (assuming a circular aperture) and may be expressed in terms of line pairs/mm by the relationship (Ref. 2).

$$\text{Limiting resolution} = \frac{1426}{f\text{-ratio}} \text{ lines/mm}$$

[1]Ratio of diameter of obscuration to diameter of primary mirror.

The constant in the above equation is a function of wavelength, the value of 1426 being for "white" light. For the case of the *Mariner* system, then, the theoretical limiting resolution would be 1426/8 = 178 lines/mm. This would be on-axis, high-contrast resolution.

The effect of the occultation produced by the secondary mirror cell and stray-light shield on the diffraction pattern is that of lowering the amount of light in the central disk (diverting this light to the rings) and slightly decreasing the diameter of the central disk (Ref. 3). This will increase the high-contrast resolution. Unfortunately, the *Mariner* optical system is expected to view low-contrast landscapes, in which case, one may expect some loss of resolution due to the diverting of energy into the diffraction rings. If the obscuration is relatively small compared to the primary aperture, the amount of energy lost in the central disk is proportional to the obscuration. Rayleigh's criteria for practical perfection in an optical system is that aberrations may cause a loss of not more than 22% of the fraction of energy falling within the central disk. For a Cassegrain system one would want the loss of energy in the central disk due to aberrations *plus* occultation not to exceed 22%. On axis, the aberrations are zero; hence, the occultation may account for the full 22%. In other words, the obscuration may be 22% of the area of the primary aperture. This allows an occultation ratio of $(0.22)^{\frac{1}{2}} = 0.47$. This analysis, however, has not considered the losses in the central disk due to the secondary cell support spider nor the effect of central disk energy which has been diverted into the diffraction rings. It does show that the *Mariner* occultation ratio of 0.51 is higher than desirable from a theoretical point of view. As stated previously, this value represents a practical minimum under the design constraints.

Before becoming concerned with occultation ratios, it is well to ask what is really required of the optical system. The spatial frequency of the vidicon image-processing system, as used in the *Mariner* television camera, is 18 optical line pairs/mm at the focal plane. This is the limiting resolution of the television system. The optical system must have a capability for a higher spatial frequency in order to not degrade, seriously, the over-all system resolution.

It is not clear from the literature whether the over-all resolution of n elements in series is expressed best by

$$\frac{1}{R_{over\text{-}all}} = \sum_{i=1}^{n} \frac{1}{R_i}$$

or by

$$\frac{1}{R_{over\text{-}all}} = \sum_{i=1}^{n} \left(\frac{1}{R_i}\right)^2$$

Assuming the latter equation to be valid, and assuming $n = 2$; then, if $R_1 = 3R_2$, the over-all resolution will be 0.95 R_2. If $R_1 = 5R_2$, the over-all resolution is increased only a few percent to 0.99 R_2. Hence, it is seen that a factor of three in the resolution capability of the optics compared to that of the vidicon readout does not degrade the over-all resolution by more than 5% (assuming the latter equation), and that no significant gain is accomplished by increasing the factor to more than three.

Thus, the optical system resolution requirement is three times 18 lines/mm, or 54 optical lines/mm. This capability should be achieved at low contrast and will restrict the over-all system resolution to a value of 17 optical lines/mm, or 34 TV lines/mm. (Note that the Kell effect has not been introduced into the above argument, nor should it be.)

The theoretical high-contrast limiting resolution has been previously stated to be 178 lines/mm minus a small amount due to occultation effects. The required low-contrast resolution is only 54 lines/mm. The difference between high-contrast performance and low-contrast performance of a Cassegrain system with good stray-light control is not expected to be as great as the above ratio of approximately 3:1. *Mariner B* experience with $f/4$ Cooke Triplets exhibiting spherical aberration has shown a low-contrast (ratio 1.6:1) resolution consistently greater than one-half the high-contrast (ratio 25:1) resolution. The Cassegrain system should perform at least this well.

It appears, then, that a "perfect lens" is not required, and quarter-wave accuracy in optical surfaces may well be adequate. The distance between a spherical surface and a parabolic surface at the edge of the primary mirror (Ref. 4) is given by

$$e = \frac{D^4}{1024\,F^3}$$

where

D = diameter of the mirror = 1.6 in.

F = focal length = 12 in.

The value of e is calculated to be 3.7×10^{-6} in. which is equal to 0.17 wavelengths at 5500 A. Hence, the primary mirror need not be parabolized. Time has not permitted

the derivation of the distance between a hyperbolic and spherical surface for the secondary mirror. However, the fact that the secondary mirror may also be spherical is attested by the fact that an all-spherical system built to this design exhibited a low-contrast (ratio 1.6:1) resolution of greater than 85 optical lines/mm on axis and greater than 60 lines/mm at 0.745 deg off-axis (edge of required field).

In summary, a Cassegrain system of spherical surfaces meets the requirements of the *Mariner* Mars 1964 television camera. This is based on the assumption that system resolution is a function of the sum of the squares of the reciprocal resolutions. Under this condition, system resolution at the focal plane will be no less than 17 line pairs/mm (before Kell effect). If the resolution of the system is a function of the sum of the reciprocal resolutions to the first power, then the degradation in limiting resolution caused by a 54 line/mm optical system would be 25 percent. System resolution, in this case, could fall as low as 13.5 line pair/mm. Furthermore, a "perfect" lens system of a relative aperture of $f/8$ would allow no more than 16 lines/mm system resolution.

B. *Mariner* C TV Development Support Equipment

No less important than the development of flight hardware is the ability to perform thorough and repeatable tests and evaluation of the flight subsystem. For this reason three sets of development support equipment (DSE) are being developed and fabricated to support the test, calibration and evaluation of the *Mariner C* TV subsystem. Every effort is being made to ensure that the three equipments are identical to provide consistent test data no matter which equipment is used, whether at JPL or AMR. Standard high quality test equipment is used wherever possible.

The DSE must be able to perform the following functions:

(1) Activate the subsystem both electrically and optically.

(2) Simulate as accurately as possible all electrical interfaces.

(3) Have access to necessary test points.

(4) Display picture data.

(5) Perform operation analysis and trouble shooting.

System activation equipment. The activation equipment is divided into two general categories, electrical and optical.

Electrical activation consists of 2400 cps square wave power plus necessary pulse inputs for proper camera operation. The pulse inputs will be discussed later in a section on interface simulation. A GTI Model #21157 2400-cps power supply is used for raw power input.

Total subsystem operation must be verified by the use of optical stimulus. Since the telescope is focused at infinity, an optical collimator must be used (Fig. 1). The collimator provides parallel light, and images appropriate test patterns on the vidicon photoconductor or target. The collimator will be used also as a calibration source, and is therefore calibrated with respect to brightness and color temperature to simulate Mars as closely as known. The collimators were procured from Farrand Optical Company to JPL Specification 30764. An identical collimator will also be used to support systems test operations on the spacecraft.

Interface simulation (data automation system [DAS] simulator). Electrical interface simulation is necessary in order to ensure that the subsystem will operate satisfactorily when mounted on the spacecraft. This portion of the DSE requires close liaison with the science DAS people to ensure that accurate simulation is accomplished (Fig. 2a and b). To this end a DAS simulator was designed and fabricated using equivalent DAS end circuits wherever possible. The DAS simulator provides the following channels for TV operation: sync channel, picture data channel, and TV engineering data channel.

The sync channel provides line start, line stop, and frame start pulses to the camera. Pulse characteristics, source impedance and timing are all important factors to duplicate in the simulator. A planet in view pulse is also generated which indicates that the planet has been seen by the narrow angle Mars gate, and that the information was received by the DAS. This pulse is generated by a front panel push button. The picture data channel of the DAS simulator receives digital ones and zeros on two separate lines, and reconstructs the nonreturn to zero (NRZ) data. The reconstructed data are then coupled to a digital-to-analog (D/A) converter for subsequent display on a picture monitor.

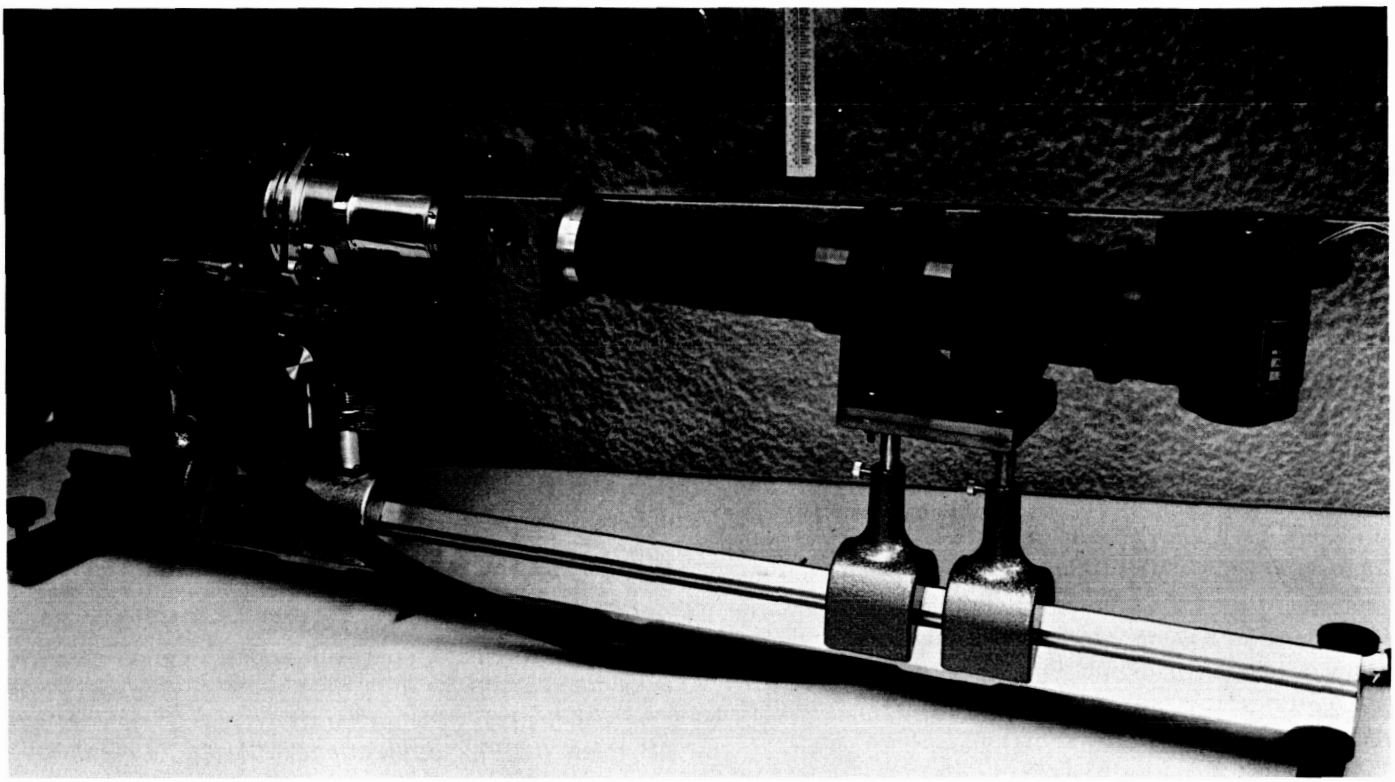

Fig. 1. Collimator and camera head

The engineering data channel provides readout and display of various engineering checkpoints of the TV subsystem. An analog-to-pulse width converter (A/PW) is used in the camera to convert the vidicon control grid voltage (E_{g1}), and an analog signal reference voltage (signal level) to pulse spacing information. The DAS simulator provides a multiplex voltage plus a read command to the A/PW converter. The simulator receives the output pulse from the camera A/PW converter, compares the time it is received to the time the read pulse was sent, and indicates the elapsed time. The elapsed time can then be converted to an analog voltage using the A/PW calibration data. Six front panel lights are used to indicate the following, reading from left to right (Fig. 2): video gain (3), shutter time, filter position, and planet-in-view signal.

Test point access. All camera test points are cabled from the camera to a patch panel where any point of interest can be connected to test equipment for evaluation (Fig. 3).

The patch panel contains terminations of the following test equipment: staircase generator, digital-to-analog converter, Conrac monitor, DAS simulator, electronic counter, and the 2400 cps power supply.

Two one-to-one transformers (one inverting and one noninverting) and two operational amplifiers are included for signal conditioning. System operating time is obtained by a timer which accumulates time whenever 2400-cps power is applied to the camera.

Picture data display. The TV picture is displayed using a slow scan direct view monitor manufactured by Conrac Division of Giannini Controls. The monitor, Model CSS-5, uses a long persistence phosphor for viewing in a darkened room. Polaroid pictures are taken of the monitor for a permanent record. The monitor requires line sync, frame sync, and analog picture data to operate. Analog picture data is obtained from the digital data out of the camera using an AdCom Model 519A digital-to-analog converter manufactured to JPL Specification 30751.

In addition to polaroid copies, a permanent record of all subsystem performance and calibration tests will be obtained using a 35-mm film recorder. Fig. 4 shows the

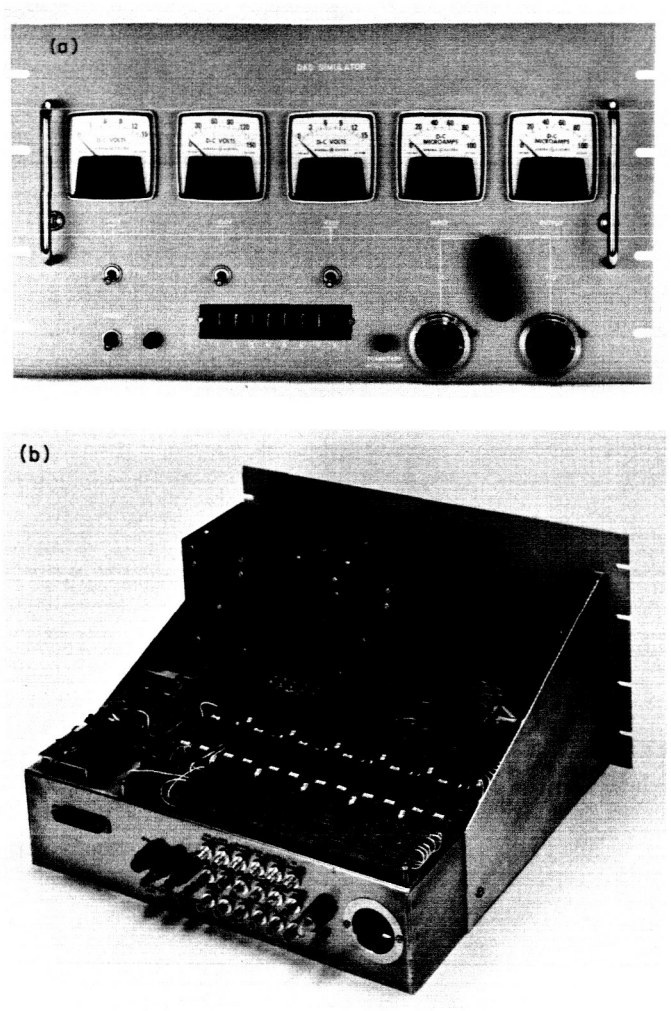

Fig. 2. DAS simulator (a) front panel; (b) rear panel and electronics

film recorder which utilizes a Conrac monitor and an automatic 35-mm camera. The camera is a Flight Research Model IV-E Multidata 35-mm camera with an A-45 camera control unit. The monitor as before requires line sync, frame sync, and analog data. The operation of the recorder is as follows:

(1) Frame sync starts the vertical sweep and opens the camera shutter.

(2) When the frame terminates, a shutter close pulse is generated in the recorder which closes the shutter and flashes two xenon lamps, thus illuminating a clock, pulse counter and data slate which is recorded with each frame. The data image does not pass through the shutter.

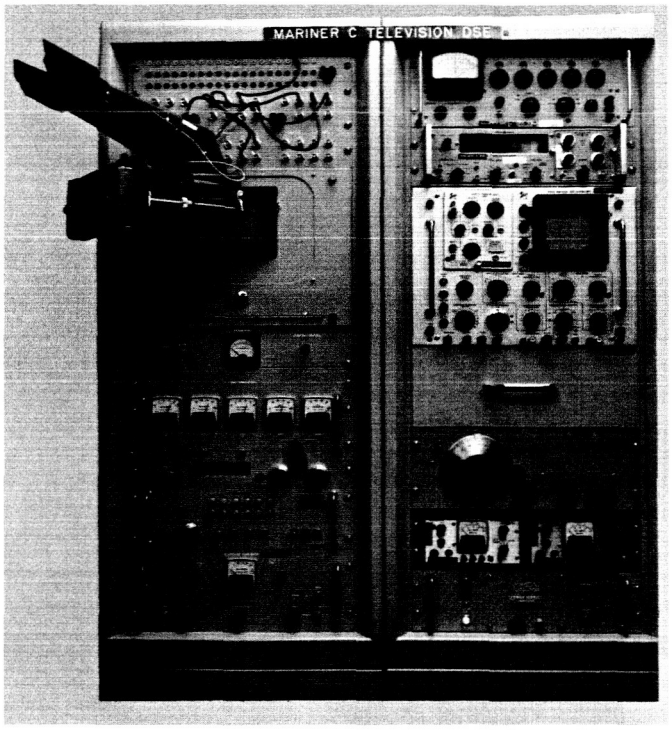

Fig. 3. DSE main console

(3) When the data are recorded and the shutter closed, the film is indexed to the next position and awaits the next frame start pulse.

In this manner a continuous film recording is made of each frame that the TV camera produces. The film camera and monitor are purchased items comprising the major components of the film recorder. The two items are assembled in a 5-ft rack along with periphery equipment designed in-house to complete the film recording function and marry it to the TV camera. To provide ease of operation the following were added:

(1) A monitor cathode current meter.

(2) Indicator lights showing the status of the recorder shutter and whether or not the TV picture was being read out.

(3) An end of film warning light and buzzer. Fig. 5a and b shows typical recorder pictures. The data slate clock and pulse counter appear in the picture for purposes of identifying the data.

A staircase generator was designed to provide linear and logarithmic electrical video signals for checking out and setting up the monitors.

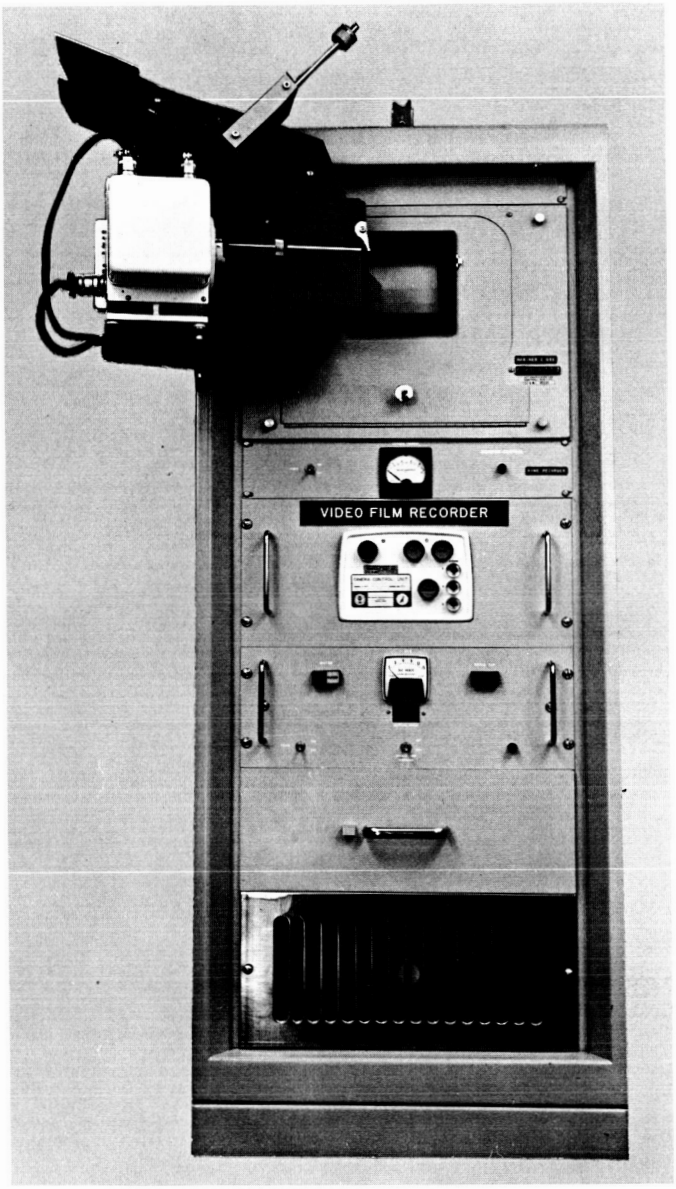

Fig. 4. Video film recorder

Operation analysis and trouble shooting equipment. Standard test equipment was included in the system to provide signal analysis and troubleshooting capability. High quality and flexible equipment was selected to eliminate early obsolescence. The following equipment has been included (Fig. 3): Fluke Mfg. Co. Model #825AR differential voltmeter, Hewlett-Packard 5243L electronic counter, Tektronics RM45A oscilloscope, Hewlett-Packard 200 CDR wide range oscillator, Kepco regulator dc power supplies (2).

Status and future plans. Two main DSE consoles have been completed and are in use. All subassemblies for the third unit have been completed with assembly and interconnecting in process. Two film recorders are to be assembled. One is complete and is undergoing checkout and evaluation. Assembly work is in process on the second, all subassemblies having been completed.

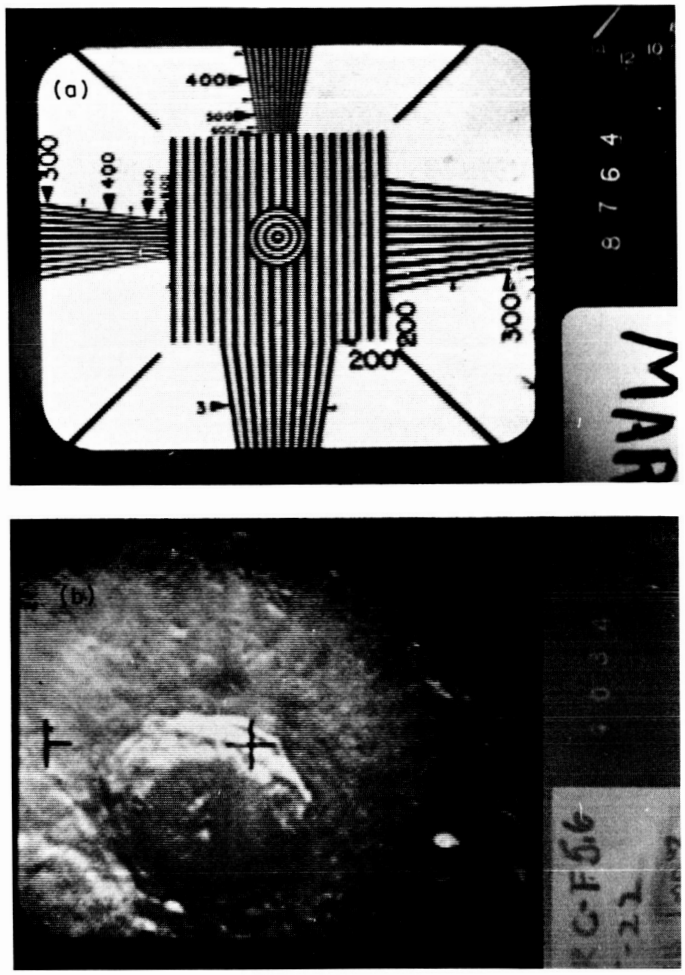

Fig. 5. Typical video film recorder pictures (a) video test chart; (b) video lunar crater

C. Efficiency of Video Data Utilization in a Space TV Camera System

The line-scanning process in a space TV system generates extensive amounts of data which must be passed through the narrow-band filter represented by the telemetry-link to Earth. As this transmission channel is

information limited, it is essential that maximum utilization be made of its capacity. The ratio between the picture information actually transmitted and the system capacity determines the channel utilization. A utilization factor may be expressed for the camera system as $U = H/2ntC$, where H is the picture information in bits, taken over a sufficiently long interval of time, $2nt$ is an integral number of frame periods and C is the channel capacity in bits/sec. Generally, in a fast real-time TV system, the transmission efficiency is determined by the scanning retrace-time and the frame and line synchronization requirements with $U = 0.8$ as typical. However, for a slow-scan TV camera these requirements represent a relatively small part of the losses and other inefficiencies are introduced that are peculiar to slow-scan operation.

A distinction may be made between U_C the camera utilization factor and U_T the transmission-channel utilization. Further subdivisions may be made with U_F and U_L representing the frame and line-time utilization. Efficient systems management can generally ensure a high U_T, even though for an isolated camera U_C may be quite low. However, as will be shown later, there are fixed information-time losses in the line scanning process that result in a value of U_T that cannot be improved upon by systems organization.

Reviewing first the relationship of U_C to U_T: for a space science TV experiment employing a single camera, $U_T = U_C = U_F U_L$. For a slow-scan camera, each picture frame must be followed by an erase mode of equal time, hence $U_F = 0.5$, $U_C = 0.5\ U_L$ so that $U_T < 0.5$. If there is more than one camera aboard, the picture frames may be interleaved so that while $U_F = 0.5$ for each camera, $U_T = U_L$. Data from other space science instrumentation may also be interleaved with a single camera so that U_T may be made to approach unity.

For a planetary experiment where data are not to be transmitted in real time, a continuous flow of transmitted data may be maintained by suitable control of the tape machine. This could be implemented, for example, by starting and stopping the machine for each frame recorded and then playing back at a continuous rate. Thus while $U_F = 0.5$, $U_T \rightarrow 1.0$. For a deep-space TV system with an extremely limited channel capacity, the data readout from the camera will be at a much greater rate than the readout from the tape. To accomplish the required reduction, data is read out line-by-line in time t_A, the active line-scan time, then stored and recorded during a lengthy line-blanking period t_B. The efficiency over the line period $U_L = t_A/(t_A + t_B)\ U_{AL}$, where U_{AL} is the efficiency over the active-scan time. For $t_B \gg t_A$, U_L will be quite low. During playback, however, the transmission efficiency $U_T = t_B/(t_A + t_B)\ U_{AL}$, a figure much closer to unity. By interleaving the data from two lines, as in the *Mariner C* TV system, U_T may be made to approach U_{AL} more closely.

Those camera losses that are not amenable to system manipulation are associated with the losses during the active line-scan time. The information generated during the active-scan time is unipolar. System mechanization requires that a dc reference-signal corresponding to optical black be established at the output terminals of the camera amplifier. The reference signal must originate as an optically black signal at the photosensitive surface of the camera tube and must be supplied for each scan line in addition to the video information. The time thus removed from effective video data is a loss that will be sustained throughout all signal processes including the reconstruction of the final image.

The electrical signal that must be derived from true optical black is created at the camera tube by scanning an opaque sector on the photosensitive surface. The scan lines are positioned so that the initial portion of each line traverses the masked sector as shown in Fig. 6. The ratio of the exposed scan to the over-all scan is a measure of the active-line transmission-efficiency U_{AL}. The time that the beam must continue to scan behind the optical mask is determined by the time required to establish a controllable dc reference level at the output terminals of the camera amplifier. In addition, sufficient overscan must be provided to allow for incidental geometrical positioning errors. These positioning errors are

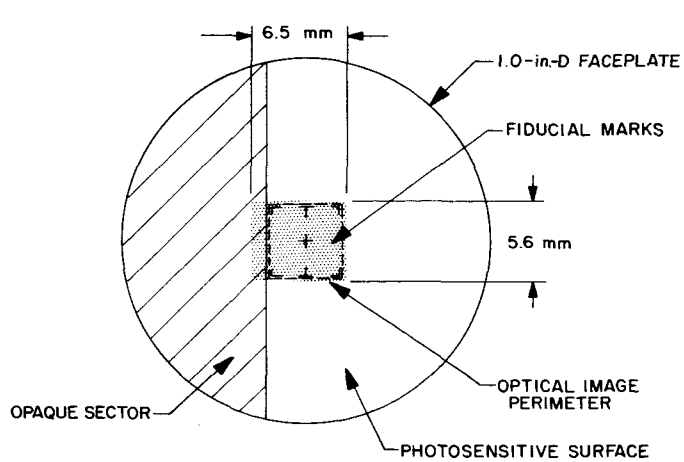

Fig. 6. Scanning raster on vidicon face plate, *Mariner C*

created by the spacecraft environment and relate to temperature and power-supply variations and the presence or absence of the Earth's magnetic field. Temperature stabilization must be implemented in the solid-state circuitry and the power-supply variations must be countered by stable electronic regulators. The influence of extraneous magnetic fields, and particularly the Earth's magnetic field on the camera scanning beam, is nullified by the use of a high-permeability axial shield around the camera tube.

A well-established clamp technique for establishing a black-reference potential will now be described for the camera output-amplifier of the *Mariner C* system. Briefly, the video output stage is ac coupled to the earlier amplifiers and a controllable dc charge is set up on the coupling capacitor at the time the camera tube is scanning optical black. The requisite charge is delivered to the capacitor during each line scan by a line-keyed pulse generator. The beam continues to scan behind the mask following the charging period to ensure that the reference signal is adequately stabilized. The transmission utilization for the line expressed in bits is then $U_{AL} = H_L/[H_L + (H_c + H_r + H_o)]$, where H_L represents the picture information in bits and H_c, H_r, H_o are the bits lost during the charging and stabilizing operations and the overscan.

A schematic diagram of the reference-signal mechanization is shown in Fig. 7. For clarification the circuit may be divided into three parts: the keyed-clamp charging function, a high-input impedance and dc blanking-level section, and a differential emitter-follower output amplifier. The blanking level provides a potential baseline against which video and dc levels can be established. Operation of the circuit is as follows. The video coupling capacitor C_{18} is charged by pulses supplied from keyed pulse generators Q_5, Q_7. Pulses are initiated and turned off by a 1-msec pulse derived by differentiation of the line synchronizing pulse, C_{19} R_{22}. Pulses of opposite

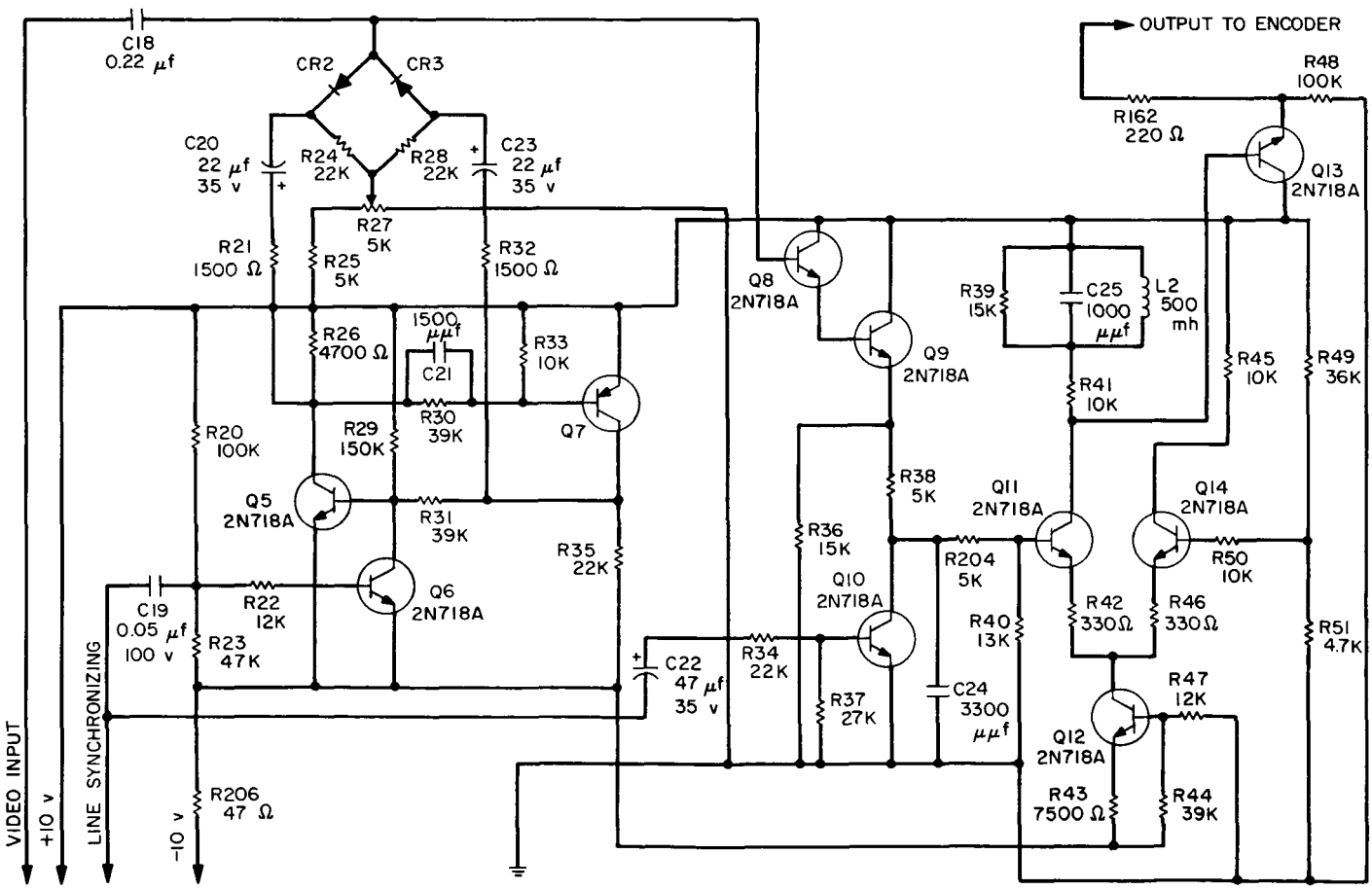

Fig. 7. Video output amplifier and black-level referencing

polarity are applied to a balanced bridge where diodes CR_2, CR_3 form two of the arms. The bridge is in balance when the dc potential controlled by R_{27} is zero. Application of a voltage by R_{27} unbalances the bridge and permits C_{18} to be charged by the keying pulses.

The bridge is followed by a high-input impedance Darlington circuit that provides a sufficiently long discharge time-constant during the line-scan time of 14.4 ms. A blanking-level is provided when amplifier Q_{11} is cut off by clamp Q_{10} being driven to saturation by the line-synchronizing pulse. The differential amplifier Q_{14} is offset so that Q_{11} operates as a unidirectional amplifier. A low output impedance for Q_{11} is secured by emitter follower Q_{13}.

The unidirectional video-output signal for *Mariner C* is PCM encoded. A single line scan with the timing and encoding functions is shown in Fig. 8. The analog signal

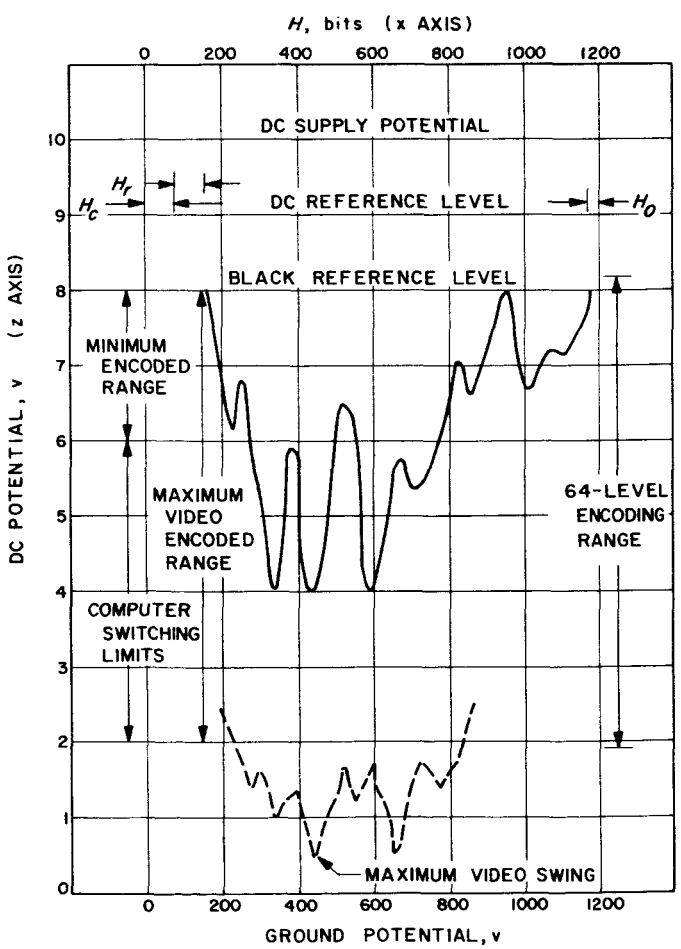

Fig. 8. Video level characterization

is quantized into 64 levels where each resolution element appears as a 6-bit word. To ensure no loss of picture information some quantizing overlap is desirable. Thus there are losses in efficiency in both the x and z axes. For a PCM system the active-line efficiency becomes $U_{AL} = H_L/H_L + [(H_c + H_r + H_o)]\ U_Z$ where U_Z is the utilization efficiency of the quantizing system. As it is impossible to maintain the video signal for all pictures at the full 64 level quantizing the U_Z for various picture frames may be expected to vary. The variation is minimized in *Mariner C* with a digitally controlled AGC computer that restrains the highlight video level between 25 and 60 quantizing levels.

U_Z is maximized within the above constraints when the black-reference level is completely stabilized. This requires an adequate time constant for the video-coupling condenser C_{18} and the high-input impedance Darlington circuit. For *Mariner C* a time constant of 1.5 sec stabilizes the black-reference signal to a half digit accuracy for the duration of the line scan. The solid-state circuitry related to the dc clamp is temperature compensated using Balco wire-wound resistors to a ±½ digit accuracy over a temperature range from 0 to +55°C with an error no greater than 3 digits from −20 to +70°C. In addition, the solid-state circuitry related to the scanning has been stabilized to achieve an objective positional stability of 0.1 mm in the horizontal or vertical directions over a temperature range of from 0 to +55°C. Preliminary tests in the *Mariner* program indicate that the positional stability achieved is of this order. However, more precise measured data are dependent upon the arrival of a newly developed digital readout oscilloscope that may be used at slow-scan rates.

Estimates of utilization efficiencies are included below for the *Mariner C* single TV camera system. The frame period is 24 sec and the erase mode time equals the frame time, hence $U_F = 0.5$ and $U_C = 0.5\ U_L$. As other space science data are inserted $U_T \rightarrow 1.0$ in accordance with the utilization of the camera dead time. From the active-line scan data of Fig. 6 or from Fig. 8, $U_{AL} = 0.86\ U_Z$. If a full amplitude video signal into the encoder is assumed, $U_Z = 60/64 = 0.94$, making $U_{AL} = 0.86 \times 0.94 = 0.81$. The active line period $t_A = 14.4$ msec, and the blanking time $t_B = 105.6$ msec so that $U_L = 0.81 \times 14.4/120 = 0.097$. After data-recording, however, the transmitted-information $U_T = 0.81 \times 105.6/120 = 0.71$, or for two interleaved lines $U_T \rightarrow 0.81$, depending on the amount of data inserted between active picture-frame scans. Thus the data transmission efficiency of the camera

encoded information is seen to be of the order of 80% and is seen to be ultimately dependent on the positional stability of the scanning raster on the vidicon camera tube.

D. Investigation of Micropolish Oxides for Recording *Ranger* Block III Data

In addition to the kinescope film recording of demodulated video data on Block III, longitudinal magnetic recording is made of the predetection signal. This magnetic recording will be used as a working copy from which further film duplicates will be generated and subsequent scientific analysis made. For this reason it is imperative that the magnetic recording be of as high a quality as possible with respect to fidelity to the original data.

Nature of the predetection signal. The *Ranger* Block III TV experiment utilizes two transmitters symmetrically displaced in frequency about the bus transponder, with each transmitted video channel occupying a bandwidth of 950 kc. For the purpose of magnetic recording, each of these signals is separately heterodyned to a center carrier of 500 kc, thus occupying the frequency spectrum from 25 to 975 kc. The major portion of signal energy is situated around the 500-kc center frequency; however, it is essential for fidelity of the demodulated waveform that the entire spectrum be preserved with good amplitude/phase characteristics. A nominal mission predetection communication signal-to-noise ratio (S/N) has been set at 21 db rms S/rms N within the 800-kc passband. The magnetic recording should, therefore, be capable of meeting or exceeding this specification so that flight data will not be severely degraded.

The constraints of bandwidth and S/N have led to the choice of Ampex FR 1400 recorders operating at a tape speed of 120 in./sec. While this resulted in a recorded magnetic packing density of 8000 cycles/in. (linear), the useful recording time was reduced to 15 min or less for a 9600-ft reel of tape. For an alternate flyby mission, useful recording times of up to 30 min are possible. For this reason, it was deemed advisable that newly available magnetic tapes be investigated with the possibility of recording mission data at 60 in./sec.

Investigation of micropolish tapes. The Ampex FR 1400 recorder is capable of recording a 750-kc signal at 60 in./sec with standard high-output instrumentation tape. The recent introduction of high-potency oxides with high surface polish indicated that it should be possible to record and play back signals with wavelengths of 60 μin., thus allowing a 1-Mc capacity at 60-in./sec tape velocity. The following types of commercial magnetic tape with micropolish characteristics were obtained: Memorex 62J, Memorex 62L, 3M 2219-22883 (prototype of Type 951), and 3M 2113-22783 (prototype).

Testing was accomplished by choosing Memorex 62J as a comparison standard and adjusting the playback equalization for the most uniform response at 60 in./sec. This playback equalization was then maintained for all tapes, while the bias and direct record levels were optimized for each tape under test. In this manner it was possible to compare the playback characteristics of each tape.

While testing these tapes, it was observed that the playback characteristics measured while the tape was in the process of being recorded were significantly different from those measured when the tape was rewound and replayed. All subsequent playback passes were identical to the first replay. This effect was definitely not due to bias leakage, record signal fringing, or magnetized heads. Furthermore, all four types of tape possessed this characteristic to varying degrees, suggesting perhaps a magnetic relaxation phenomenon.

Results of the frequency response tests for playback while recording are given in Table 1, and the replay responses are given in Table 2. For each tape the zero reference level was the point of 1% third-harmonic distortion, with second-harmonic distortion set for minimum.

Check of the effect on the predetection signal. The results of the frequency response runs demonstrated clearly that all four tapes were capable of recording the predetection TV signal at 60 in./sec. As a check, test recordings were made of a composite TV signal that is electrically generated within the ground station. Since both Memorex tapes were essentially identical, only one (62L) was used for this test; both 3M tapes were used. Kinescope photographs of the TV signals demodulated from these tapes are shown in Fig. 9. Frame 0006 was taken from Memorex 62L, and Frames 0021 and 0035 were from 3M 2219-22883 and 3M 2113-22783, respectively. Neither amplitude nor phase distortion is evident in the photographs. The demodulated video S/N was identical for all three tapes and equalled 35 db peak-to-peak S/rms N unweighted. The fact that all tapes had the

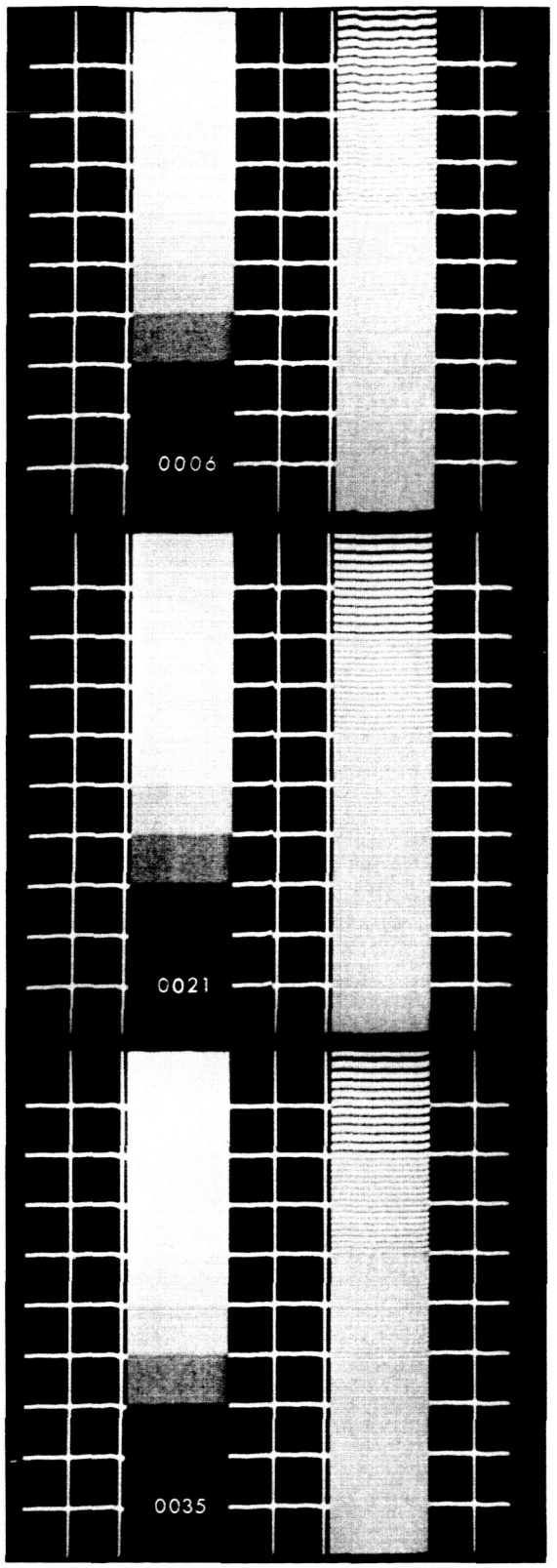

Fig. 9. Kinescope photographs of TV signals demodulated from micropolish tapes

Table 1. Test results for playback while recording

Frequency, kc	Tape response, db			
	Memorex 62J	Memorex 62L	3M 2113-22783	3M 2219-22883
1	0	0.4	2.0	0
10	−0.2	0	1.7	−0.6
100	0.3	0.3	1.4	0
200	0.1	−1.0	0.4	−1.2
300	—	−0.2	1.2	1.2
400	−0.2	−0.8	0.6	1.0
500	0	−1.0	0.5	1.0
600	0.8	−0.6	1.0	2.8
700	1.0	−0.9	1.2	2.8
800	0.9	−1.1	1.2	3.1
900	−1.9	−3.6	−1.6	0.7
1000	−6.2	−8.0	−5.8	−3.4

Table 2. Test results for playback following rewind

Frequency, kc	Tape response, db			
	Memorex 62J	Memorex 62L	3M 2113-22783	3M 2219-22883
1	0.1	0.4	2.0	−0.3
10	−0.5	−0.2	1.4	−1.0
100	−0.6	−0.6	1.3	−1.0
200	−2.0	−2.3	−0.4	−2.5
300	—	−1.8	0.2	−0.4
400	−2.5	−2.7	−0.8	−1.0
500	−2.9	−3.1	−1.0	−1.3
600	−2.3	−2.8	−0.4	0.1
700	−2.8	−3.2	−0.6	−0.2
800	−3.6	−3.4	−0.9	0.2
900	−5.8	−6.0	−4.0	−2.6
1000	−10.8	−10.5	−8.5	−7.1

same S/N is proof that, even at 60 in./sec, the tape medium does not limit data S/N.

Conclusions. It has been established that presently available tapes will allow useful predetection recording of the *Ranger* Block III TV signal at 60 in./sec. Should it be required that a mission recording extend to 30 min, prime mission data will not be jeopardized by using a tape speed of 60 in./sec instead of the 120 in./sec presently used.

References

1. "Mariner Television Subsystem," *Space Programs Summary No. 37-18*, Vol. VI, pp. 67–70, December 31, 1962.

2. "Method of Determining the Resolving Power of Photographic Lenses," Circular 533, National Bureau of Standards, U.S. Government Printing Office, Washington, D.C., 1953.

3. Grey, D., *Journal of the Optical Society of America*, Vol. 39, No. 9, September 1949, p. 727.

4. Wright, F. B., "Accuracy in Parabolizing a Mirror," *Amateur Telescope Making*, Vol. I, Scientific American Publishing Co., New York, N.Y., 1935, p. 257.

VIII. Space Instruments Systems

A. Mechanization of the Nonreal-Time Data Automation System

The nonreal-time portion of the Science Data Automation System (NRT DAS) provides the necessary functions for acquiring science data during the planetary encounter phase of the spacecraft mission, and transferring these data to a tape recorder in the telecommunications system. The complete DAS is described in Ref. 1. This report reviews the design constraints and hardware trade-offs involved in the design of the NRT system.

1. Science Instrument Planetary-Encounter Data Requirements

Photographic subsystem (Ref. 2). Data from a television vidicon exceeds 250,000 bits per picture. The video data are generated by line scanning. Each line generates 200 samples, encoded to 6 binary bits per sample, for a total of 1200 bits per line. A total of 200 lines are scanned per picture. In addition, it is necessary to provide frame and line identification data. A mission storage capability in the tape recorder of 20 pictures is desired. Pictures are to be taken in overlapping pairs, using two different color filters. The picture data are played back after encounter at a rate compatible with the telecommunication bandwidth capability.

Infrared spectrometer. This instrument was deleted from the *Mariner C* spacecraft in March 1963, but it is reviewed here because its data requirements influenced the design of the DAS in its present form. A provision for 10 samplings of the infrared (IR) spectra was desired, arranged so that each sampling would cover the same planetary area as each picture pair. Each sampling generated approximately 6,000 bits of data over a time interval of about 1 min. This data rate exceeded the telecommunications bit rate by a factor of more than 10. It was necessary to store the data from this instrument for post-encounter transmission, unless an onboard data-reduction computer was included. The latter alternative was rejected as too sophisticated for this spacecraft.

Fields and particle instruments. The remainder of the scientific instruments (Ref. 3) chiefly measure particles and fields and transmit their data essentially as it is gathered, i.e., in real-time. A later retransmission of this data is desirable, if possible.

2. System Design Criteria and Constraints

The storage medium chosen for *Mariner C* is the magnetic tape recorder. Sufficient capacity for 20 pictures is provided. After recording is fully completed, the recorder is played back at a speed reduction consonant with the telecommunication rate of 8⅓ bits/sec.

The recording characteristics of the tape recorder which the NRT DAS must meet are as follows.

Digital recording is accomplished on a single track which accepts binary data one bit at a time (tracks are switched after the original starting point is reached on the continuous tape loop). The source data must be clocked by a stable oscillator because the clock is recorded and employed on playback as an element of the servo-control loop which maintains playback at the stable 8⅓ bits/sec telecommunication rate.

A mission constraint is the necessity for taking picture pairs at presented intervals chosen to maximize the likelihood of having the planet in view (as the spacecraft passes the planet). The total interval of time is about 22 min. If the tape recorder had been made to run continually, more than 1 min. would have been required for the recording of each picture. However, this interval imposes engineering restrictions on the TV camera which cannot easily be met. The overlap of picture pairs which are utilized for color information is also eliminated. As a consequence, it was necessary to stop the recorder between pictures.

The requirement for stopping and starting the tape recorder was examined for its effect on recording the IR and real-time data. The storage of these data on a magnetic core matrix, or buffer, was preferable to use of a second tape recorder.

One of the limitations on the length of the recording period for the TV picture is a minimum vidicon line-scan rate which will yield a satisfactory video signal-to-noise ratio (Ref. 2). This factor limits the picture time to a maximum of 3 sec. However, it was not feasible to build the *Mariner C* recorder so that it could start, record for 3 sec, and stop (this sequence repeating 20 times), without wasting an excessive amount of tape. It is possible to increase the total picture recording time without decreasing the scan velocity of each TV line, and yet provide a continuous flow of data for the recorder, if a buffer is provided to store each line.

In the system mechanized, each TV line is scanned in only 14.3 msec out of the 120-msec interval between lines. The video data rate is 83.33 kc, and is written directly into the buffer. Data are read out of the buffer at a 10.7 kc $\pm 1\%$ rate. This rate yields a continuous flow of data to the tape machine. It was immediately recognized that the same buffer could be used for buffering video, IR and real-time data during picture recording, and for storing the IR and real-time data only between pictures.

After the detail design phase of the DAS, the IR instrument was deleted from the *Mariner C* payload. However, this possibility had been anticipated and the system was modified to provide for the storage of real-time data only between pictures.

A choice of precisely 24 sec for recording each picture was made because it permits the TV line rate to occur at the telemetry bit rate, 8⅓ bits/sec (200 lines divided by 8⅓ lines per second equals 24 sec.) This arrangement simplifies the arrangement for recording real-time data. Each real-time bit, as it becomes available, is recorded with each TV line. The TV line identification, which is in fact spacecraft time, plus the *a priori* knowledge of the real-time data format, uniquely identifies each real-time bit. Synchronization between the real-time bit rate and the video system also significantly simplifies the arrangement for transmitting video system performance data and video AGC (automatic gain control voltage, a measure of the average picture illumination) in real-time. An interval of 24 sec is allowed between pictures for erasing the vidicon. The NRT format is described in Ref. 1 and is repeated in Fig. 1.

3. Detail Mechanization

The following functions are mechanized by the NRT (Nonreal-Time) DAS:

(1) Generation of TV frame and line sync.

(2) Generation of TV frame and line identification codes to precede the video data.

(3) Control the passage of video data through the buffer.

(4) Command the start and stop of the tape recorder.

(5) Accumulate video system performance data and sequence it into the flow of video data through the buffers to the recorder.

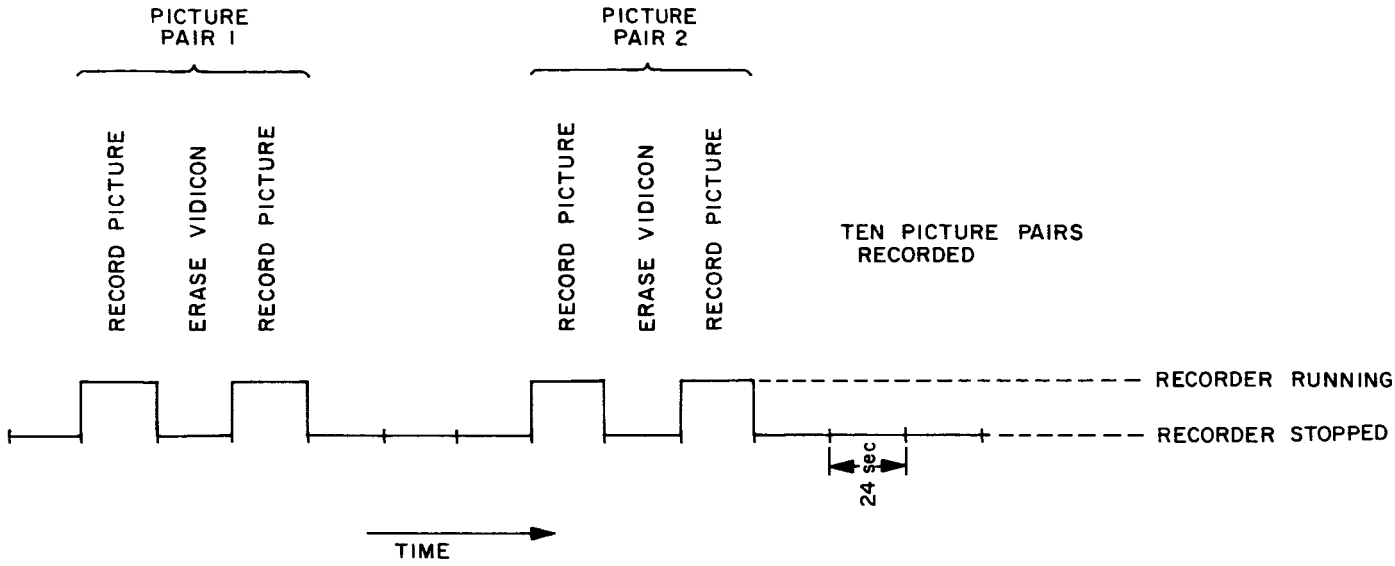

Fig. 1. NRT format

(6) Sequence the real-time data into the buffers.

(7) Provide video performance data to the RT (Real-Time) DAS for real-time transmission.

(8) Provide for the necessary control and command functions for the planetary encounter data mode (Mode 3) as follows:

(a) Accept the wide-angle acquisition of the planet as seen by the planetary scan system. At this time, telemetry data Mode 3 begins (14 words of science replace spacecraft engineering data, as in Ref. 1). Also at this time, picture sequencing commences, without actually recording pictures, and the transmission of video performance data and NRT DAS events (status) begins.

(b) Accept the narrow-angle acquisition from the Mars Gate and/or the TV system, backed up by ground command. At this time, the scan system is commanded to cease scanning and recording of pictures commences.

(c) Accept the end-of-tape command from the recorder, backed up by the counting of 22 pictures internal to the DAS. After this time, no more start-tape commands are issued, and telemetry Mode 3 is terminated (Mode 2, the time sharing of telemetry with spacecraft engineering data, is resumed by the telecommunications system until Mode A, recorder playback commences).

The NRT DAS is mechanized independently of the RT DAS, including a separate power supply, in order to provide against a possible short circuit in the RT DAS which could otherwise eliminate the video data along with the RT data. The RT DAS uses about twice as many electronic components as the NRT DAS (not counting the buffer memory cores, whose individual failure would produce only scattered loss of data). Since the deletion of the IR Spectrometer, the NRT DAS could almost be described as the Video DAS, since the sequencing of RT data onto the tape recorder constitutes a very small proportion of the total components.

4. NRT DAS Block Diagram

Fig. 2 is a simplified block diagram of the NRT DAS (Ref. 1). In the detail mechanization of the DAS, the block labeled "buffer" consists of two buffers, each of the type in which no interlace of the writing and reading functions occurs. They are serially addressed, of the type frequently referred to as "first-in, first out." An identical unit is symmetrically located on the reverse side of the tray. During picture recording, as one buffer accumulates a single line of video data, line identification, video system performance data and one bit of RT data, the second buffer is being read out into the recorder. During the next video line, the buffers are reversed in status. One

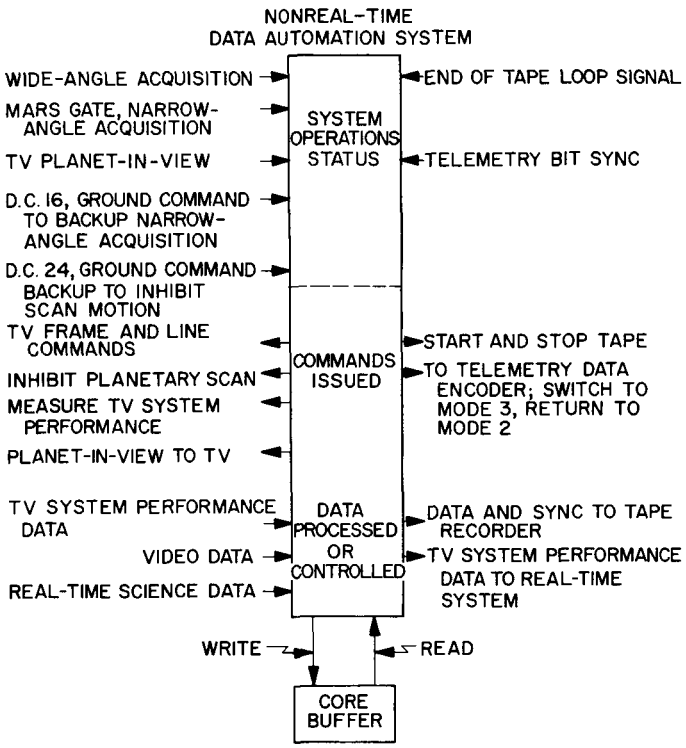

Fig. 2. NRT DAS simplified block diagram

buffer load, during the recording of pictures, totals 1261 bits, as follows:

Bits	Function
31	PN sequence
4	NRT frame count
3	Subframe count
9	TV line number
3	TV system status
1	Real-time science data from RT DAS
10	TV performance data
1200	Video data, 200 elements

The format in use between the recording of pictures is given in Ref. 1.

B. Planetary Simulation for *Mariner C* Planetary Scan Subsystem

The design and construction of a planetary simulator for the *Mariner C* planetary scan subsystem has been completed. The device is used to evaluate the instrument in both bench and environmental testing.

Theoretical calculations. In order to design the simulator, the amount of solar energy reflected from Mars and incident at the scan subsystem has been calculated. When the planet is observed through an optical system, the flux incident in the image (Ref. 4) is

$$e(\alpha, \gamma, \Delta, \lambda) = \frac{E_v \, \phi(\alpha) \, S \, T}{\gamma^2 \, \Delta^2} \int_{\lambda_1}^{\lambda_2} \frac{f(\lambda)}{f(v)} P(\lambda) \, d\lambda \qquad (1)$$

where

e = Energy available at the sensor

E_v = Monochromatic energy flux at $\lambda = 0.55\,\mu$ corresponding to visual albedo, $\alpha = 0$ deg., $\gamma = 1$, $\Delta = 1$.

α = Phase angle (Sun-planet-spacecraft angle)

$\phi(\alpha)$ = Phase function

S = Aperture area of optical system

γ = Mean distance from planet to Sun in astronomical units

Δ = Distance from planet to spacecraft in astronomical units

$\frac{f(\lambda)}{f(v)}$ = Relative spectral energy flux of the planet

$P(\lambda)$ = Spectral response of the sensor

T = Transmission efficiency of the optics

λ_1, λ_2 = Cutoff wavelengths of the optical system

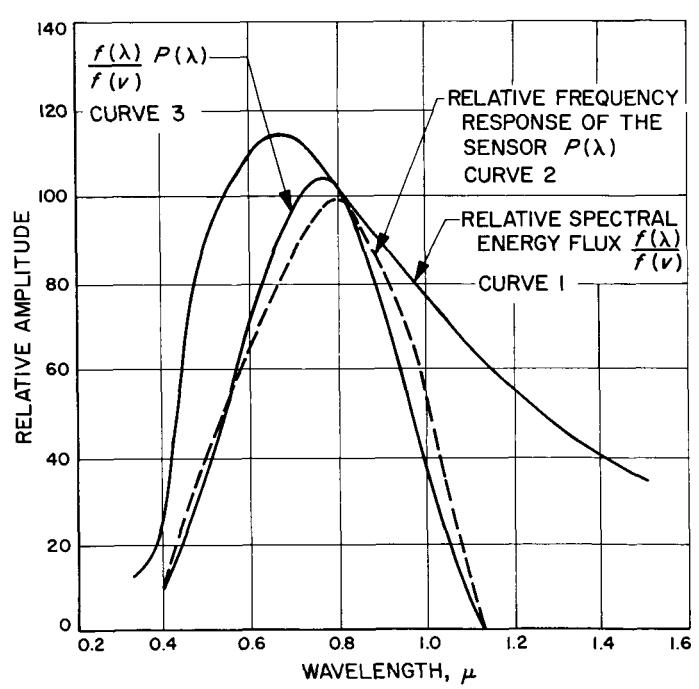

Fig. 3. Relative spectral response of the planet and sensor

The relative spectral energy flux of the planet (Ref. 4) is shown as Curve 1 together with the spectral response of the sensor shown as Curve 2 on Fig. 3. The resultant spectral response of $\left(f(\lambda)/f(v)\right)P_{(\lambda)}$ was calculated and plotted as Curve 3 on Fig. 3.

The amount of energy available at the sensor can be calculated by means of Eq. (1). The monochromatic energy flux at $\lambda = 0.55\,\mu$, when measured at $\alpha = 0$ deg., $\gamma = 1$, and $\Delta = 1$, is 1.52×10^{-8} erg/cm² sec A or 1.52×10^{-11} w/cm² μ (Ref. 4). The phase function has a numerical value of 0.406 for $\alpha = 60$ deg.; this is the anticipated phase angle at the spacecraft and planet encounter. The integral representing the area under Curve 3 of Fig. 3 is 0.42. The remaining terms of Eq. (1) are as follows:

$$\gamma = \frac{227.8 \times 10^6\,\text{km}}{149.5 \times 10^6\,\text{km}} = 1.524\ \text{AU}$$

$$\Delta = \frac{\text{Planet-spacecraft distance in km}}{149.5 \times 10^6}$$

$$ST = \frac{\pi (d)^2}{4}\,T$$

$$ST = 0.85\,\text{cm}^2, \text{for } d = 1.2\,\text{cm}, T = 0.75$$

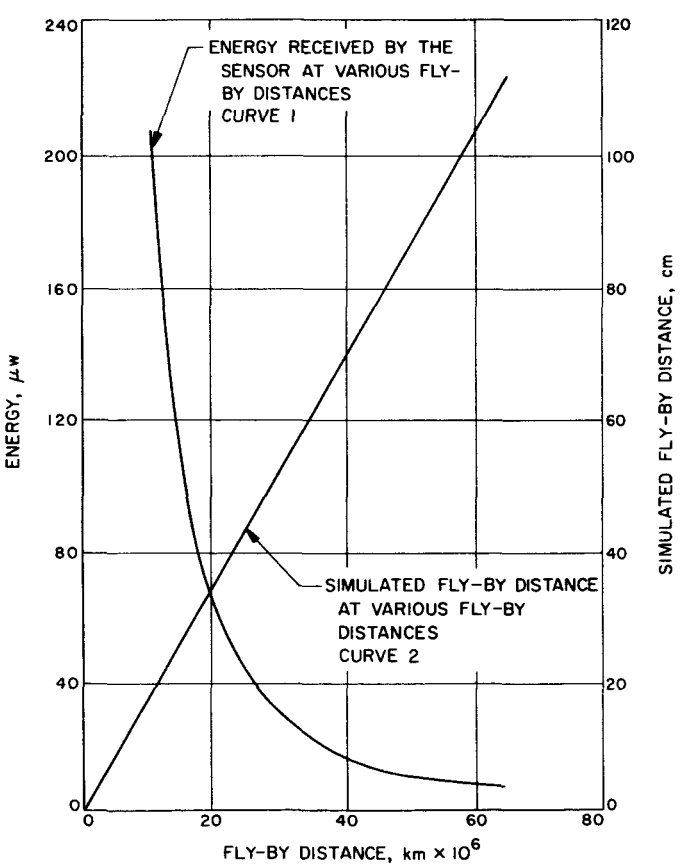

Fig. 4. Energy received and simulated fly-by distance

The energy received as a function of planet-spacecraft distance is calculated and shown as Curve 1 in Fig. 4.

Planetary simulator. To provide planetary simulation during subsystem development and testing, a simulator was designed and constructed. This device, shown in Fig. 5, consists of an illuminated disk having a radius of 6.0 cm, an incandescent lamp source, filters, and iris diaphragm in a metal housing. The transmission characteristics of the filters are such that only energy having a spectrum and distribution approximating the spectral reflectivity curve of the planet is allowed to reach the disk. Experiments were performed in order to obtain combined transmission characteristics of filters capable of satisfying these requirements. Fig. 6 shows the

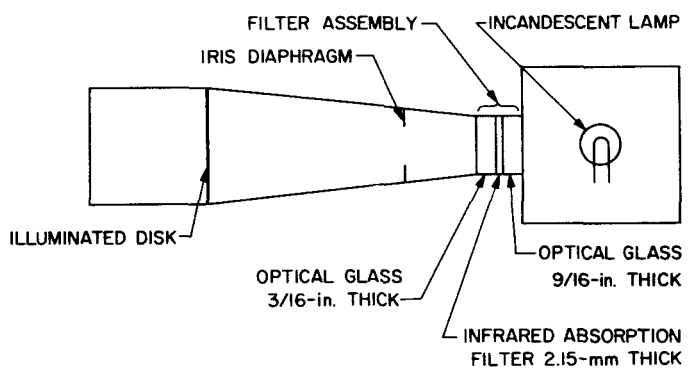

Fig. 5. Planetary simulator

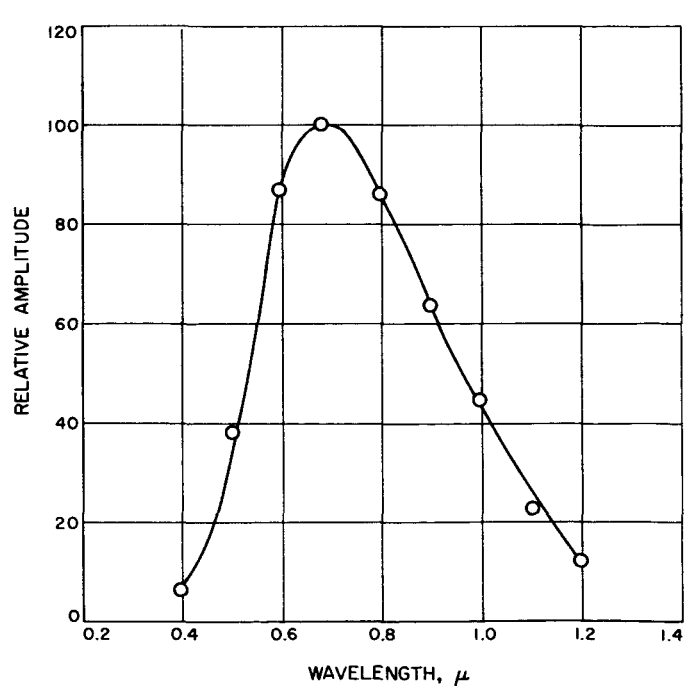

Fig. 6. Relative spectral distribution of the simulator

measured spectral response curve of the simulator. An iris diaphragm is used to adjust the output energy without altering its spectrum. The output energy is measured by means of a thermopile.

To simulate the various fly-by conditions, the simulated fly-by distances as a function of the actual fly-by distance were calculated and results are shown as Curve 2 in Fig. 4.

Conclusion. The theoretical calculations described in this report are based on spectral characteristics of Mars as presented in Ref. 4. Although the calculated results were utilized as basic data in the design and performance evaluation of the subsystem, an adequate margin has been incorporated to insure satisfactory performance.

C. Analysis of Anomalies in *Mariner* 2 Data

The analysis of the anomalies in the scientific data on *Mariner* 2 is about 50% completed. Inasmuch as the final report on the analysis will not be completed for some time, it is felt that a summary of the analysis to date would be worthwhile and timely. There might be some facet of the *Mariner* 2 study which would focus attention upon an area in the *Mariner C* spacecraft that might otherwise be overlooked.

The experimental tests made in conjunction with the analysis have been of three types:

(1) Those pertaining to data automation system (DAS) effects:

(a) Voltages were varied within the DAS.

(b) Pertinent circuits were opened, shorted, partially opened, partially shorted, transistor gains were degraded, diode characteristics degraded.

(2) Those pertaining to Science Subsystem effects:

(a) Voltages in the radiometer, infrared radiometer (IR), magnetometer and solar plasma detector were varied.

(b) Partial short and open circuits were simulated in the radiometer.

(c) A complete partial short and open circuit interconnection was made between all scientific analog outputs.

(3) Those pertaining to temperature effects:

(a) The DAS was run at 47°C for one week and 67°C for one week to determine whether or not operation at elevated temperatures for long periods of time created effects similar to those observed.

(b) The radiometer and IR were also subjected to special temperature tests.

The results of these tests clearly indicated that 2 (c) was the only simulation which produced effects similar to those observed on *Mariner* 2.

The sequence of observed degradations on *Mariner* 2 was:

(1) The magnetometer was noisy. (September 20, 1962)

(2) The solar plasma calibration reading drifted 1 to 2% over a period of 16 hr. (October 20, 1962)

(3) Cross-talk existed between microwave radiometer, IR, scan position, magnetometer off output, temperature readings (1 to 2% full scale readings). (October 8, 1962)

(4) An increase occurred in radiometer time constant (continuous).

(5) The DAS clock readout was erratic during solar flare. (October 23, 1962)

The circuit which successfully duplicated the observed anomalies is shown in Fig. 7.

Typical values of shunt resistance to the system common are 5 to 50 kΩ. Typical values of shunt resistance to the +6 line are 100 to 500 kΩ. All effects could be duplicated with shunt resistance except the radiometer scan position offset; this anomaly required a small series resistance (500Ω). All the connections are made in the same plug through the same cable. The plasma sensor was not available for the combined tests.

At this point in the analysis the tentative conclusions concerning the failure include the following:

(1) The anomalies were *not* the result of a single, isolated failure, such as a short, a voltage change, or a component failure.

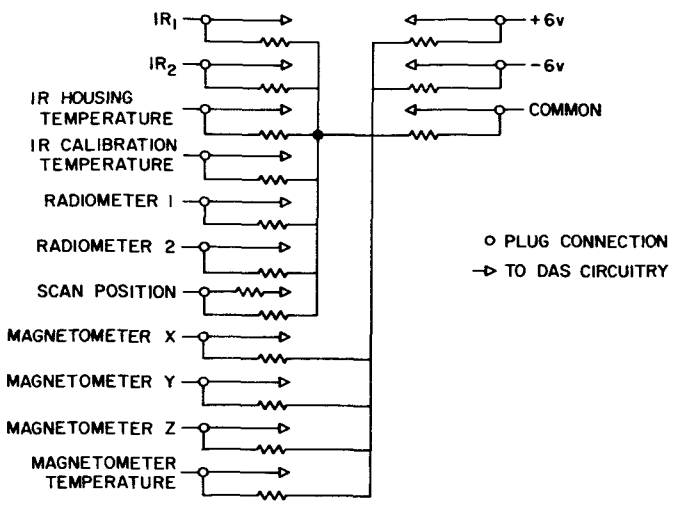

Fig. 7. Circuit used to simulate *Mariner* 2 anomalies

(2) The consequence of the failure became apparent in several circuit areas at about the same time.

(3) The failure took place over a period of time of about 8 to 16 hr and the degradation continued at a slower rate for the remainder of the flight.

(4) The deviation in the data amounted to 1 to 2% of full-scale readings and was higher for those sensors with higher operating output impedances.

Possible causes of the degradation include the following:

(1) General diminishing of effectiveness of case harness cabling insulation properties.

(2) General breakdown of connector insulation.

(3) General breakdown of circuit board insulation.

The possibility (1) suggests that the problem may apply to all spacecraft systems and is partially supported by an observed change in the residual spacecraft magnetic field during the same interval of time when the degradation rate was the highest. The fact that the DAS clock readout was erratic during a solar flare may also be pertinent because it suggests that the radiation caused an arcing somewhere on the spacecraft. This observation could indicate that there is a correlation between the solar radiation and the performance of electronic systems after they are in the space environment for extended periods of time. The observation of the degradation in other areas may not have been readily observed because the readings were less accurate, or taken less frequently or made in circuits with relatively low impedances. Possibility (2) is the next most probable cause; however, it would be confined to those areas which used the same type of connector potting compound. Possibility (3) is considered because the circuit boards were physically located next to the magnetometer power supply. The magnetometer executed some unscheduled calibrations prior to the analog anomalies. The evidence indicated that these unscheduled calibrations were attributable to jumps in the magnetometer power supply voltage. Thus, the possibility exists that a power supply filter capacitor failed and resulted in the deposition of a conductive layer on the circuit board. However, the mechanism for introducing a series resistance by this process has not been conceived and consequently conflicts with the fact that the radiometer scan position anomaly cannot be duplicated without introducing a small series resistance.

The analysis needed to complete the anomaly report includes the following:

(1) A complete solution to the circuit equations and derivation of the values of resistors. A comparison of the experimental and theoretical values of resistance.

(2) A derivation of the values of resistance shunting the radiometer utilizing the variation in time constant observed.

This derivation will allow an independent calculation of two of the shunt resistances. The agreement between the values derived from the independent equations will be related to the confidence in the realism of the simulated mode of failure.

References

1. "The *Mariner* C Science Data Automation System," *Space Programs Summary No. 37-24*, Vol. VI, pp. 77–84, December 31, 1963.

2. "*Mariner* Mars 1964 Photographic Subsystem," *Space Programs Summary No. 37-20*, Vol. VI, pp. 104–108, April 30, 1963.

3. "Mariner C Science Subsystem," *Space Programs Summary No. 37-24*, Vol. VI, pp. 71–77, December 31, 1963.

4. de Vancouleurs, G., and Baker, J. G., *A Study of the Optical System for a Mars Probe* (Final Report under JPL Contract 950014), Harvard College Observatory, Harvard University, Cambridge, Mass., June 30, 1961.